SEMI-ACTIVE SMART-DAMPERS AND RESETABLE ACTUATORS FOR MULTI-LEVEL SEISMIC HAZARD MITIGATION OF STEEL MOMENT RESISTING FRAMES

A thesis

submitted in fulfilment

of the requirements of the Degree

of

Master of Mechanical Engineering

in the

University of Canterbury

by

S. J. Hunt

University of Canterbury
2002

ABSTRACT

This thesis explores the creation and assessment of semi-active control algorithms for both squat shear buildings and tall flexible structures. If cost-effective, practicable, semi-active structural control systems can be developed, the potential reduction in loss of both property and lives due to seismic events is significant. Semi-active controllers offer many of the benefits of active systems, but have power requirements orders of magnitude smaller, and do not introduce energy to the structural system. Previous research into semi-active controllers has shown their potential in linear simulations with single earthquake excitations. The distinguishing feature of this investigation is the use of appropriate non-linear modelling techniques and realistic suites of seismic excitations in the statistical assessment of the semi-active control systems developed.

Finite element time-history analysis techniques are used in the performance assessment of the control algorithms developed for three and nine story structural models. The models include non-linear effects due to structural plasticity, yielding, hysteretic behaviour, and P-delta effects. Realistic suites of earthquake records, representing seismic excitations with specific return period probability, are utilised, with lognormal statistical analysis used to represent the response distribution.

In addition to displacement focused control laws, acceleration and jerk regulation control methods are developed, showing that potential damage reduction benefits can be obtained from these new control approaches. A statistical assessment of control architecture is developed and undertaken, examining the distribution of constant maximum actuator authority for both squat shear buildings, and tall slender structures, highlighting the need to consider non-linear structural response characteristics when implementing semi-active control systems. Finally, statistical analysis of all results and normalised values shows the efficacy of each control law and actuator type relative to different magnitude seismic events. As a result, this research clearly presents, for the first time, explicit tradeoffs between control law, architecture type, non-linear structural effects, and seismic input characteristics for the semi-active control of civil structures.

ACKNOWLEDGMENTS

I would like to sincerely thank Dr Geoff Chase, my principal advisor, for his guidance and patience during the development of this work. His constant enthusiasm and commitment were an inspiration to me, and without his willingness to share his experience, knowledge, and appreciation of good coffee, this research may never have flown. I also wish to thank my external advisor, Assistant Professor Luciana Barroso, from Texas A&M University, whose friendly support and willingness to help during the hard times were invaluable.

The steep learning curve required in this research was aided with guidance and encouragement from Professor John Mander and Dr Bruce Deam from the University of Canterbury Department of Civil Engineering, and Associate Professor Greg MacRae from the University of Washington College of Engineering.

I would like to thank the University of Canterbury Research Office for the summer research scholarship that helped kick this research into life. In addition, thanks are extended to Dr Geoff Shaw and the Christchurch Hospital ICU Research Trust, who provided me with an opportunity to broaden my research horizons, as well as pay the rent!

I would like to thank my fellow post-grads, Dean Kirk, Mark Carey, Manda Batchelor, Blair Liddell, Chris Pretty, Bram Smith, and Zhu Hui Lam, whose encouragement and suggestions have been invaluable. Particular thanks to Jonathan Harrington for the late night cups of tea and company when everyone else was smart enough to be home in bed, and Dave Arnold for taking an active interest in my research and being willing to wade through my drafts. Thanks also to my two best mates, Nick (Nanna) Thompson and Andy Gibbs, whose close friendship make living life more special.

The mission of producing this thesis has been made easier through the support and constant encouragement of my family. Mum and Dad, I appreciate your guidance and wisdom, and the faith you have given me that I can succeed, with God's help, at whatever I put my heart into. Maree, your friendship is something I cherish, and I thank you for your down-to-earth words of reassurance that always remind me that life is bigger than school. Matt, the chats about our coming adventures have helped me see the light at the end of the tunnel, and even

though you are on the other side of the world, I am always aware that my big brother is looking out for me.

Finally, I would like to dedicate this thesis to my fiancé Kate, who throughout my University career has had a level of dedication and patience greater than I'd have thought humanly possible. Kate, you have constantly lightened the burden with your unconditional love and support, and I hope that in our life together I can in some way give you back a little of what you have given me. Let the good times roll! J

CONTENTS

LIST OF FIGURES

LIST OF TABLES

1. INTRODUCTION

1.1 MOTIVATION

With the world's human population increasing at a high rate, the use of high-rise buildings is seen as an effective way of utilising limited ground space within cities. Although these tall structures have been proven to retain integrity under normal loading conditions through the utilisation of sound design practices, their increased flexibility makes them prone to failure under large environmental loadings, such as seismic excitation or wind loads, that can fall outside their linear, damage-free design envelope. Modern structural design codes include considerations of seismic loadings through the concept of acceleration magnification factors, however, it is impractical to build all structures strong enough to sustain large near-field seismic excitations.

Over the past three decades, intensive investigation into how structures respond to seismic excitation has been undertaken. The idea of using active structural control to enable a structure to alter its dynamic characteristics in accordance with environmental loading was published as early as 1972 [Yao 1972]. Frequently, we are reminded of the impact of earthquakes by images such as that in Figure 1.1, which depicts the effect of the Afyon Earthquake (M=6.2) that struck central Turkey early in 2002, on a residential steel reinforced concrete building. If cost-effective, practically applicable, robust, semi-active or active, structural control systems can be developed for both new and retrofit applications, the potential reduction in loss of both property and lives is significant.

Structural control methods can be partitioned into three main groups; passive, active, and semi-active controllers:

i) Passive control was the first type of structural control to be widely accepted and implemented by the civil engineering community. Although a restoring force is imparted as the structure displaces, passive controllers are tuned to a particular response and unable to tailor their characteristics to match a range of excitation levels and building responses. Common examples would include tuned mass dampers (TMDs), which are designed to reduce first mode vibration of tall structures, and base isolators for shorter, squatter structures [Den Hartog 1947, Villaverde 1994, Palazzo and Petti 1994]. These control mechanisms are designed to attenuate response over a specific small frequency range, whereas passive draped cables attached to viscous or friction dampers are designed to minimise response over a larger spectrum range [Pekcan et al. 1999].

ii) An active control system has the ability to both add and/or dissipate structural energy through the application of actuator control forces. Through the use of appropriate sensor feedback the level of actuation may be controlled to give a desired structural response for a variety of seismic characteristics. The requirement of a large energy source and/or sink makes the practical implementation of an active control system potentially complex and expensive. With seismic events occurring randomly, it is not feasible to use fully active control systems that may require large hydraulic pumps to operate continuously to provide power to the seldom-used system, especially when power outage is a common result of seismic activity. However, there are examples of active tuned mass dampers (ATMD's) implemented in Japan, designed primarily to ameliorate wind-loading response [Kobori 1990, Sakamoto et al. 1994, Chase and Smith 1995(a)].

iii) Semi-active controllers are the most recent evolution in structural control and offer many of the benefits of active control with power requirements several orders of magnitude smaller, thus eliminating the need for a large external power source. As many forms of

semi-active controllers do not impart energy to the structural system, they have the additional benefit of guaranteed bounded-input bounded-output stability. Semi-active controllers are currently seen as being the most viable type of active control for widespread acceptance and application by the civil engineering community [Yi et al. 2001]. Examples of semi-active controllers include hydraulic actuators and dampers used as energy sinks, where orifice size is the controller parameter used to vary controller response [Sack et al. (1994)]. More recent advances in "smart fluids", such as magneto- and electro-rheological fluids, have led to more advanced systems [Carlson 1994, Gavin 1994, Dyke et al. 1996].

Figure 1.1: Devastating effects of 2002 Afyon Earthquake (M=6.2) on a residential concrete building.

Although the study of structural control is not new, a large proportion of control algorithm development has been implemented and assessed such that extrapolation to practical applications is not entirely realistic. In order to obtain a practical evaluation of structural performance it is necessary to include two key factors in models and simulations. The first is the inclusion of structural non-linear behaviour, as both the structural damage and large-

motion hysteretic structural damping processes are inherently non-linear. As the response of a structure, and damage that may result, is highly dependent on the nature of the excitation, the second key factor is the use of a wide variety of realistic ground motion excitations that are representative of broad ranges of potential inputs.

The focus of previous structural control design investigations has been the reduction of transient story drifts, which have historically been used as an indicator of structural damage. As internal damage and occupant safety are approximately proportional to floor accelerations [Barroso et al. 2000, Spencer et al. 1994.], a controller which weights the floor accelerations rather than displacements will reduce damage to equipment and people inside the building. The link between accelerations and permanent non-linear deformation may also result in a reduction of external structural damage.

The time rate of change of acceleration is known as “jerk”, and is a control variable that has previously been considered primarily in vibration mitigation for computer hard disc drives [Misoshita et al. 1996]. The inclusion of jerk within the control cost function for structural control is a new line of investigation, and although transient drifts may increase slightly as the controller smoothes the response, the reduction in seismic shock loading should result in a decrease in permanent deformations and damage.

1.2 OBJECTIVES AND SCOPE

The primary objective of this investigation is to use realistic modelling, excitation, and evaluation methods to advance the development of semi-active and active structural control systems. This study focuses on the seismic response of steel moment resisting frames, and its scope looks at three main areas:

i) The application of magnetorheological (MR) dampers and resetable actuators as semi-active controllers.

ii) The effect of different control objectives (displacement and energy, acceleration, jerk) on building response.

iii) The impact of actuator architecture on the controlled response of both squat shear buildings and tall slender buildings.

The structures selected for this investigation are from the SAC Phase II Project [http://quiver.eerc.berkeley.edu:8080/], with the three story SAC3 building typical of a squat shear building, and the nine story SAC9 building used to characterise the control requirements for tall slender buildings which may behave more like a Bernoulli-Euler beam. Responses of these two structures will be evaluated by non-linear finite element simulations using three suites of earthquakes representing a wide range of large seismic excitation characteristics. As with the SAC3 and SAC9 structures, the time history records of these earthquakes were developed under the SAC Phase II Project.

1.3 LITERATURE SURVEY ON SEMI-ACTIVE STRUCTURAL CONTROL

Semi-active control strategies appear to combine the best features of both passive and active control systems, with low power requirements, bounded-input bounded-output stability, and the ability to tailor energy dissipation characteristics [Housner et al 1997]. Semi-active controllers can be classed into two broad categories; those that dissipate energy via damping and those that both store and dissipate energy by varying stiffness [Patten et al. 1994]. For

these types of devices the force-deflection properties are modified during a dynamic event by small electrical commands without the need for a large energy source, which is particularly critical during seismic events in which the main power source to the structure may fail [Breneman 2000, Spencer et al. 1997]. Examples of these types of devices are variable orifice dampers [Sack et al. 1994, Mizuno et al. 1992], friction controllable braces [Dowdell and Cherry 1994], friction controllable isolators [Kawashima et al. 1992], variable stiffness devices [Kobori et al. 1993], and controllable-fluid dampers [Dyke et al. 1996, Dyke et al. 1998, Spencer et al. 1997].

Interestingly, the first full-scale implementation of structural control in the United States was that of the variable-orifice damper class of semi-active devices on an Oklahoma vehicle bridge in 1996 [Housner et al. 1997, Patten 1997]. The impact of the semi-active clipped-optimal controller was to reduce the stress range by 55% giving an additional 100 years of safe life. A key point to note is that this retrofit control system was fully installed for approximately 25% of the cost required to replace the bridge, a level of affordability not likely to be matched by fully active systems.

MR dampers are a more recent type of semi-active controllable fluid damper that have rapidly become a leading candidate for many semi-active control applications due to their large energy dissipation. MR fluids have the ability to reversibly change from a free-flowing, linear viscous fluid to a semi-solid with controllable yield strength in a matter of milliseconds with the application of a magnetic field from a low-current coil [Dyke et al. 1998, Spencer et al. 1997]. MR fluids are magnetic analogues to ER fluids, and typically consist of micron-sized magnetically polarisable particles dispersed in a suspension oil [Housner et al., 1997]. MR dampers are generally cheaper to manufacture than their ER counterparts, as their

performance is relatively insensitive to the presence of contaminants within the MR fluid [Jansen and Dyke 2000].

A great deal of research has been focused on the development of an appropriate model for the MR damper, which includes the actuator dynamics in reaching rheological equilibrium as well as its inherent hysteretic properties [Spencer et al. 1997; Dyke et al. 1996]. The usefulness of these models is yet to be extended to full scale MR dampers, as non-linear model optimisation and experimental verification has only been undertaken on small prototype units applied to model structures. Although a lot of emphasis has been placed on developing non-linear models of the MR damper, their performance has never been investigated with the inclusion of the non-linear structural effects that are considered essential for an accurate model of a structural system [Barroso et al. 2001]. The importance of the actuator dynamics in relation to structural dynamics is not fully investigated, but if the natural frequencies of interest are separated by a sufficiently large interval, any interaction will have little impact. MR dampers have shown promising results in laboratory testing [Dyke et al. 1998], however, for real-life earthquake applications very large forces are required. Although the Lord Corporation have developed a 20-ton MR damper, shown in Figure 1.2, the practicality of installing this actuator into a full-scale structure has not yet been investigated [Yi et al. 1998].

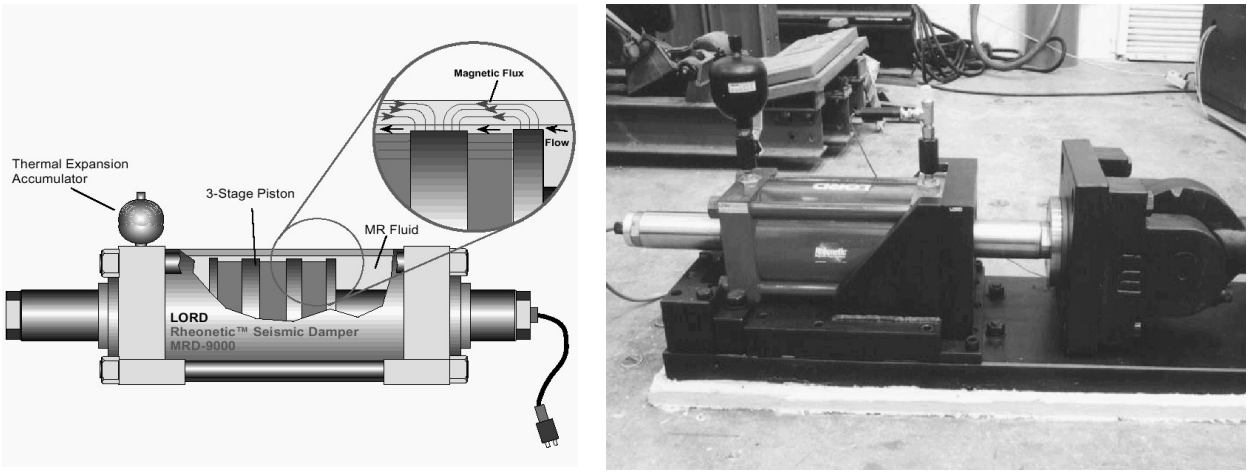

Figure 1.2: 20-ton MR damper developed by the Lord Corporation.

One of the most interesting recent advances in semi-active actuators has been the development of the resetable actuator. This actuator effectively behaves as a spring with an adjustable unstressed length, with a controllable valve releasing stored energy before it is returned to the structure [Bobrow et al. 1995]. More specifically, it simply compresses air with actuator motion, storing energy which is released at the peak of vibration oscillation, releasing the energy before it is put back into the structure. A key factor in the suppression of vibration is the rapid removal of energy from the vibrating structure, and linear simulation and experimentation have shown resetable actuators to be extremely successful at rapid energy dissipation [Bobrow and Jabbari 1997, Yang et al. 2000(b)]. Previous investigations into resetable actuators have focused on the development of the control law and have limited verification to either linear lumped mass simulations, or laboratory testing of small models subjected to cyclic excitations [Bobrow et al. 1995, Thai et al. 1995]. As discussed previously, it has been shown that the lack of realistic non-linear structural effects and excitations makes it unreasonable to assume this verification will directly extend to practical applications [Barroso et al. 2001, Breneman 2000].

Performance-based evaluation of control methods is an important step in relating the benefits of these non-traditional structural solutions to the earthquake engineering community. The United States Building Seismic Safety Council (BSSC) has developed guidelines that relate structural drifts to the estimated structural damage of steel moment frames as part of the National Earthquake Hazards Reduction Program (NEHRP) [BSSC 1997]. As presented in Table 1.1, the qualitative performance levels are described in terms of both transient and permanent drifts. The peak transient drifts are indicative of damage to low strength rigid elements, such as building cladding and partition walls, while permanent drifts provide an indication of cumulative damage to structural members [Barroso et al. 1998]. The drift limits presented in Table 1.1 are defined as the ratio of maximum interstory drift over story height, in percentage form.

TABLE 1.1: GENERAL STRUCTURAL PERFORMANCE LEVEL DEFINITIONS AND INDICATIVE DRIFTS FOR STEEL MOMENT FRAMES [BSSC 1997].

Performance Level	**Description**	**Approximate Drift Limit (%)**	
		Transient	**Permanent**
Collapse Prevention	Little residual stiffness and strength, but load bearing columns and walls function. Large permanent drifts. Building is near collapse.	4	4
Life Safety	Some residual strength and stiffness. Some permanent drift. Building may be beyond economical repair.	2	1
Immediate Occupancy	No permanent drift. Structure retains all of its pre-earthquake strength and stiffness.	1	Negligible

Using permanent drifts as the sole measure of structural damage can be misleading, as an earthquake excitation may have simultaneous jolts in different directions, resulting in a small permanent deformation but extensive structure damage [Barroso et al. 1998]. In addition, peak floor accelerations are indicative of the level of occupant safety, which is an important

additional consideration in structural control evaluations, particularly for structures such as hospitals [Dyke and Spencer 1996].

The difficulty with undertaking an investigation based fully on simulations is the verification that the simulation contains the attributes necessary to give a sufficiently accurate representation of real behaviour. When a study is concerned with structural response on the global or individual story level, it is appropriate to model the structure's frame elements as lumped mass linear frame elements with non-linear behaviour modelled by non-linear torsional connecting elements at the ends of the beam-column elements [Barroso 1999, Breneman 2000]. A Bouc-Wen model describes the non-linear hysteretic behaviour of the torsional elements which model structural dissipation during large motions, as this functional representation fits well with continuous derivative integration routines commonly used for time history analysis [Breneman 2000]. The significance of other types of non-linear characteristics has also been investigated, with P-delta effects noted as having a small effect on model accuracy [Barroso 1999].

1.4 OVERVIEW

Chapter 2 presents a description of the structures and earthquake suites that are used in the simulations to assess the various controller designs. Two types of structures are presented, the three story SAC3 building, and the nine story SAC9 building, both of which are steel moment resisting frames. A discussion of the structural models and the basic control simulation techniques is presented in Chapter 3. The development of a finite element model with the inclusion of structural non-linear effects is outlined, followed by a brief outline explanation of how this is used as part of a time-history analysis. Five different control algorithms are investigated:

i) Clipped quasi-bang-bang.

ii) LQR clipped optimal.

iii) LQRy clipped optimal.

iv) Resetable actuator.

v) JQR clipped optimal.

A brief example of the benefits of a base isolation hybrid controller is also developed. The details of the design and optimisation of these controllers is presented in Chapter 4. Simulation results for the SAC3 structure are presented in Chapter 5, while those for the SAC9 structure are presented in Chapter 6. Chapter 7 presents a selection of results for the SAC3 and SAC9 structures normalised using structural hysteretic energy and the L_2-norm of control input energy, enabling effective comparisons of the different types of control systems. In addition, Chapter 7 presents a comparison with previous research on passive viscous dampers, highlighting the benefits of semi-active control strategies. A brief summary of previous discussions is presented in Chapter 8, along with the primary conclusions of this research. Finally, suggestions for future developments leading from this research are discussed in Chapter 9.

1.5 CHAPTER SUMMARY

This research explores the creation and assessment of semi-active controllers for both squat shear buildings and tall flexible structures. If cost-effective, practically applicable, robust, semi-active or active, structural control systems can be developed for both new and retrofit applications, the potential reduction in loss of both property and lives due to seismic events is significant.

This chapter has introduced the motivation for this investigation, and briefly outlined the development from passive controllers which are tuned for a particular response, to active controllers that use sensor feedback to control the level of actuation, giving a desired structural response for a variety of seismic characteristics. A discussion of previous research into semi-active controllers, which offer many of the benefits of active control with power requirements several orders of magnitude smaller, was presented. The distinguishing feature of this investigation is the use of appropriate non-linear modelling techniques and realistic suites of seismic excitations in the assessment of the semi-active controllers developed. The following chapter presents a basic overview of the three and nine story structures used, and the three suites of earthquake records applied as input excitations.

2. BUILDINGS AND EARTHQUAKE SUITES

The structural systems used in this investigation were both developed as part of the SAC Phase II Project. The SAC Project was primarily concerned with the impact of connection fractures of steel moment resisting frames, and buildings were designed for three locations: Los Angeles, Seattle, and Boston [Krawinkler and Gupta 1998]. The two structures and three sets of earthquake suites used in this research were developed for the Los Angeles area. Los Angeles was selected as it has the highest level of seismic hazard of the three SAC locations, and would be a primary candidate for implementation of semi-active control systems.

2.1 SAC3 STRUCTURAL SYSTEM

The SAC3 structure is a three-bay, three-story steel structure with exterior moment resisting frames. Each bay has centreline dimensions of 30 feet by 13 feet, and all columns are fixed at the base and extend the full height of the structure. Figure 2.1 shows the configuration of a North-South SAC3 frame, with centreline dimensions and US steel member sections as shown. The structure is approximately uniform in the two orthogonal directions, hence a two dimensional analysis of this single North-South frame will give a sufficiently accurate representation of the building response. A more detailed description of the structural system modelling techniques may be found in Chapter 3. The SAC3 building is essentially a short squat structure with very linear, shear building structural response at a fundamental period of approximately one second.

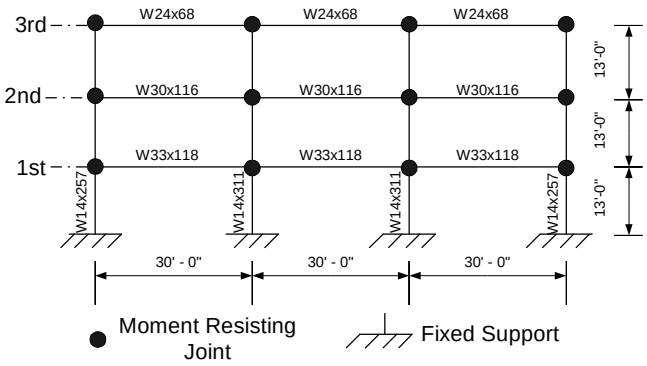

Figure 2.1: SAC3 structural system showing centreline dimensions and member sections.

2.2 SAC9 STRUCTURAL SYSTEM

The SAC9 structure is a five-bay, nine-story building, with four moment resisting bays and one partially moment resisting bay with simple shear connections to avoid bi-axial bending in the corner columns. The SAC9 structure has a soft first story with isolation properties that may be beneficial to structural control. Although each bay has a width of 30 feet, the first story has a height of 18 feet while the eight stories above have a height of 13 feet. The extra height ensures the first floor is approximately 62% less stiff or "softer" than subsequent floors. Below this first floor there is a basement level, which has a depth of 13 feet and is horizontally restrained at ground level. A schematic of a North-South SAC9 frame is shown in Figure 2.2, with centreline dimensions and beam sections as annotated. Each structural column is simply supported at the base and is fabricated from different sized sections with splices between alternate floors. For clarity, column sizes for each numbered section are omitted from Figure 2.2, but are shown in Table 2.1. As with the SAC3 structure, the use of this single North-South frame in modelling is sufficient due to the building's orthogonal symmetry (see Chapter 3 for further explanation).

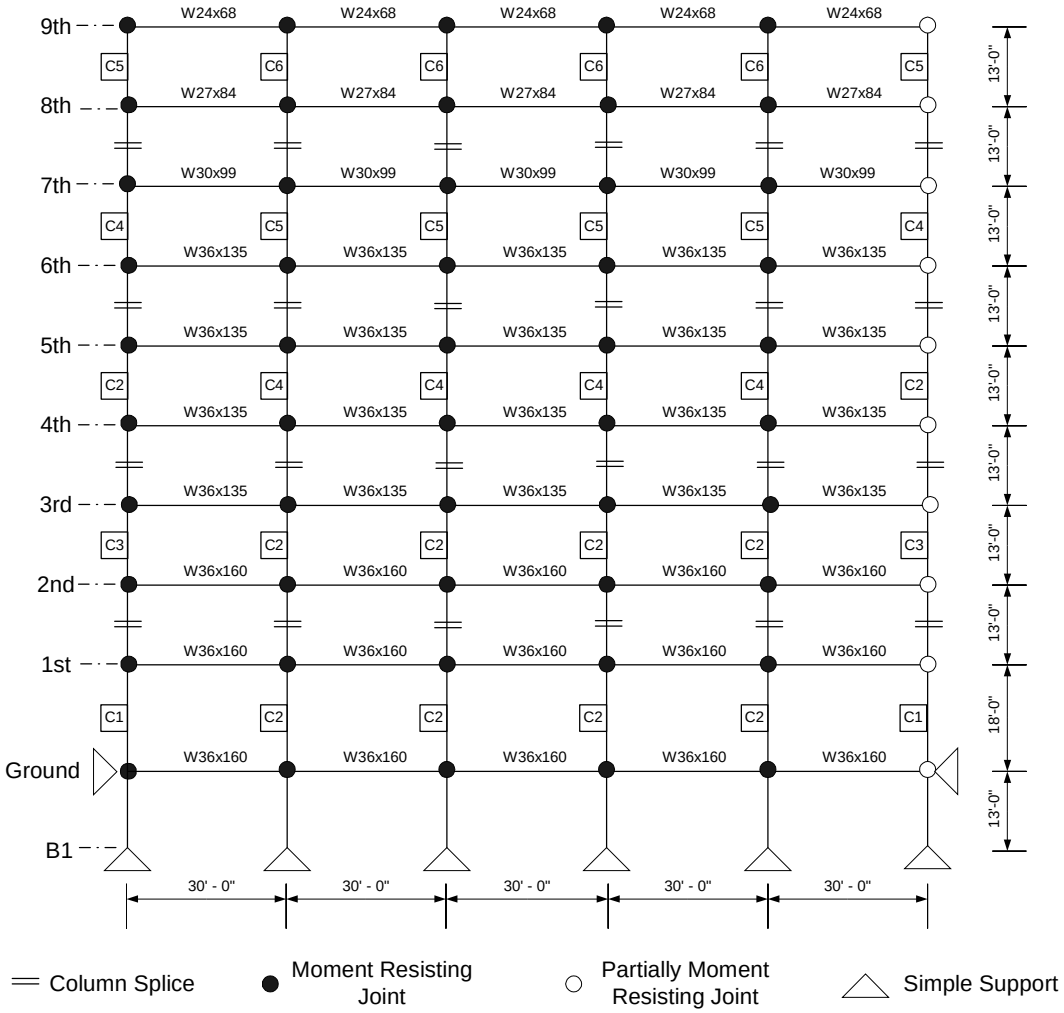

Figure 2.2: SAC9 structural system showing centreline dimensions and beam sections.

TABLE 2.1: SPLICED COLUMN SECTIONS FOR SAC9 STRUCTURE (REFER TO FIGURE 2.2 FOR COLUMN NAMES).

Column Name	Column Section
C1	W14x500
C2	W14x370
C3	W14x455
C4	W14x283
C5	W14x257
C6	W14x233

2.3 EARTHQUAKE SUITES

The use of accurate seismic time histories is a key feature of this research, with little prior research focusing on the importance of examining a wide range of excitation characteristics, and the use of statistical methods to evaluate structural response. Previous research into semi-active controllers employed either sinusoidal, random, or single earthquake excitation to prove the benefits of clipped-optimal or Lyapunov-derived controllers [Yi et al. 1998, Jansen and Dyke 2000, Bobrow et al. 1995]. As the characteristics of seismic excitation are entirely random and unlike other types of vibrational excitation, the use of multiple time history records over a range of seismic levels is essential for effective controller evaluation.

Three suites of 20 earthquake acceleration records were developed to represent the seismic hazard at the SAC Phase II Los Angeles site [Sommerville et al. 1997]. The high, medium, and low suites are grouped according to a probability of excedance of 2%, 10%, and 50% in 50 years, respectively. These excedance probabilities are approximately equivalent to mean return periods of 2,475, 474, and 72 years for the high, medium, and low suites respectively. The low and medium level suites are comprised solely of recorded ground motions pairs, while the high level suites contain five recorded and five simulated motion pairs. The time histories for the low suite are from earthquakes at a distance range of 5 to 100km, while those for the medium and high suites, with the exception of the 1992 Landers earthquake which was recorded at a distance of 40km, are near-field recordings. Near field recordings have rapid spikes in acceleration and hence, will effectively test the benefits of acceleration and jerk control. Each of the ground motion pairs represent the same earthquake measured in orthogonal directions, each of which is at 45 degrees to the fault strike, which is the angle, with respect to north, at which the fault plane intersects a horizontal plane. The earthquakes contained within the three suites are shown in Table 2.2. It should be noted that although in

some cases multiple pairs of earthquake pairs have the same name, these are in fact distinct pairs of time histories from different recordings of the same earthquake.

In order to accurately represent the seismic hazard at the Los Angeles site, each earthquake was scaled by a scalar value so that their response spectra, for a given probability of excedance, were comparable with the spectrum from the United States Geological Survey (USGS) probabilistic seismic hazard maps for the Los Angeles area, in the period range of 0.3 to 4.0 seconds for stiff local soil conditions. The error between the suites of ground motions and the USGS hazard maps was minimised over the selected period range as the damped natural frequencies of the SAC3 and SAC9 structural models fall within this band.

TABLE 2.2: NAMES OF EARTHQUAKES SCALED WITHIN SUITES.

Suite	Probability of Excedance for Entire Suite	Earthquakes Scaled within Suite
High	2% in 50 years	Kobe (1995) Loma Prieta (1989) Northridge (1994) Tabas (1974) Elysian Park (simulated)
Medium	10% in 50 years	Imperial Valley (1979) Landers (1992) Loma Prieta (1989) Northridge (1994) North Palm Springs (1986)
Low	50% in 50 years	Coyote Lake (1979) Imperial Valley, El Centro Array 6 Kern County (1952) Landers (1992) Morgan Hill (1984) Parkfield (1966) North Palm Springs (1986) San Fernando (1971) Whittier (1987)

Due to the scaling method used to ensure each suite of earthquakes falls within the prescribed probability of excedance, the entire suite must be used for probability groupings to hold. Although the median spectral acceleration for the entire suite at a given period will closely match the desired USGS value, the value for an individual scaled earthquake may not. Due to the computational time involved for simulations of the SAC9 structural system, it was not possible to efficiently run the full 20 earthquakes per suite, rather, odd-half suites were used. Although this does introduce potential error in the excedance probabilities, taking the first earthquake in each pair is expected to still give a fair indication of the building response for the prescribed excitation level. Spectral acceleration diagrams allow the relative intensity of earthquakes to be assessed, and are developed by determining the response of a 1 degree-of-freedom system over a spectrum of different periods. Intensity comparisons can then made using the fundamental frequency of the structure of interest. As can be seen in Figure 2.3, the spectral acceleration plots of the odd half suites are close to those of the full suites, however, to reduce any potential skewing of the results, comparisons will only be made between suites that contain the same earthquakes.

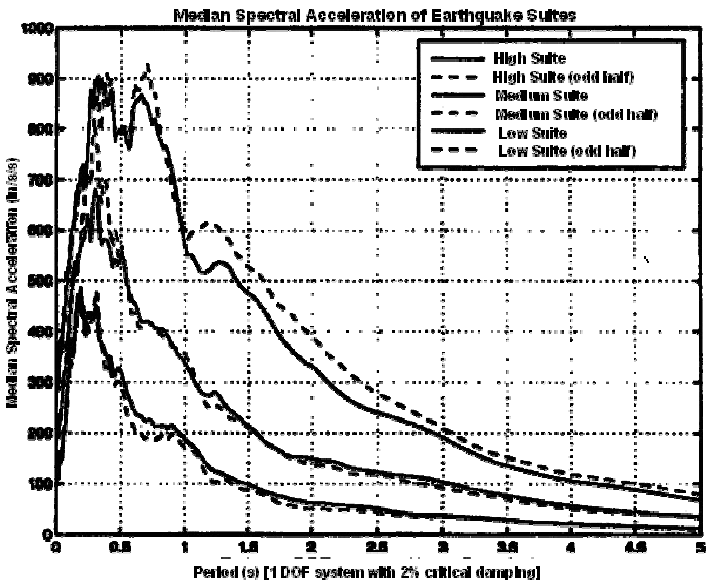

Figure 2.3: Spectral acceleration plots for full and odd half earthquake suite (1 DOF system with 2% critical damping) [Breneman 2000].

2.4 CHAPTER SUMMARY

This chapter has described the three-story and nine-story structures and earthquake suites used in the control assessment simulations. The buildings were developed as part of the SAC Phase II Project, and are structures designed and built for the Los Angeles area. Of the three SAC Project locations, Los Angeles has the highest seismic risk and is seen as a primary candidate for implementation of semi-active control systems. Both structures have moment resisting steel frames and are approximately uniform in orthogonal directions. The development of the three earthquake suites from the SAC Phase II Project was presented, with a brief description of the required time-history record adjustment to represent probabilities of excedance of 2%, 10%, and 50% in 50 years according to USGS Los Angeles probabilistic seismic hazard maps. Details of the finite element formulation and non-linear modelling techniques are presented in the following chapter, along with a brief description of the MATLAB simulation implementation.

3. MODELS AND CONTROL SIMULATION

3.1 STRUCTURAL MODELS

In order to evaluate the potential benefits afforded by semi-active controllers, a computer simulation algorithm was developed. The development of a structural model that represents the actual structure to the required level of detail is a crucial step in the development of seismic simulations. The methods used to formulate a non-linear structural model accounting for the contribution of hysteresis, plasticity, yielding, and P-delta effects are detailed within this section.

3.1.1 Finite Element Formulation

The section describes the development of a finite element formulation for the two structures presented in Chapter 2. As each structure is approximately uniform in the two orthogonal directions, a two dimensional model of the North-South frame will give an accurate representation of the building's structural response. The two dimensional models are of a single moment resisting frame with half the seismic mass distributed across each floor level. The distribution of half the structural weight between the floors for the SAC3 and SAC9 models are shown in Tables 3.1 and 3.2 respectively.

TABLE 3.1: DISTRIBUTION OF SAC3 STRUCTURAL WEIGHT.

Floor Level	Weight (kips)
1	1056
2	1056
3	1143
TOTAL	**3255**

TABLE 3.2: DISTRIBUTION OF SAC9 STRUCTURAL WEIGHT.

Floor Level	Weight (kips)
B1	0
Ground	1063
1	1111
2-8	1092
9	1179
TOTAL	**10997**

As this investigation is concerned with the structural response on the global level, a commonly accepted structural analysis method is implemented, using centreline dimensions with stiffness contributions from non-structural components such as cladding and internal walls neglected. Although the use of centreline dimensions does result in a slight overestimate of beam-column moments, with moments taken at the centreline and not at connected member faces, the effect of this on global response values is small [Gupta 1998]. It is also assumed that the members used in the original buildings have sufficient lateral bracing to allow local and lateral buckling instability to be neglected. It should be noted that column buckling effects may need to be examined during any subsequent experimental investigations due to the effect of the vertical components of applied actuator forces.

For the level of detail required in these simulations, a lumped plasticity model for the frame elements is appropriate [Breneman 2000]. Although the plastic zone may extend down a member during large joint rotations, this has a detrimental effect on column performance, and is limited through design using strong column-weak girder (SCWG) methods. SCWG design methods ensure that the column moment capacities at a given joint are at least 1.2 times that of the attached beams. The building's frame elements are modelled as linear-elastic beam-column elements with non-linear behaviour assumed to be lumped at the ends of the beams and columns. The non-linear behaviour is added by modelling non-linear connection

elements at each end of the beam-column elements, as schematically represented in Figure 3.1.

Figure 3.1: Lumped plasticity model for beam-column elements.

These non-linear torsional spring-dampers are zero length elements and produce a restoring force due to relative beam-column rotation. Due to the assumption that the plastic zone has zero length, the interior nodes have the same displacement as their adjacent external nodes. A very high initial stiffness relative to the beam elements is enforced, and torsional spring-damper strength is set to the plastic moment capacity of the beam in order to limit the maximum rotation of the torsional elements. The torsional spring-damper post-yielding stiffness is calculated based on the elastic flexural stiffness of the beam. The overall effect is to provide joint connections with non-linear hysteretic elastic-plastic behaviour to account for hysteretic structural damping and permanent structural deformation under large deflections or excitation.

Using the assumption that the floor slabs are rigid in-plane, the horizontal degrees-of-freedom of each floor are slaved, leaving only one horizontal degree-of-freedom per floor level. This degree-of-freedom coupling decreases computational intensity and simplifies the application of earthquake loading and actuator forces. The final finite element model for the SAC3 building, shown in Figure 2.1, with fixed constraints imposed at the base of each column and appropriate degree-of-freedom coupling, has a total of 49 degrees-of-freedom. The model for

the SAC9 structure, shown in Figure 2.2, with simple support constraints at the basement level and horizontal restraint at ground level, has 327 degrees-of-freedom.

The modal properties of the resulting models for both structures are shown in Table 3.3. It should be noted that 2% Rayleigh damping is enforced at the first mode period for both the SAC3 and SAC9 structure. This value is lighter than might be expected for this structure under strong motion, however, with the inclusion of the non-linear connection elements, represents the linear damping term for smaller motions only. Reduced order, 3 and 9 degree-of-freedom, linear models used for some of the controller design were tuned to match the first modes of Table 3.3.

TABLE 3.3: MODAL PROPERTIES OF SAC3 AND SAC9 STRUCTURAL MODELS.

	SAC 3 Structural Model		**SAC9 Structural Model**	
	Period (s)	**Damping (%)**	**Period (s)**	**Damping (%)**
1st Mode	1.02	2.0	2.27	2.0
2nd Mode	0.33	1.5	0.85	1.1
3rd Mode	0.17	2.2	0.49	1.1

3.1.2 Non-linear Modelling Techniques

Previous research into the effect of non-linear aspects within simulated models for controller evaluation has highlighted the necessity to included two main types of non-linear effects if models are to accurately represent actual structural demands [Breneman 2000, Barroso et al. 2001]. The inclusion of a non-linear hysteretic model to account for structural dissipation and yielding during large motions is the first of these aspects, while the second is the effect of geometric non-linear P-delta effects on flexural stiffness. Although many other non-linear effects exist, for example the degradation of column bending strength due to P-M interaction,

the impact of these aspects on parameters at the global level are small and hence are neglected in this investigation [Barroso et al. 2001].

The inclusion of these non-linear effects in the structural models dramatically changes the response of the structure, particularly for the tall, slender SAC9 structure. Table 3.4 presents the modal participation percentages for the linear and non-linear SAC9 structural models. The impact of the non-linear response is to increase the contribution of higher modes, particularly the 3rd and 4th modes. This change in modal response characteristics can greatly alter how each of the different control systems perform. Hence, their inclusion is vital to the accurate assessment of controller performance.

TABLE 3.4: MODAL CONTRIBUTION FOR LINEAR AND NON-LINEAR SAC9 STRUCTURAL UNCONTROLLED RESPONSES.

Mode	Modal Contribution (%)	
	Linear Structural Model	Non-linear Structural Model
1st	89.4	57.3
2nd	7.2	6.1
3rd	1.1	16.7
4th	1.8	11.3
5th	0.1	2.4
6th	0.3	2.5
7th	0.0	1.4
8th	0.0	1.1
9th	0.1	1.1

3.1.2.1 NON-LINEAR FRAME ELEMENT BEHAVIOUR

Previous research has investigated the identification and/or development of models to represent the dynamics of civil structures under large excitation and deflection [Iwan and Cifuentes 1986, Peng 1992]. A Bouc-Wen smooth varying hysteretic model is used in this

investigation as its functional representation fits well with the continuous derivative time integration routines used to solve the structural simulations [Breneman 2000]. This model is also easily manipulated to provide a desired level of hysteretic behaviour through the adjustment of model parameters. Although this model is non-linear, for both small and large deflections the force-deflection relationship is linear, with two different stiffness values as depicted in Figure 3.2. If the total torsional spring-damper stiffness is denoted as $K_{T,}$ then the linear restoring moment, M_R, for small rotational deflections, r(t), is given as:

$$M_R = K_T r(t) \tag{3.1}$$

For rotational deflections outside the linear range, the minimum post-yielding stiffness is defined as the elastic stiffness, K_E, and the remainder of the total stiffness that may yield is defined as the hysteretic stiffness, $K_H=K_T-K_E$. This definition of K_H can be clearly seen in Figure 3.2. For the hysteretic model, the total restoring moment, M_R, for a single element can then be written in terms of the elastic and hysteretic restoring moments as:

$$M_R = M_E + M_H = K_E r(t) + K_H z(t) \tag{3.2}$$

where z(t) is a new time varying, non-physical displacement defined by the Bouc-Wen model, and is related to the real displacement, r(t) by the relationship:

$$\dot{z}(t) = \dot{r}(t)\left[1 - 0.5(1 + \mathrm{sgn}(\dot{r}(t)\, z(t)))\left|\frac{z(t)}{Y}\right|^n\right] \tag{3.3}$$

where Y is the yield deflection for each non-linear element, n is a hysteretic shape parameter, and sgn() denotes the sign of the internal function [Wen 1976]. Equation (3.2) may be

rewritten in terms of the post-yielding stiffness ratio, α, which is the ratio of residual stiffness to nominal stiffness, $\alpha = (K_E/K_T)$. A post-yielding stiffness ratio of α=0.03 (3%) was selected for these simulations, representing a 97% post-yield reduction of stiffness in the plastic region. This is an idealisation of plastic resistance and response that is seen as appropriate for use when the focus is on the global structural response [Breneman 2000, Barroso 1999]. Each non-linear element has its own yield deflection, which is dependent of the plastic moment capacity of the member, M_P, and is defined:

$$Y = \frac{M_P}{K_T} \tag{3.4}$$

A large initial value of the total stiffness is used as a small displacement corresponds to a large rotational deflection which leads to large outer fibre strains, and subsequently rapid onset of plastic deformation. For each of the non-linear torsional spring-dampers a value of 1e12 was used for the total initial stiffness, as a large number representative of the rotational stiffness of a 1-inch member.

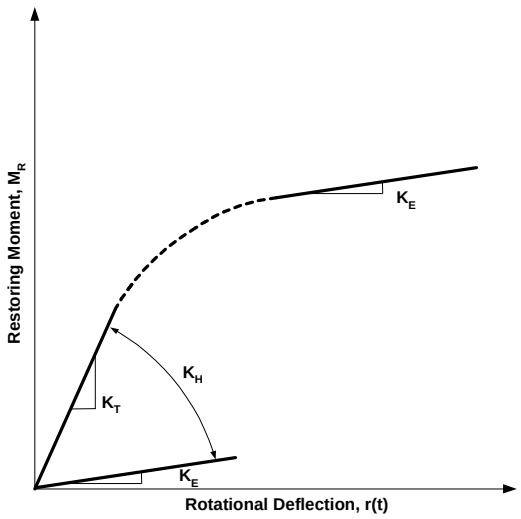

Figure 3.2: Stiffness definitions for hysteretic torsional spring-damper model.

The relationship between z(t) and r(t) described in Equation (3.3) is shown schematically in Figure 3.3, where Y is the yield deflection value defined in Equation (3.4). It can be clearly seen that at small deflections z(t) is proportional to r(t), with allowance made for residual plastic deformations. The shape parameter, n, from Equation (3.3) determines the effective width between linear segments, with large values tending towards a bi-linear relationship. A shape parameter of n=10 was selected for each of the non-linear torsional spring-dampers used in this investigation, providing a smooth bi-linear transition.

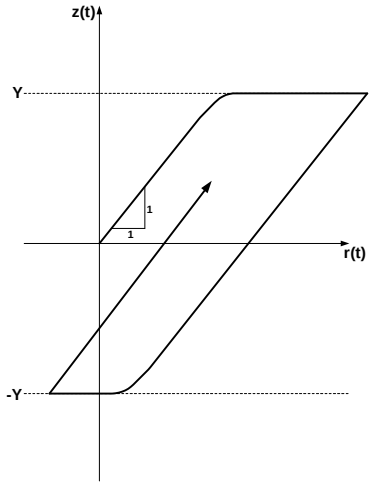

Figure 3.3: Schematic of Bouc-Wen hysteretic relation.

Figure 3.4 shows the form of the smooth Bouc-Wen hysteretic loop. The essential characteristics that should be noted are the limit of restoring moment due to the torsional spring-damper plastic moment capacity, as well as the weighted yielding in one direction which results in a net plastic deformation – a feature observed in the earthquake simulations undertaken in this investigation. It should be noted that stiffness degradation due to cumulative damage is not included in the model, with stiffness values independent of how much permanent deformation has occurred.

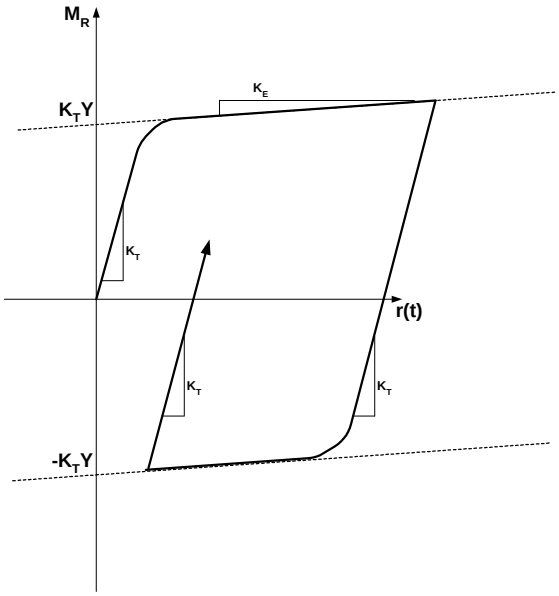

Figure 3.4: Schematic of the Bouc-Wen hysteresis loop.

3.1.2.2 P-DELTA EFFECTS

When columns are subjected to gravity loads, their lateral stiffness is decreased by an amount proportional to the axial load. The procedure for inclusion of this effect is derived directly from the theory of P-delta effects on the individual cantilever column show in Figure 3.5(a) [Barroso 1999]. As illustrated in Figure 3.5(b), as the column deflects laterally an additional bending moment at the base of the column results from the axial load. This additional bending moment can be represented by an increased lateral load as shown in Figure 3.5(c). Using the lateral stiffness of the column, k, the equilibrium equation may be written as:

$$F_x + F_y\left(\frac{d}{L}\right) = kd \tag{3.5}$$

where F_x is the lateral end load, F_y is the axial end load, d is the cantilever lateral tip displacement, and L is the cantilever length.

Equation (3.5) may now be rearranged to eliminate the vertical force by introducing a reduced lateral stiffness term, k_{red}:

$$\left(k - \left(\frac{F_y}{L}\right)\right)d = k_{red}d = F_x \tag{3.6}$$

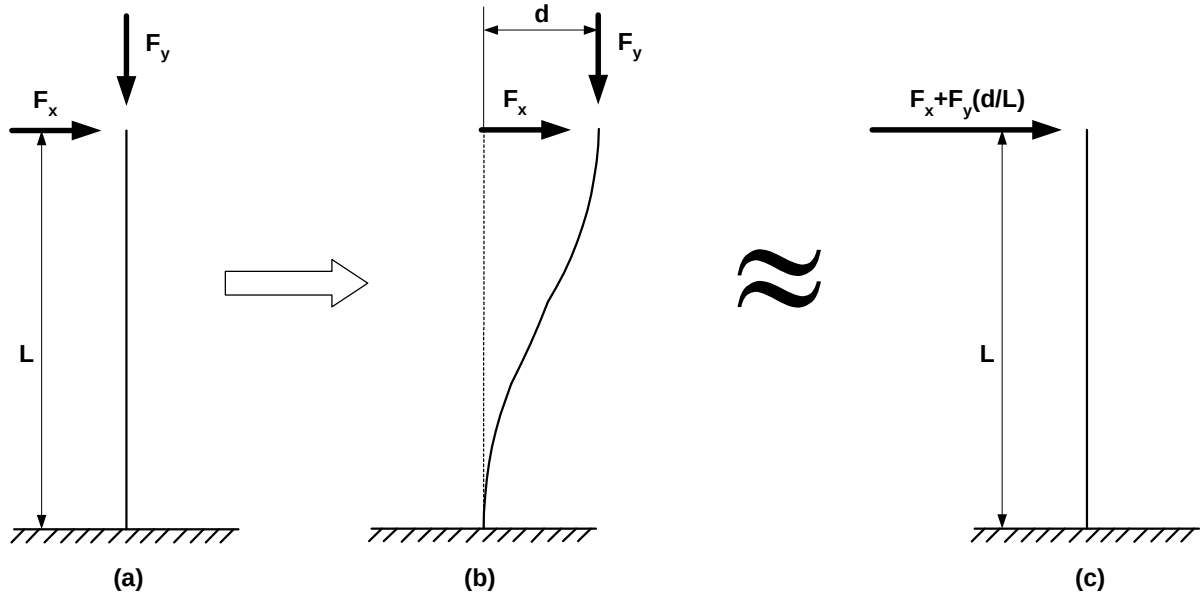

Figure 3.5: P-delta effects on a cantilever column.

This P-delta theory for a cantilever column is simply extended into matrix form for the frame elements used in this investigation, with a geometric stiffness matrix obtained upon assembly for each element subjected to gravity loading. The geometric stiffness matrix is assembled and added to the global stiffness matrix, thus accounting for the structure's reduced lateral stiffness. By making the assumption that the columns are subject only to gravity loads with no additional dynamic axial loading due to actuators loads or floor slab rotation, the geometric stiffness is not time dependent and is therefore only calculated once during model formulation.

3.1.3 Assembled Non-linear Structural Model

The dynamic equations of motion for the assembled non-linear system are given by Equation (3.7), where **M**, **K**, and **C**, are the assembled global mass, stiffness, and damping matrices, respectively. The stiffness matrix, **K**, includes the adjustment for P-delta effects described previously. The $\mathbf{K_H}$ matrix is the assembled hysteretic stiffness matrix due to the non-linear torsional spring-dampers, and **z**(t) is a vector of hysteretic non-physical displacement values, z(t), for each element. The terms on the right hand side of Equation (3.7) account for the external loading applied by the earthquake, gravity, and actuator forces. The vector $\mathbf{S_g}$ maps the earthquake ground acceleration, $\ddot{\mathbf{x}}_{\mathbf{g}}(t)$, to the slaved horizontal degrees-of-freedom for each floor.

$$\mathbf{M}\ddot{\mathbf{v}}(t) + \mathbf{C}\dot{\mathbf{v}}(t) + \mathbf{K}\mathbf{v}(t) + \mathbf{K}_{\mathbf{H}}\mathbf{z}(t) = -\mathbf{M}\mathbf{S}_{\mathbf{g}}\ddot{\mathbf{x}}_{\mathbf{g}}(t) + \mathbf{F}_{\mathbf{ext}}(t) \tag{3.7}$$

where v, $\dot{v}$, $\ddot{v}$ are the relative displacement, velocity, and acceleration respectively.

The vector $\mathbf{F_{ext}}$(t) is defined in Equation (3.8), where the matrix $\mathbf{S_{act}}$ maps the actuator force matrix, $\mathbf{F_{act}}$(t), to the appropriate horizontal degrees of freedom, and the vector $\mathbf{S_{grav}}$ maps the gravity load vector, $\mathbf{F_{grav}}$(t), to the appropriate nodal positions.

$$\mathbf{F}_{\mathbf{ext}}(t) = \mathbf{S}_{\mathbf{act}}\mathbf{F}_{\mathbf{act}}(t) + \mathbf{S}_{\mathbf{grav}}\mathbf{F}_{\mathbf{grav}}(t) \tag{3.8}$$

The system of second order differential equations in Equation (3.7) can be expressed as a system of first order differential equations by creating a standard state-space model employing an augmented state vector:

$$\mathbf{x}_s(t) = \begin{bmatrix} \mathbf{v}(t) \\ \dot{\mathbf{v}}(t) \\ \mathbf{z}(t) \end{bmatrix} \tag{3.9}$$

where $\mathbf{v}(t)$, $\dot{\mathbf{v}}(t)$, and $\mathbf{z}(t)$ are as defined previously. The description of the hysteretic behaviour can also be assembled into a form written as:

$$\dot{\mathbf{z}}(t) = \left[\frac{d\mathbf{z}(t)}{d\mathbf{v}(t)} \right] \dot{\mathbf{v}}(t) \tag{3.10}$$

Using the definitions in Equations (3.7)-(3.10), the state space form of the assembled non-linear system may be defined:

$$\dot{\mathbf{x}}_s(t) = \begin{bmatrix} \mathbf{0} & \mathbf{I} & \mathbf{0} \\ -\mathbf{M}^{-1}\mathbf{K} & -\mathbf{M}^{-1}\mathbf{C} & -\mathbf{M}^{-1}\mathbf{K}_H \\ \mathbf{0} & \dfrac{d\mathbf{z}}{d\mathbf{v}} & \mathbf{0} \end{bmatrix} \mathbf{x}_s(t) + \begin{bmatrix} \mathbf{0} \\ -\mathbf{S}_g \\ \mathbf{0} \end{bmatrix} \ddot{\mathbf{x}}_g(t) + \begin{bmatrix} \mathbf{0} \\ \mathbf{M}^{-1} \\ \mathbf{0} \end{bmatrix} \mathbf{F}_{ext}(t) \tag{3.11}$$

3.2 SIMULATION IMPLEMENTATION

The time-history analysis required to solve Equation (3.11) was performed using MATLAB V6.0/R12. MATLAB offers the benefit of built-in toolboxes for linear controller design as well as output visualisation functions, however, the computational intensity of manipulating large matrices coupled with the performance of the in-built ordinary differential equation (ODE) solver meant the solution time for a suite of earthquakes could be large. In an attempt to reduce solution time, sparse matrices were used wherever possible and the Jacobian matrix

for the time varying ODE solution was explicitly calculated rather than depending on an internal finite difference approximation which can lead to an unstable solution.

Following the assembly of the system structural matrices and formation of the state-space equations, the solution is obtained used MATLAB's ODE solver, ode15s. This solver was selected due to the stiff nature of the system, and is a variable-order multistep solver. For each simulation run the same integration tolerances were used, with the relative tolerance set to 1e-2, and the absolute tolerance set to 1e-4 for translational degrees-of-freedom, 1e-5 for rotational degrees-of-freedom and 1e-6 for hysteretic degrees-of-freedom.

Once a solution has been obtained, the following metrics were calculated from the time history response and used for assessment of the structural performance:

i) Peak story drift

ii) Permanent story drift

iii) Peak floor absolution acceleration

iv) Structural hysteretic energy

These results are stored for each individual earthquake and then compiled at the end of the suite assuming a lognormal distribution for drift metrics, and a standard counted distribution for hysteretic energy values, which determines statistical terms based on the number of response values that lay below the desired statistical value.

3.3 CHAPTER SUMMARY

This chapter has detailed the methods used to construct and implement the models necessary to obtain an accurate representation of the non-linear structural response for the SAC3 and SAC9 buildings. Using a lumped-plasticity model for beam-column elements, the effect of structural hysteretic behaviour and yielding is accounted for. Each beam-column element is constructed from a combination on a linear-elastic frame element and zero-length non-linear hysteretic torsional spring-dampers acting as connection elements. The hysteretic behaviour of the non-linear torsional spring-dampers is described by a smooth varying Bouc-Wen hysteretic model. Non-linearities due to P-delta effects are included through the use of a constant geometric stiffness matrix, which acts to reduce the structural lateral stiffness as a function of axial load. The multi-degree-of-freedom equations of motion are presented, and through the use of an augmented state vector to account for the hysteretic deflections, the state-space formulation developed. The chapter concluded with a brief description of how the simulation is implemented using the MATLAB ODE solver, ode15s – a variable order, multi-step solver for use with stiff differential equations.

The following chapter discusses the controllers implemented using the simulation model and system presented in this section. Control algorithms for five different types of controller are presented, along with a brief description of a base isolation hybrid semi active-passive system.

4. ACTUATOR ARCHITECTURE & CONTROL DESIGN

4.1 INTRODUCTION

This chapter describes the actuator architectures utilised in the structural control simulations, and focuses on the development of controller logic for the SAC3 and SAC9 buildings. Two types of actuators are investigated, MR dampers and resetable actuators, with the MR damper implemented using clipped quasi-bang-bang, LQR, LQRy, and JQR controller logic types. Although the use of clipped-optimal displacement regulation control algorithms has previously been investigated for semi-active control, their potential benefit has not been fully examined using non-linear structural modelling techniques, which introduce significant challenges and modifications to control design.

By investigating several types of control logic the objective is to compare the different characteristics of each controller, to assess their relative benefit in the reduction of structural demands. It should be noted that the use of percentage performance reductions is to facilitate these comparisons and not to show the absolute benefit of each controller. Controller performance is highly dependent on the choice of the maximum actuator forces, with high percentage demand reductions achievable as the maximum actuator forces grow comparable with the weight of the structure. Previous research into MR dampers applied to a linear model of the SAC20 structure, a five-bay 20-story building developed as part of the same project as the SAC3 and SAC9 structures used in this research, attained 22-56% reductions in maximum drifts [Dyke 1998]. Although this is a notable achievement which shows the potential of MR dampers, these reductions were achieved using 30 MR dampers, each with a maximum force of 200kips, resulting in total actuator forces corresponding to approximately 50% of the structural weight.

Semi-active controllers act as energy dissipaters, removing energy from the system as efficiently as possible, as determined by the control algorithm. If actuator forces are extremely large, the amount of energy that is dissipated by the actuator may become unrealistic for a limited capacity energy sink. In an attempt to ensure the practical applicability of the research, the total of the maximum actuator forces used in this research are limited to approximately 13% of the structural weight. In addition, this amount is held constant for all architectures and controllers for each building structure. Hence, the study of the impact of different architectures is independent of total actuator authority.

4.2 ACTUATOR ARCHITECTURE

A major objective of this research is to assess the effect of actuator placement on control benefit. This section presents the different actuator architectures used for the SAC3 and SAC9 building studies. Much of the previous research into actuator architecture has examined the effect of placing different numbers of actuators on each floor, for example one 1000kip actuator on the ground floor compared to 1000kip actuators on each floor [Breneman 2000, Dyke and Spencer 1996, Chase and Smith 1995(b), Reinhorn et al. 1989, Yang and Giannopolous 1978, Soong et al. 1991]. Percentage structural demand reduction comparisons between the two cases is largely unjustified as the architectures have different total actuator authority. In this investigation a uniform total control input force is maintained across each architecture, with the distribution of this total force between different floor levels used to represent different actuator architectures, allowing valid comparison of structural demand reduction. Hence, a very strict comparison of energy management efficacy is obtained as a function of actuator placement given a fixed actuator authority.

4.2.1 SAC3 Actuator Architecture

A maximum actuator force of 450kips was selected for control of the SAC3 building, representing 13.8% of the total building weight of 3255kips, which is distributed as shown in Table 3.1. The main control assessment was undertaken with actuators placed between the ground and first floors only, however, control architectures with actuators on the second and third floors were also investigated. The effect of different force distributions was initially assessed using only the high earthquake suite, with trends used to select the best architectures for further simulation under all three full earthquake suites. Figure 4.1 shows the three actuator architectures used, with the naming convection SAC3-A1, -A2, and -A3 representing actuators on the first floor, first and second floors, and all three floors, respectively.

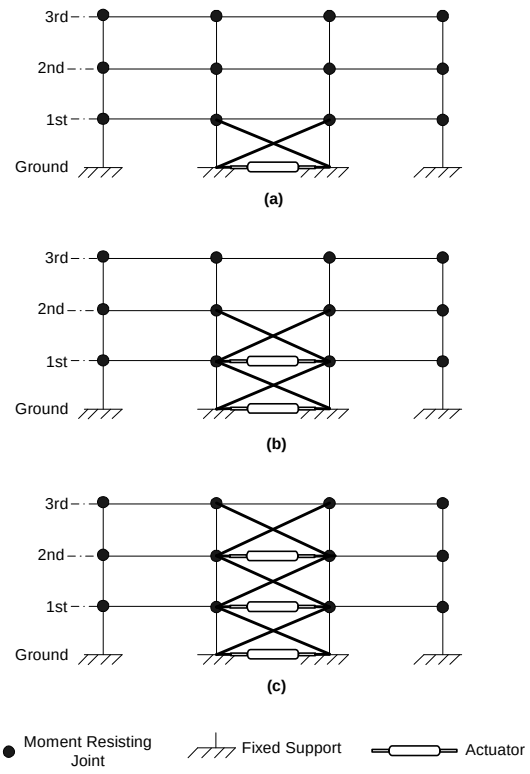

Figure 4.1: SAC3 actuator architectures: (a) SAC3-A1 (b) SAC3-A2 (c) SAC3-A3.

In addition to the distinction as to where actuators are located within the building, the distribution of the total 450kip actuator force is also specified. The actuator force distributions shown in Table 4.1 were selected to assess where the maximum control effort should be focused, and whether it is beneficial to spread the available actuator force over the full height of the structure, or lump it in one particular area. Note that the SAC3 tendon connections in Figure 4.1 are at an angle of 23 degrees. Hence, these peak actuator forces are reduced by cos(23)=0.92 as they are applied as lateral loads to the structure.

TABLE 4.1: SAC3 DISTRIBUTIONS OF MAXIMUM ACTUATOR FORCES.

	Maximum Actuator Force Distribution (kips)			
Architecture	**Floor 1**	**Floor 2**	**Floor 3**	**Total Force (kips)**
SAC3-A1-1	450	0	0	***450***
SAC3-A2-1	315	135	0	***450***
SAC3-A2-2	225	225	0	***450***
SAC3-A2-3	135	315	0	***450***
SAC3-A3-1	270	135	45	***450***
SAC3-A3-2	150	150	150	***450***
SAC3-A3-3	45	135	270	***450***

4.2.2 SAC9 Actuator Architecture

The distribution of actuators in tall structures is crucial, as poor placement of actuators can be detrimental to the dynamic response by changing the balance of structural modes in the response. To assess the effect of actuator architecture on the response of the SAC9 building, two different arrangements were used. Each architecture has all of the actuators placed on the ground floor of the structure, with tendons used to apply actuator authority to the required floors. Due to the large tendon angle that would result when attached to the top floor, an active tuned mass damped (ATMD) is placed on the roof of the building in an attempt to reduce top-whip, as is already implemented in some existing structures [Chase and Smith

1995(a), Housner et al. 1997]. This arrangement differs from that used for the SAC3 structure, and is necessary due to the impact of actuator-actuator interaction during the multi-mode response of the SAC9 structure, as is discussed in Section 6.3.1.

As shown in Figure 4.2(a), the first architecture, SAC9-A3, has tendons attached to the second and third stories only, with the soft first story retained, as discussed in Section 6.3.2. The SAC9-A8 architecture, shown in Figure 4.2(b), has tendons attached to floors 2 through 8, with an ATMD positioned on the roof. In both actuator architectures, the tendons span two horizontal bays, effectively reducing the application angle of the actuator forces. Practically, if installation of these long tendons is difficult due to structural members, it may be possible to install them into elevator shafts, which commonly extend through the centre of the building. These two architectures were selected primarily to determine whether it is necessary to have actuators attached to each floor when controlling tall buildings, of whether it is sufficient to use a combination of large actuator forces low in structure, and smaller forces applied to the top floor through an ATMD.

The maximum actuator force is set at 1500kips, which represents 13.6% of the structural weight of 10997kips. The distribution of the maximum actuator authority is shown in Table 4.2. It is important to note that the maximum actuator authority on each floor is in fact the force within the tendon, hence, actual lateral forces applied to the structure are reduced by the cosine of the tendon angle. For example, the force applied to the eighth floor is reduced by a factor of 0.48.

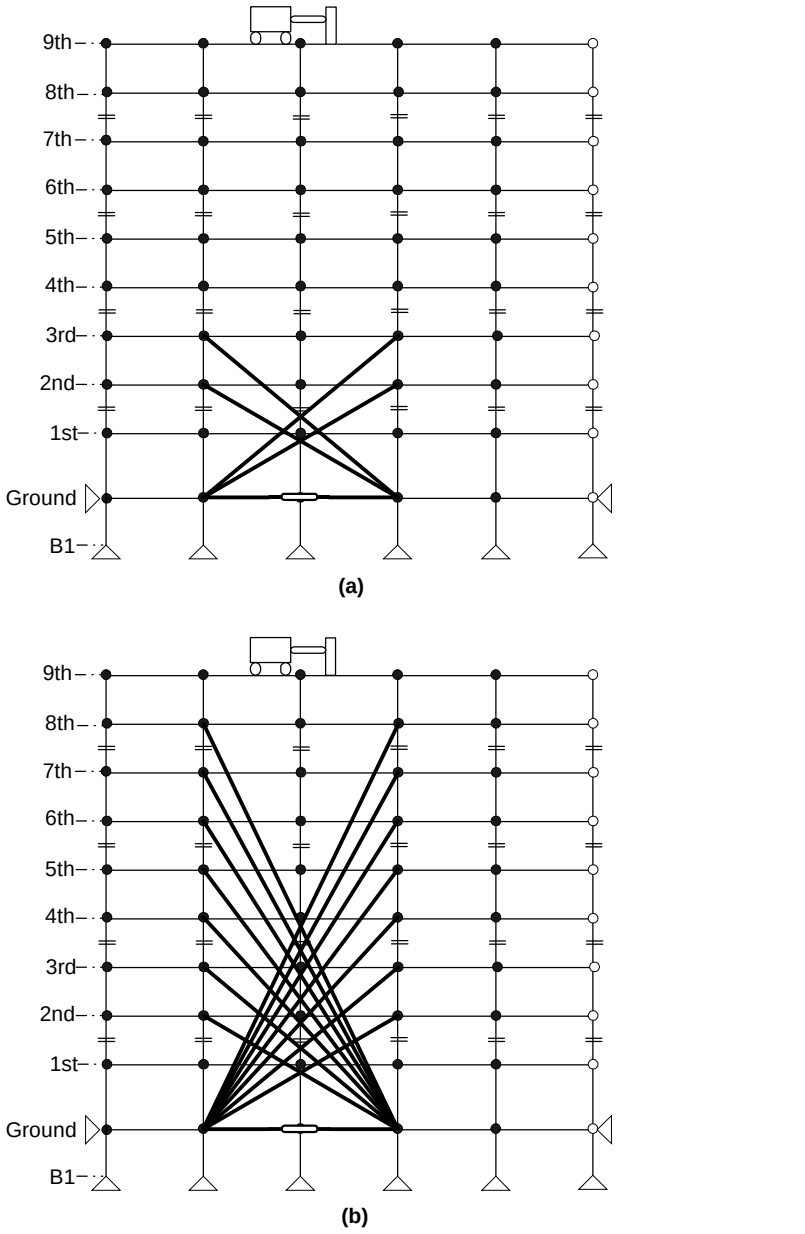

Figure 4.2: SAC9 actuator architectures: (a) SAC9-A3 (b) SAC9-A8.

TABLE 4.2: SAC9 DISTRIBUTIONS OF MAXIMUM ACTUATOR FORCES.

	Maximum Actuator Force Distribution (kips)									
Architecture	**Fl 1**	**Fl 2**	**Fl 3**	**Fl 4**	**Fl 5**	**Fl 6**	**Fl 7**	**Fl 8**	**Fl 9**	**Total Force (kips)**
SAC9-A3	0	750	550	0	0	0	0	0	200	***1500***
SAC9-A9	0	450	350	100	100	100	100	100	200	***1500***

4.3 MR DAMPER CLIPPED QUASI-BANG-BANG CONTROLLER

4.3.1 Introduction

Although MR dampers are a relatively new development in semi-active control, intensive research has been undertaken to develop models of their dynamic response. Through experimental testing of the 20-ton MR damper shown in Figure 1.2, it has been determined that the actuator achieves 95% of the commanded actuator force in approximately 60msecs [Yang et al. 2000(a)]. This finding implies that for full-scale MR dampers, their dynamic peak-to-peak response is in the order of 20Hz. As shown in Table 3.3, the dynamic response of the SAC3 and SAC9 structures are 0.98Hz and 0.44Hz respectively. Hence, the dynamic range of the structures is approximately 95% less than that of the full-scale MR dampers, meaning the dynamics of the actuator should not significantly affect the building response. For this reason, actuator dynamics were not included in the control algorithm or models, although control-structure interaction can be important if this gap is not sizable [Dyke et al. 1993].

The quasi-bang-bang control algorithm for the application of the MR dampers uses two distinct control laws depending on whether the building is moving towards, or away from, its static equilibrium, or rest, position that is the zero state for linear analysis and represents the permanent deflected state for non-linear analyses. The use of a two-stage control law is an effective method of representing the different MR damper characteristics that occur depending on whether power is supplied to the magnetic coil. The desired action of the MR damper at any time is that which acts to restore the structure to its equilibrium position. Hence, whenever the structure is moving away from its equilibrium position the MR damper is powered to apply a strong resisting force. This logic is schematically represented in Figure 4.3, with power supplied to the MR damper for cases (a) and (b) only, when the product of

displacement and velocity is greater than zero. When the structure is moving back towards its equilibrium position, as in cases (c) and (d) of Figure 4.3, the MR damper acts as a passive fluid damper with a two stage damping force accounting for its hysteretic nature. The displacement and velocity values used in the control law are extracted from the full state vector for the lateral degrees-of-freedom to which each actuator is attached, so the control law is completely decentralised.

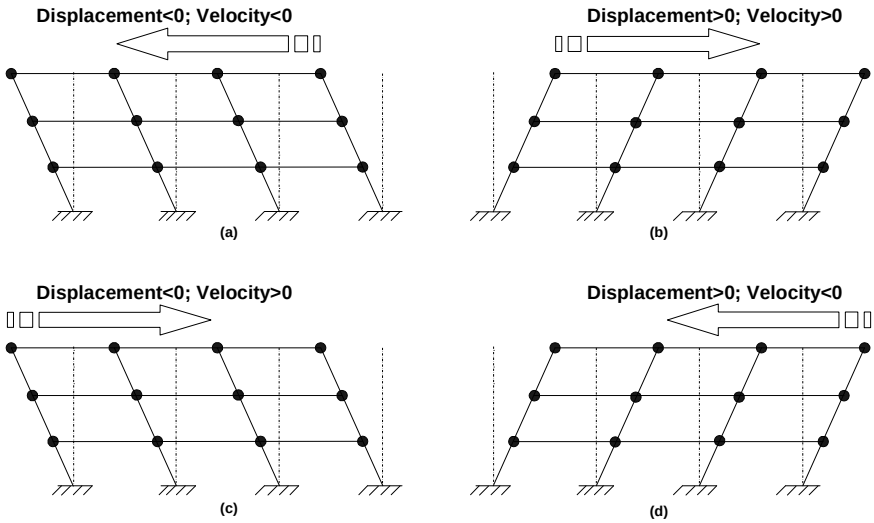

Figure 4.3: Schematic showing possible combinations of structural displacement and velocity used for MR damper quasi-bang-bang controller.

4.3.2 Moving-Zero Definition

As the actuator force is dependent on the floor displacements relative to the equilibrium position of the structure, the definition of the equilibrium point is important. When using a linear structural model, as has been done in previous semi-active controller investigations, the equilibrium point is clearly the original building position, as the model does not account for permanent deformations. However, when a memory of non-linear structural damage is included in the model, the permanent deformations that result from strong motions lead to an equilibrium position that changes with time.

The decision to restore the structure back to its yielded, rather than original, position is based on the structural damage that is likely to result as well as the lack of significant force. Through the use of much larger actuator forces it may be possible to re-yield the structure back to its original position, resulting in an apparent improvement in performance through decreased permanent drift. When a beam-column joint is damaged through large joint rotations, the flexibility of the joint is increased dramatically. Hence, if large actuator forces act to restore the building back to its un-yielded position, the decreased structural stiffness can result in very large structural deformations and more extreme structural damage.

The time-varying equilibrium point, called the moving-zero hereafter, is obtained using a moving average of floor displacements. At each time step in the iteration process, a new displacement value is added to a column vector which is then averaged to provide a low-pass filtered mean displacement. It was determined that a vector 200 displacement values in length provides a moving-zero that is sufficiently insensitive to transient peaks while still providing adequate tracking with acceptable lag. An example of the moving-zero tracking is shown in Figure 4.4 for the uncontrolled SAC3 first floor drift subject to the Elysian Park earthquake, where the bold line represents the time-varying equilibrium point. Displacement values used in the control law are then computed relative to the instantaneous moving-zero value for the relevant lateral degrees-of-freedom, rather than to the absolute zero.

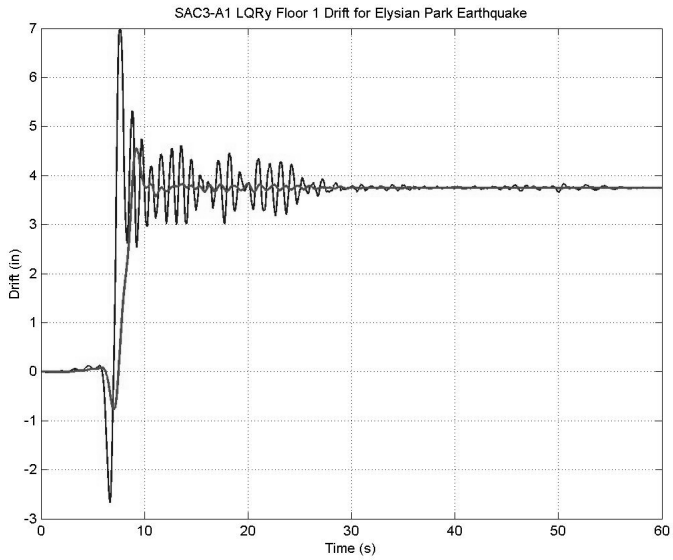

Figure 4.4: Example of time-varying equilibrium tracking for the SAC3 LQRy controlled floor 1 drift – Elysian Park earthquake.

4.3.3 Dead-band Definition

When floor displacements or velocities are close to the moving-zero it is undesirable for the controller to apply moderate or large control forces, as this can increase the duration of the structural response and is sensitivity to sensor noise and jitter. Although the two-stage control force is proportional to either displacement or velocity depending on the motion of the building, the effective bandwidth of the control law produces actuator forces at near-zero displacements or velocities that are larger than desired, as it is necessary to have forces with sufficient magnitude at larger displacements and velocities. Rather than lose actuator performance during maximum demand, displacement and velocity dead-bands were introduced. By carefully examining the performance of the control law, the limits of the dead-bands were selected to minimise the undesirable control forces during small motions, while also minimising the actuator idle time when control forces are beneficial. Hence, when either the displacement or velocity is below the dead-band limits, the control force is set to zero.

4.3.4 Control Law Description

The quasi-bang-bang control method uses a two-stage control force that is dependant on the motion of the building, as discussed in Section 4.3.1. A diagram showing the basic stages in the control law is shown in Figure 4.5. Information relating to the placement of the actuators, which is defined outside the time-history analysis, is used in the control law to map the transformed control forces to the appropriate lateral degrees of freedom, accounting for the tendon angle. At each time step in the time-history analysis the moving-zero low-pass filter is recalculated using the appropriate instantaneous displacement values, and the lateral displacement and velocity values for each controlled floor are extracted from the state vector. A check is then made to determine if the displacement or velocity values lie inside the dead-band, in which case the control force is set to zero. The direction of building motion is then determined using the product of displacement and velocity, and a selection of whether to use the active or passive control mode is made.

The distinction between using either a semi-active resistance control force, u_{sa}, or a passive fluid damping force, u_d, is shown in Equation (4.1):

$$u_i(t) = \begin{cases} u_{sa} & \text{(if moving away from centre)} \\ u_d & \text{(if moving towards centre)} \end{cases} \tag{4.1}$$

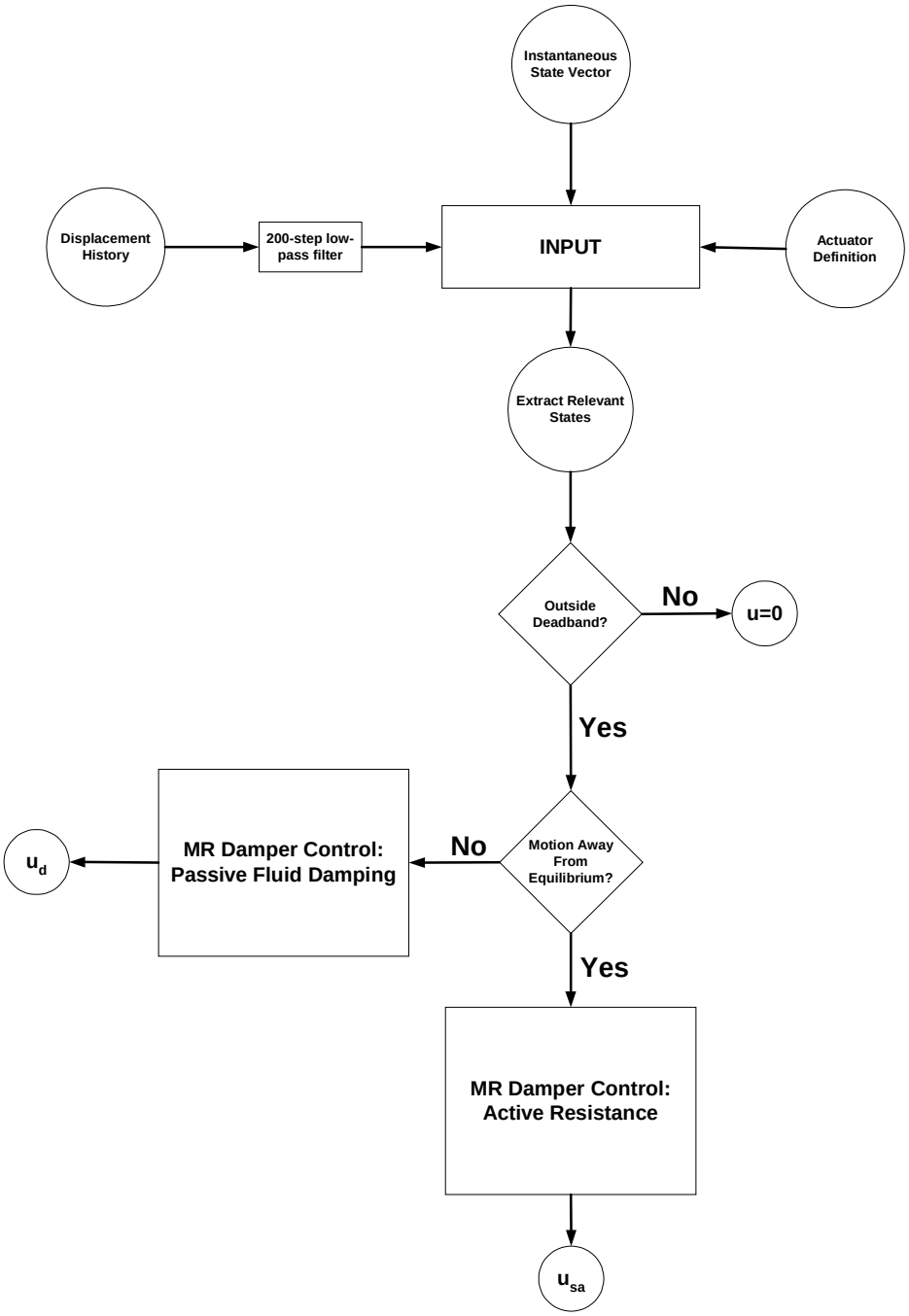

Figure 4.5: Schematic of MR damper quasi-bang-bang control law for a single actuator.

The active resistance force is essentially proportional control, with an additional step in the control logic to account for actuator saturation. Actuator saturation limits the total control force to approximately 13% of the building weight, and is necessary to ensure controller effort is limited within practical bounds. The active resistance control force is given as:

$$u_{sa} = \begin{cases} -\dfrac{F_{max}}{v_{max}} v & (\text{if } u_{sa} < F_{max}) \\ -F_{max}\,\mathrm{sgn}(v) & (\text{if } u_{sa} > F_{max}) \end{cases} \tag{4.2}$$

where F_{max} is the actuator saturation force, v_{max} is the floor displacement at which maximum control force is desirable, v is the floor displacement relative to the moving-zero obtained from the low-pass filter moving average, and sgn() is the sign of the internal variable. The value of v_{max} is a constant value for each floor, and is determined from observations of the uncontrolled structural response over a range of earthquake magnitudes, with a value selected to, on average, provide maximum actuator forces during the strong motion of the earthquakes. This approach provides linear proportional feedback over a limited range beyond the dead-band to minimise impulse inputs to the structure that can excite higher modes or cause local damage.

When power is not supplied to the MR damper it performs as a passive fluid damper – an advantageous feature should power fail during a seismic event. A two-stage damping force was implemented to represent the hysteresis that is apparent in experimental damping curves, modelling the hysteresis as a bi-linear relationship. The velocity at the bi-linear transition was selected from experimental damping plots that were scaled to represent a 20-ton MR damper using the ratio of saturation forces [Dyke et al. 1996]. The passive damping control force law is then defined:

$$u_d = \begin{cases} -\xi \dfrac{F_{max}}{\dot{v}_{max}} \dot{v} & (\text{if } \dot{v} < \dot{v}_{max}) \\ -\xi F_{max}\,\mathrm{sgn}(\dot{v}) & (\text{if } \dot{v} > \dot{v}_{max}) \end{cases} \tag{4.3}$$

where $\dot{v}_{max}$ is the bi-linear transition velocity, $\dot{v}$ is the floor velocity, F_{max} is as previously defined, and ξ is the damping saturation force proportion. From experimental investigations in which the MR damper was run in both passive and semi-active modes, it is apparent that the maximum passive force is approximately 25% of the maximum semi-active force, hence $\xi = 0.25$ [Dyke and Spencer 1996, Dyke et al. 1996].

4.4 LQR CLIPPED OPTIMAL CONTROLLER

The linear quadratic regulator (LQR) control design system is a well known method of optimal control, and is used in this investigation to develop clipped optimal controllers for use with MR damper semi-active actuators. A primary benefit of the LQR controller is the guaranteed stability that results from the solution of the Algebraic Riccati Equation (ARE) to determine the optimal state feedback gains. Although the LQR design method is primarily for use with linear systems, the structural response of the SAC3 and SAC9 buildings is not highly non-linear and LQR is often employed for structural control applications. Hence, it is studied here to determine the efficacy of this approach for this type of system model.

The LQR control design essentially seeks to find the optimal trade-off between performance and control cost, with weighting values used to define their relative importance. For multi-input multi-output (MIMO) systems, the LQR controller determines the control output which minimises the cost function:

$$J = \int_0^\infty (\mathbf{x}^T(t)\mathbf{Q}\mathbf{x}(t) + \mathbf{u}^T(t)\mathbf{R}\mathbf{u}(t))dt \qquad (4.4)$$

where **x**(t) is the linear state vector, **Q** is a real symmetric positive semi-definite matrix containing the weighting factors for structural performance measures, **u**(t) is a vector of control inputs, and **R** is a real symmetric positive definite matrix containing weighting factors relating to the cost of control effort. For most applications, **Q** and **R** are diagonal, weighting only autocorrelations of the states and control inputs, and not the cross correlation terms. Hence, this cost function is a sum of squared weighted L_2-norms of states and control inputs. The state feedback control output is defined as:

$$\mathbf{u}(t) = -\mathbf{K}\mathbf{x}(t) \tag{4.5}$$

where **K** is the state feedback gain matrix obtained from the LQR control solution, with **u**(t) and **x**(t) as previously defined.

The LQR control design was undertaken using the MATLAB control toolbox, with a lumped mass reduced state model of each structure. The use of a lumped mass model, in which the structure is represented by its lateral degrees of freedom only, is an appropriate simplification as it is the global structural response that is of interest, with assessment of structural performance based primarily on transient and permanent relative lateral displacements. The modal properties of the linear lumped mass models were adjusted as necessary to ensure a close match with those of the full model. Following the formation of the reduced model mass, stiffness, and damping matrices, the reduced actuator force mapping vector was obtained, with the appropriate degrees-of-freedom multiplied by their relative proportion of the total maximum force in order to obtain gains in the correct proportions for each actuator saturation level. The effect of these relative force proportion factors on the gain magnitudes was removed through re-multiplication of the final state feedback gain matrix by the relevant

proportions. This approach to design is necessary when considering variable actuator saturation levels, and represents a new approach to LQR designs for civil structural control.

The primary difficulty with using optimal control techniques is in the selection of the appropriate weighting factors to give the best performance attainable for the available control effort. An iterative process was used, with weighting factors adjusted until the control force magnitudes gave sufficient actuator saturation during strong structural motions but not during smaller transient cases. As building damage is commonly assessed using floor drifts, the weighting of displacements in the state vector were set higher than the velocity performance weightings. Hence, the LQR designs are heavily weighted toward displacement reduction.

The LQR control law for the force in the i^{th} actuator is defined:

$$u_i = \begin{cases} -\mathbf{K}_{LQR}(i,:)\mathbf{v}_{temp} & (\text{if } u_i < F_{imax}) \\ -F_{imax}\,\text{sgn}(v_i) & (\text{if } u_i > F_{imax}) \end{cases} \tag{4.6}$$

where $\mathbf{K}_{LQR}(i,:)$ is the i^{th} row of the matrix optimal gains, $\mathbf{v}_{temp}$ is the reduced state vector containing displacements and velocities of the lateral degrees-of-freedom for that moment in time, F_{imax} is the i^{th} actuator saturation force, and v_i is the displacement of the floor to which the i^{th} actuator is attached, relative to the moving-zero discussed in Section 4.3.2. Note that the control force is applied to the floor above the actuator by tendons, as shown in Figures 4.1 and 4.2. Hence, the floor below, to which the actuator is attached, has an equal and opposite reaction load.

4.5 LQRY CLIPPED OPTIMAL CONTROLLER

The LQRy control design method is a linear optimal control method that is very similar to the LQR method, hence much of the discussion in Section 4.4 is applicable to LQRy design. Rather than applying performance weightings to the linear state vector, the LQRy design method allows the application of performance weightings on the user-defined output vector **y**(t). The LQRy cost function, for which control outputs are designed to minimise, is defined as:

$$J = \int_0^\infty (\mathbf{y}^T(t)\mathbf{Q}\mathbf{y}(t) + \mathbf{u}^T(t)\mathbf{R}\mathbf{u}(t))dt \tag{4.7}$$

where **y**(t) is the desired weighted output, and all other variables are as previously defined. This approach is used to control the total lateral accelerations of the structure since these accelerations are also associated with internal damage and occupant safety. This approach is particularly important for structures with a strong occupant safety requirement.

As it is the effect of acceleration control that is under investigation, **y**(t) is defined as:

$$\mathbf{y}(t) = \mathbf{C}_1\mathbf{x}(t) = [-\mathbf{M}^{-1}\mathbf{K} \quad -\mathbf{M}^{-1}\mathbf{C}]\mathbf{x}(t) \tag{4.8}$$

where all variables are as previously defined. Hence, using a linear version of Equation (3.11), it can be seen that the weighted output, **y**(t), is the total acceleration of each floor, including the acceleration due to ground excitation and control force:

$$\mathbf{y}(t) = \ddot{\mathbf{v}}(t) + \mathbf{S}_g\ddot{\mathbf{x}}_g(t) - \mathbf{M}^{-1}\mathbf{S}_{act}\mathbf{F}_{act}(t) = \mathbf{C}_1\mathbf{x}(t) \tag{4.9}$$

where $\ddot{\mathbf{v}}$ is the absolute floor acceleration relative to the ground, with all other variables defined previously.

As with the LQR design, state feedback gains were obtained using the MATLAB control toolbox with a linear lumped mass reduced order structural model. The performance and control cost weighting factors, Q_{ij} and R_{ij} respectively, were the same for each floor, and were selected using a performance-based iterative process.

The LQRy control law for the force in the i^{th} actuator is summarised:

$$u_i = \begin{cases} -\mathbf{K}_{LQRy}(i,:)\mathbf{v}_{temp} & (\text{if } u_i < F_{imax}) \\ -F_{imax}\,\text{sgn}(v_i) & (\text{if } u_i > F_{imax}) \end{cases} \tag{4.10}$$

where $\mathbf{K}_{LQRy}$ is the i^{th} row of the optimal state feedback gain matrix, $\mathbf{v}_{temp}$ is a reduced state vector containing displacements and velocities of the lateral degrees-of-freedom, F_{imax} is the i^{th} actuator saturation force, and v_i is the displacement of the floor to which the i^{th} actuator is attached, relative to the moving-zero discussed in Section 4.3.2. It should be noted that although the selection of gains is based on the minimisation of accelerations, the gains that are obtained are still multiplied by the linear state vector, $\mathbf{v}_{temp}$.

4.6 RESETABLE ACTUATOR CONTROLLER

4.6.1 Introduction

Resetable actuators are essentially hydraulic spring elements in which the un-stretched spring length can be reset to obtain maximum energy dissipation from the structural system. Figure 4.6 shows a schematic of a resetable actuator attached to a one degree-of-freedom spring-

mass system, where k_o is the structural stiffness and the attached mass is the structural mass. With the actuator value closed, as the actuator is either compressed or extended, energy is stored within the actuator's bi-directional piston-cylinder arrangement. At the point when the energy storage rate is stationary, the valve between the two cylinder halves is opened and then re-closed, rapidly releasing the energy from the system before it is returned to the structure. The range of attainable resetable actuator spring stiffness is extensive, with stiffness dependent on the piston area, piston stroke, and hydraulic fluid bulk modulus. As an example, an actuator with a piston area of 2 in^2, a stroke of 4 in, and a fluid with a bulk modulus of 250,000psi, which is typical for hydraulic fluids, would have a stiffness of 500,000lb/in. Hence, attainable actuator stiffness is not a significant limit of the control design space.

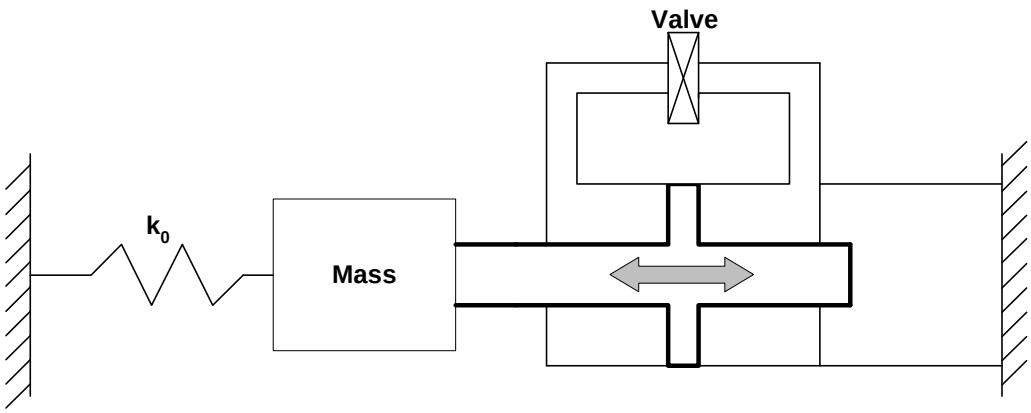

Figure 4.6: Schematic of a resetable actuator attached to a 1 DOF system.

Although full-scale resetable actuators have yet to be developed, testing on existing actuators has found that the reset time is approximately 20msecs, implying structures with natural frequencies up to about 20 Hz may be effectively controlled [Bobrow et al. 2000, Jabbari and Bobrow 2002]. Both the SAC3 and SAC9 structures fall well within this controllable frequency band as shown in Table 3.3. As the energy stored within the actuator is dissipated

as heat, success of full-scale implementation will be primarily dependent on the available size of the energy sink. Without data from full-scale actuator testing available, the actuator force limit of approximately 13% of the building weight is explicit recognition of this limitation.

4.6.2 Control Law Description

The control law for the resetable actuator is dependent on the rate of energy storage, with the free length of the hydraulic spring reset when the energy storage is maximised. The energy in a single actuator, U_{act}, is given by:

$$U_{act} = \frac{1}{2} K_{act} (v - v_o)^2 \tag{4.11}$$

where v is the relative displacement of the actuator ends, v_o is the free length of the hydraulic spring which is at the last reset position, and K_{act} is the effective spring stiffness. As the idea of the control law is to remove energy from the structural system as quickly as possible, the control law waits until the energy in the hydraulic spring is maximised, thus dissipating maximum packets of energy before re-applying the control force. Discarding maximum packets of energy is advantageous, as it then minimises the actuator valve-open time during which the actuator applies no control force to the structure. Taking the time derivative of Equation (4.11), the rate of change of energy is given as:

$$\dot{U}_{act} = K_{act} \dot{v}(v - v_o) \tag{4.12}$$

where $\dot{v}$ is the relative velocity of the actuator ends, and other variables are as defined for Equation (4.11). From Equation (4.12) the control logic can be clearly seen, as the energy

stored in the actuator is stationary when $\dot{U}_{act} = 0$, giving the trivial case of minimum energy storage when $(v - v_o) = 0$, and maximum energy storage when $\dot{v} = 0$. This recognition of simple energy principles gives an effective method of determining the ideal time for energy dissipation, as defined:

$$\text{Set } v_o = v \text{ whenever } \dot{v} = 0 \tag{4.13}$$

where v_o is the free length of the hydraulic spring, v is the relative displacement between the actuator ends, and $\dot{v}$ is relative velocity of the actuator ends. As it is unlikely that the relative velocity will exactly equal zero at the iteration time step, a more robust method of detection is required. As the sign of the velocity values at time steps before and after the stationary point will be different, a simple sign comparison will effectively detect the stationary point, with the introduction of an insignificant maximum lag of one time step. The control law shown in Equation (4.13) may now be rewritten as:

$$\text{Set } v_o = v \text{ whenever } \text{sgn}(\dot{v}_t) \neq \text{sgn}(\dot{v}_{t-1}) \tag{4.14}$$

where the subscripts (t) and (t-1) represent current and previous time steps respectively.

The control force applied to the structure for a single actuator, u_i, is then simply that of a displaced spring with the additional logic incorporating actuator saturation:

$$u_i = \begin{cases} -K_{iact}(v_i - v_{io}) & (\text{if } u_i < F_{imax}) \\ -F_{imax}\,\text{sgn}(v_i - v_{io}) & (\text{if } u_i > F_{imax}) \end{cases} \tag{4.15}$$

It should be noted that the displacement of the i^{th} actuator, v_i, is measured relative to the time-varying dynamic equilibrium point. As discussed in Section 4.3.2, the inclusion of the structure's yielded position during strong motions reduces the likelihood of the actuator forces attempting to re-yield the structure back to its original static position, which would result in increased structural damage.

4.7 JQR CLIPPED OPTIMAL CONTROLLER

The design and implementation of the JQR clipped optimal controller is similar to the LQRy optimal control method, however the focus is reduction in total structural jerk. Structural jerk is the time derivative of the structural acceleration, and may be closely related to the damage to people and equipment within a building subjected to seismic events. The cost function, for which the state feedback gains are designed to minimise, is the same on used for the LQRy methods:

$$J = \int_0^\infty (\mathbf{y}^T(t)\mathbf{Q}\mathbf{y}(t) + \mathbf{u}^T(t)\mathbf{R}\mathbf{u}(t))dt \tag{4.16}$$

where each variable is as defined for Equation (4.7). The vector of weighted outputs, $\mathbf{y}(t)$, for the JQR controller is defined:

$$\mathbf{y}(t) = \mathbf{C}_1 \dot{\mathbf{x}}(t) = [-\mathbf{M}^{-1}\mathbf{K} \quad -\mathbf{M}^{-1}\mathbf{C}]\dot{\mathbf{x}}(t) \tag{4.17}$$

Using a linear version of Equation (3.11), it can be seen that the weighted output, $\mathbf{y}(t)$, is the total structural jerk of each floor, including the jerk due to ground excitation and control forces:

$$\mathbf{y}(t) = \dddot{\mathbf{v}}(t) + \mathbf{S}_g \dddot{\mathbf{x}}_g(t) - \mathbf{M}^{-1}\mathbf{S}_{act}\dot{\mathbf{F}}_{act}(t) \tag{4.18}$$

where $\dddot{v}(t)$ is a vector of floor jerks relative to the ground, $\dddot{\mathbf{x}}_g(t)$ is the jerk of the earthquake motion, $\mathbf{M}$ is the structural mass matrix, $\dot{\mathbf{F}}_{act}(t)$ is the time derivative of the actuator force, and $\mathbf{S_g}$ and $\mathbf{S_{act}}$ are vectors mapping earthquake and actuators forces to the appropriate lateral degrees of freedom, respectively.

A penalised Lyapunov function, V(x,u), can be determined as the sum of a quadratic Lyapunov function and the cost function, J:

$$V(\mathbf{x},\mathbf{u}) = \mathbf{x}^T\mathbf{P}\mathbf{x} + \int_0^\infty (\mathbf{y}^T(t)\mathbf{Q}\mathbf{y}(t) + \mathbf{u}^T(t)\mathbf{R}\mathbf{u}(t))dt \tag{4.19}$$

where $\mathbf{x}$ is the linear state vector, $\mathbf{P}$ is a symmetric positive definite matrix, and the other variables are as defined previously. For guaranteed system stability and optimality, the derivative of this Lyapunov function must be less than zero for all time. Using the transient system definition with no external input, $\dot{\mathbf{x}} = \mathbf{A}\mathbf{x} + \mathbf{B_1}\mathbf{u}$, and state feedback, it can be shown that for the optimal case:

$$\overline{\mathbf{A}}^T\mathbf{P} + \mathbf{P}\overline{\mathbf{A}} - \mathbf{P}\mathbf{B_1}\overline{\mathbf{R}}^{-1}\mathbf{B_1}^T\mathbf{P} + \overline{\mathbf{Q}} = 0 \tag{4.20}$$

where:

$$\overline{\mathbf{R}} = \mathbf{B}_1^T\mathbf{C}_1^T\mathbf{Q}\mathbf{C}_1\mathbf{B}_1 + \mathbf{R}$$
$$\overline{\mathbf{Q}} = \mathbf{A}^T\mathbf{C}_1^T\mathbf{Q}\mathbf{C}_1\mathbf{A}$$
$$\overline{\mathbf{M}} = \mathbf{B}_1\overline{\mathbf{R}}^{-1}\mathbf{B}_1^T\mathbf{C}_1^T\mathbf{A}\mathbf{C}_1$$
$$\overline{\mathbf{A}} = (\mathbf{I} - \overline{\mathbf{M}})\mathbf{A}$$
$$\mathbf{u} = -\overline{\mathbf{R}}^{-1}\mathbf{B}_1^T\mathbf{P}\mathbf{x} = -\mathbf{K}\mathbf{x}$$

Equations (4.20) are developed by taking the derivative of Equation (4.19) with optimality as the condition where $\dot{V} = 0$. Note that if we rewrite Equation (4.19) as $V(\mathbf{x}, \mathbf{u}) = \bar{v} + J$, where $\bar{\mathbf{v}} = \mathbf{x}^T\mathbf{P}\mathbf{x}$ is the quadratic Lyapunov function, and taking the time derivative assuming zero initial and final conditions, we obtain:

$$\dot{V}(\mathbf{x}, \mathbf{u}) = \dot{\bar{v}} + \dot{J} = \dot{\bar{v}} + (\mathbf{y}^T\mathbf{Q}y + \mathbf{u}^T\mathbf{R}\mathbf{u}) \tag{4.21}$$

As $\dot{J}$ is a quadratic function, it is positive for all time. This result implies that if $\dot{V} < 0$ and $\dot{J} > 0$ for all time, then $\dot{\bar{v}} < -\dot{J} < 0$, proving that the controlled system is quadratically stable. In addition, a reasonably minimal solution for J is obtained simultaneously. It should be noted that this formulation is basic and could be augmented using more advanced optimisation theory to provide a potentially larger feasible region and design space.

As with the LQRy design, state feedback gains were obtained using the MATLAB control toolbox with a linear lumped mass reduced order structural model. The performance and control cost weighting factors, Q_{ij} and R_{ij} respectively, were the same for each floor, and were selected using a performance-based iterative process. This approach weights the structural jerk on each floor equally.

The JQR control law for the force in a single actuator is defined:

$$u_i = \begin{cases} -\mathbf{K}_{JQR}(i,:)\mathbf{v}_{temp} & (\text{if } u_i < F_{imax}) \\ -F_{imax}\,\text{sgn}(v_i) & (\text{if } u_i > F_{imax}) \end{cases} \tag{4.22}$$

where $\mathbf{K}_{JQR}$ is the i^{th} row of the optimal state feedback gain matrix, $\mathbf{v}_{temp}$ is a reduced state vector containing displacements and velocities of the lateral degrees-of-freedom, F_{imax} is the i^{th} actuator saturation force, and v_i is the displacement of the floor to which the actuator is attached, relative to the moving-zero discussed in Section 4.3.2.

As the effect of the control law is to smooth accelerations to reduce the structural jerk, floor drifts may actually increase. To avoid the control law applying undesirable forces during small motions, displacement and velocity dead-bands were included, as described in Section 4.3.3. It should be noted that although the selection of gains is based on the minimisation of structural jerk, the gains that are obtained are still multiplied by the linear state vector, $\mathbf{v}_{temp}$, as the feedback quantities are displacement and velocity.

4.8 BASE ISOLATION HYBRID CONTROLLER

Hybrid control systems are seen as an effective method of combining the advantages of passive and semi-active controllers, while minimising their disadvantages. In this section a brief overview of the development of a basic passive base isolation system for the SAC3 building is presented, with response of a base-isolated MR damper hybrid control system detailed in Chapter 5. Rather than an in-depth study into the development of hybrid controllers for structural applications, hybrid control is presented as a simple example of the effectiveness of using semi-active systems to augment passive methods.

Base isolation systems act to reduce the seismic response of structures by shifting the fundamental frequency of the structure to a value lower than the main seismic excitation frequencies. Base isolators offer an effective method of control when assessing occupant safety, however, they are ineffective at reducing peak structural response and may in fact

increase structural damage in tall, slender buildings if used as the sole control method during near-field excitations [Kageyama and Yuzuru 1990]. As base isolation systems are designed to attenuate response over a specific small frequency range, their application in tall, multi-mode structures subjected to a large range of excitation levels is extremely limited. In addition, base isolation is practicable primarily for short-squat structures with aspect ratios less than 1.0 [Kelly 1986]. Hence, it is appropriate for the SAC3 building but not for the SAC9 structure.

Passive base isolation is incorporated into the time history analysis by employing it as a pre-filter of the ground excitation records. The pre-filtering method allows the code designed for the solution of semi-active controllers to be used in its original form, with the filter design undertaken outside the time history analyse using Simulink. A schematic of the structural system with the addition of the base isolation is shown in Figure 4.7, where M_b is the total structural mass of the building, k_b and c_b are the effective fundamental mode stiffness and damping of the building respectively, M_f is the approximated mass of the foundation set at 5% of the building weight, and k_f and c_f are the designed stiffness and damping of the base isolator respectively. It can be clearly seen that the original seismic excitation, $\ddot{x}_g$, is filtered by the base isolator so that the building then sees the filtered excitation, $\ddot{x}_f$. The performance of this filtering is a function of how effectively the foundation and fundamental building modes are decoupled. With good isolation, the structural control system has a significantly reduced "ground" motion excitation to manage. It is emphasised that this isolator design method does not consider the multi-mode response of the building, and is hence designed for a first mode response of the SAC3 building – a squat shear-building with a predominantly first mode response.

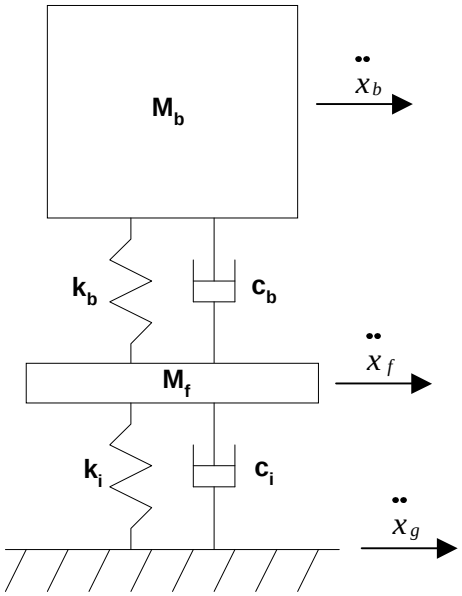

Figure 4.7: Schematic of base isolation and structural system.

The base isolator alters the response of the building by introducing an additional lower fundamental mode to the isolator-building system. The effect of this new isolated fundamental mode is to dramatically reduce the magnitude of the building's fundamental frequency. New fundamental frequencies of 0.26Hz and 0.51Hz, which represent 4:1 and 2:1 reductions in fundamental frequency respectively, were investigated. However, the 2:1 reduction was found to excessively increase the peak excitation acceleration for the Loma Prieta and Elysian Park earthquake records for linear simulations. Hence, the 4:1 reduction system was used in the hybrid control implementation.

4.9 CHAPTER SUMMARY

This chapter has presented the actuator architectures and control laws used for the SAC3 and SAC9 buildings. Previous investigations into the application of semi-active controllers have used peak actuator forces in excess of 50% of the building weight, however, to retain the practical applicability of this research, total actuator authority is limited to approximately 13% of the building weight for both the MR and resetable actuators. It should be noted that

clipping of the actuator force occurs prior to force mapping and horizontal transformation, hence the actual peak lateral forces applied to the structure are dependent on the actuator angle, but are typically reduced by 10-20%. Therefore, the effective lateral force applied to the structure is limited to approximately 11% of total building weight.

Three different actuator architectures are used for the SAC3 building, with actuators placed on the first, first and second, and on all three floors. These three architectures allow assessment of the effect of actuator placement on the response of a squat shear-building. Due to the interaction of actuators on adjacent floors during the multi-mode response of the SAC9 structure, actuators were positioned on the ground floor, with actuator forces applied to higher stories through diagonal tendons. In addition, an ATMD is placed on floor 9 to control the effects of top-whip. Two actuator architectures were investigated for the SAC9 building, with the SAC9-A3 architecture applying actuator authority to floors 2, 3, and 9, while the SAC9-A8 architecture applies authority to floors 2 through 9. In both architectures, the soft first story is not directly controlled, retaining the isolation properties for which it was designed.

Following the description of the actuator architectures, the clipped quasi-bang-bang controller for the MR damper was presented. It has been determined from previous experimental investigations that a MR damper can achieve 95% of its commanded actuator force in approximately 60msecs. This dynamic response on the order of 20Hz is much higher than that for the SAC3 and SAC9 buildings, and as a result, the MR damper model does not include actuator dynamics. The inclusion of a low-pass filtered moving-zero for each displacement measure of interest and force dead bands was presented, with the moving-zero a key part of ensuring a stable response when models account for significant hysteresis and permanent deformation. The two-stage actuator law was presented, with active resistance applied to the structure when its motion is away from the equilibrium point, and passive fluid

damping when the motion is towards equilibrium. A two-stage fluid damping force that is dependent on the velocity of the structure was established using scaled experimental data, effectively modelling the hysteretic behaviour of the MR damper. The control logic for the clipped quasi-bang-bang MR controller is summarised:

$$
\begin{aligned}
u_i(t) &= \begin{cases} u_{sa} & \text{(if moving away from centre)} \\ u_d & \text{(if moving towards centre)} \end{cases} \\
u_{sa} &= \begin{cases} -\dfrac{F_{max}}{v_{max}} v & \text{(if } u_{sa} < F_{max}\text{)} \\ -F_{max}\,\mathrm{sgn}(v) & \text{(if } u_{sa} > F_{max}\text{)} \end{cases} \\
u_d &= \begin{cases} -\xi \dfrac{F_{max}}{\dot{v}_{max}} \dot{v} & \text{(if } \dot{v} < \dot{v}_{max}\text{)} \\ -\xi F_{max}\,\mathrm{sgn}(\dot{v}) & \text{(if } \dot{v} > \dot{v}_{max}\text{)} \end{cases}
\end{aligned}
\qquad (4.23)
$$

where u_{sa} is the active resistance force, u_d is the passive fluid damping force, and other variables are as previously defined.

Three types of linear optimal control design were presented, LQR, LQRy, and JQR. Each of these control types determines an optimal state feedback gain to minimise a cost function, with weighting factors used to differentiate between the cost of control and the value of performance. The difference between the three controllers is the metric used to measure performance. In the LQR controller, displacements and velocity are used as performance measures with heavy emphasis on displacement, whereas structural accelerations and jerks are the focus in the LQRy and JQR controllers, respectively. Although the form of the cost function is different for each of the control types, the implementation of the control law is the same and is summarised for the i^{th} actuator:

$$u_i = \begin{cases} -\mathbf{K}_{gains}(i,:)\mathbf{v}_{temp} & (\text{if } u_i < F_{imax}) \\ -F_{imax}\,\text{sgn}(v_i) & (\text{if } u_i > F_{imax}) \end{cases} \tag{4.24}$$

where $\mathbf{K}_{gains}(i,:)$ represents the i^{th} row of the state feedback gain matrix which is obtained from either the LQR, LQRy, or JQR control design methods, and other variables are as previously defined. The lateral displacements obtained from the state vector are set relative to the moving-zero before being used in the control law. Each of these controllers are designed using reduced order lateral shear building models and implemented on the full model using only those measurements.

Resetable actuators are essentially hydraulic spring elements in which the un-stretched spring length can be reset to obtain maximum energy dissipation from the structural system. In order to maximise the energy dissipation from the system, the control law resets the actuator at the point when the energy storage is maximised, thus dissipating the stored energy before it is returned to the structure. Energy storage is maximised when the relative velocity of the actuator ends is zero, hence the control law is summarised:

$$\text{Set } v_o = v \text{ whenever } \dot{v} = 0 \tag{4.25}$$

To allow reliable detection of the stationary energy point, the control law in Equation (4.25) may be re-written into an equivalent statement using the change in the sign of the velocity at the stationary point, as shown in Equation (4.26).

$$\text{Set } v_{io} = v_i \text{ whenever } \operatorname{sgn}(\dot{v}_t) \neq \operatorname{sgn}(\dot{v}_{t-1})$$

$$u_i = \begin{cases} -K_{iact}(v_i - v_{io}) & (\text{if } u_i < F_{imax}) \\ -F_{imax}\operatorname{sgn}(v_i - v_{io}) & (\text{if } u_i > F_{imax}) \end{cases} \tag{4.26}$$

This chapter concluded with a brief explanation of the design of a passive base isolation system for use in a hybrid passive-semi active controller. Passive base isolation is incorporated into the time history analysis by designing it as a pre-filter of the ground excitation records. The base isolated fundamental frequency was selected to be 25% of the structural fundamental frequency for the SAC3 building.

This chapter ends the development of the analyses tools used in this investigation, with the following chapters presenting, comparing, and discussing the results that were obtained. Chapter 5 presents the results for simulations of the SAC3 building under all three earthquake suites using the actuator architectures and control laws developed in this chapter, while the results for the SAC9 building simulations are presented in Chapter 6.

5. SAC3 SIMULATION RESULTS

5.1 INTRODUCTION

This chapter presents the simulation results for the SAC3 building using the actuator architectures and controllers presented in Chapter 4. Although a brief discussion is presented with the results, an in depth comparison of controllers, actuator architectures, and structural characteristics is discussed in Chapter 7. This chapter is divided into three main sections: results for actuators on the first floor only, results for multi-floor actuator architectures, and results for a simple passive/semi-active hybrid control system.

The primary assessment of controller performance is undertaken using actuators on the ground floor only, utilising each of the five control methods described in Chapter 4. This simple actuator architecture was selected to allow efficient control comparison without the effect of actuator-actuator interactions between floors. To compare the effect of actuator architecture in an efficient manner, an initial study of actuator authority distribution for the SAC3-A2 and SAC3-A3 architectures was undertaken using the resetable controller with the high earthquake suite only. Using these simulations, the most effective architectures were selected for application with all three earthquake suites using resetable and LQRy controllers. The JQR controller is also tested for the SAC3-A3 architecture to investigate its effectiveness on multiple stories.

The structural performance for each earthquake suite is evaluated using:

i) Peak story drift.

ii) Permanent story drift.

iii) Peak floor absolute acceleration.

iv) Structural hysteretic energy.

These metrics were selected to give an indication of both the potential structural damage due to structural hysteretic energy dissipation, transient story drifts, and permanent story drifts, as well as the level of occupant hazard through the assessment of floor accelerations. The reduction in structural hysteretic energy is also used to give an indication of the amount of work done by the controller, as through conservation of energy it is clear that the decrease in hysteretic energy between controlled and uncontrolled cases should be approximately equal to the energy dissipated by the actuators. For each of the controlled structural simulations, the four response metrics were calculated as percentage reductions from the uncontrolled response rather than solely using the absolute drift ratios, for which limits are described in Table 1.1. Percentage performance reductions allow comparisons between control systems and architectures to be easily undertaken, which is the primary objective of this investigation rather than obtaining maximum absolute reductions in performance metrics.

5.2 STATISTICAL TOOLS

The performance measures of interest are evaluated statistically from the individual structural responses for the 20 seismic records within each earthquake suite. Therefore, the choice of statistical tools must ensure the simulation results are accurately represented. It is widely accepted that the structural response of seismically excited buildings closely follows a lognormal distribution. The lognormal distribution can be justified since the statistical variation of many material properties and seismic response variables may be well represented by this distribution provided one is not primarily concerned with the extreme tails of the distribution [Kennedy et al. 1980]. In addition, the central limit theorem states that a

distribution of a random variable consisting of products and quotients of several random variables tends to be lognormal even if the individual variable distributions are not lognormal.

The lognormal distribution differs from the more widely know Gaussian (Normal) distribution in that the data is always greater than zero and is skewed to the low end of the distribution. Figure 5.1 shows the distribution of maximum first floor drifts for the SAC3 building for one earthquake suite for both the uncontrolled and resetable controller simulations. The figure shows the absolute peak story drift for the first floor, over all 20 excitations in the high suite. The figure also shows an approximate lognormal shape overlaid on the data distribution. Although the appearance of the distribution is limited by the number of data points, two key points should be noted from these distributions:

i. Both the responses are clearly skewed to the left with a single earthquake situated at the tail of the distribution. This type of skewed distribution is accurately represented by a lognormal distribution, which is ideal for a distribution in which mean values are low and variances are large.

ii. The impact of the resetable controller can be clearly seen from the difference between the two distributions. Firstly, the drift response at the tail of the controlled distribution is less than for uncontrolled, showing the control has a positive effect even during the most extreme seismic events. Secondly, the effect of the resetable controller is to shift the distribution to the left, meaning that a greater number of responses within the distribution are closer to zero.

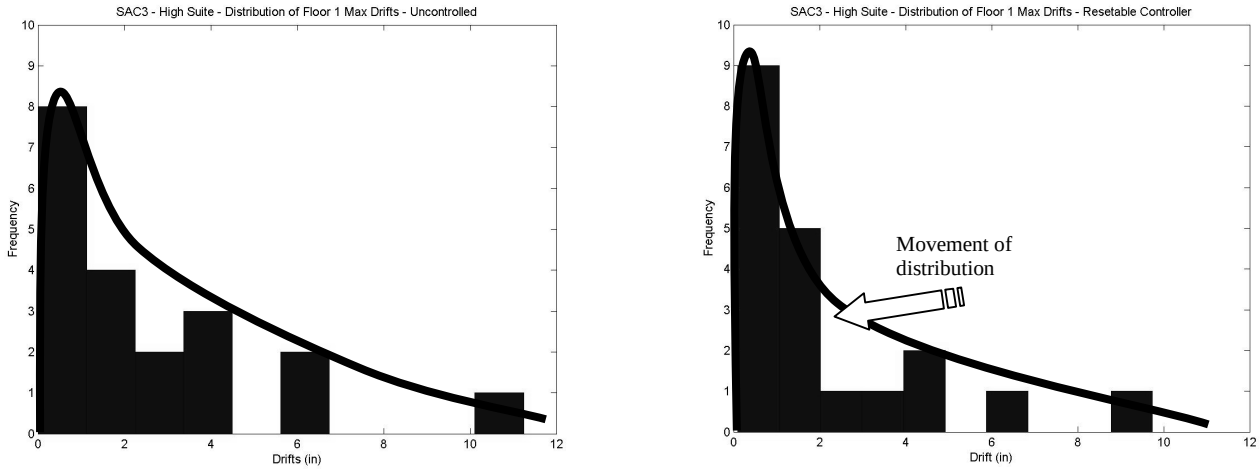

Figure 5.1: Maximum drift distribution for SAC3 floor 1 - uncontrolled and resetable controller.

Variables within each earthquake suite may be combined using the lognormal distribution geometric-mean and variance [Limpert et al. 2001]. For a lognormal distribution of "n" samples, x_i, the geometric-mean, $\hat{x}$, is defined:

$$\hat{x} = \exp\left(\frac{1}{n}\sum_{i=1}^{n}\ln(x_i)\right) \tag{5.1}$$

Similarly the lognormal based coefficient of variation, or standard deviation, $\hat{\sigma}$, is defined:

$$\hat{\sigma} = \exp\left(\sqrt{\frac{1}{n-1}\sum_{i=1}^{n}(\ln(x_i) - \ln(\hat{x}))^2}\right) \tag{5.2}$$

To present a summary of the distribution change between the controlled and uncontrolled data sets, while providing accurate statistical measures that are not highly affected by changes in any single variable, the geometric-mean or 50^{th} percentile, and the 84^{th} percentile are presented. The 84^{th} percentile for a lognormal distribution is defined as the geometric-mean, $\hat{x}$, multiplied one lognormal standard deviation, $\hat{\sigma}$. The numerical average, or Gaussian

mean, is also presented for completeness, representing approximately the 65th percentile for a lognormal distribution [Limpert et al. 2001].

By presenting the 50th, 65th, and 84th percentile levels the change in lognormal distribution shape for the different controlled cases may be observed. The shape changes between the uncontrolled and controlled cases may be classed into three general categories:

i) *Case 1* – the geometric-mean decreases while the 84th percentile increases. This type of movement is a result of an increase in distribution variance, which is likely due to the extreme outliers at the tail of the distribution. A performance improvement may be observed for these very large excitations, however, due to a potentially greater decrease for the smaller earthquakes and the subsequent lowering of the geometric mean, the distribution is stretched and the 84th percentile level increases. Hence, for this case the numerical average (65th percentile) may give a clearer indication of the response improvement.

ii) *Case 2* – geometric-mean increases while the 84th percentile decreases. For this case, there is a decrease in distribution variance. This is potentially due to effective controller performance for the larger excitations where the level of actuation is high, with smaller improvements in performance during the smaller excitations.

iii) *Case 3* – both geometric-mean and 84th percentile levels decrease. A decrease in both the 50th and 84th percentiles indicates improvements in all of the response, from the small magnitudes up to the largest in the tail of the distribution.

It should be noted that the structural hysteretic energy does not follow a lognormal distribution, unlike peak drift, permanent drift, and peak acceleration [Breneman 2000]. To define a statistical measure of the energy dissipation response values, the standard "counted" mean and 84th percentile are presented. The counted mean is the data point at which half of the response values fall below, meaning that for a sample of 20 values, linear interpolation is used to obtain the value between the 10th and 11th highest data points. Similarly, the counted 84th percentile is the data point below which 84% of the response values fall, again using linear interpolation between the 16th and 17th data points of a 20-value sample.

5.3 SAC3 UNCONTROLLED RESPONSE

Results for each of the controllers used in the SAC3 building simulations are presented as a percentage change from the uncontrolled response. The time-history analysis for the uncontrolled case is implemented using the same models as for the controlled cases, with the control input set to zero.

The structural response of the uncontrolled SAC3 building for the high earthquake suite is shown in Tables 5.1. Across all three floors, the average geometric-mean peak drifts and permanent drifts are 6.5in and 1.2in respectively, while the average 84th percentile results are 10.4in and 4.7in respectively. The large difference between these two statistical measures highlights the skewed nature of the lognormal response distribution, with one or two very large responses situated at the tail of the distribution. As a result, it is easily seen that different earthquakes of similar magnitude may have very different responses. Hence, the benefit of using the suites of earthquakes rather than just a few. The yielded shape, which can be estimated from the permanent drift of the building, is approximately linear as expected for a squat, shear building with first mode dominated response.

TABLE 5.1: SAC3 UNCONTROLLED RESULTS FOR HIGH SUITE

	Numerical Average				Geometric-mean/50th Percentile				84th Percentile			
	Gr	**F1**	**F2**	**F3**	**Gr**	**F1**	**F2**	**F3**	**Gr**	**F1**	**F2**	**F3**
Peak Drift (in)		6.35	7.33	7.91		5.60	6.60	7.17		9.48	10.57	11.22
Permanent Drift (in)		2.53	2.27	2.26		1.13	1.11	1.22		6.17	4.33	4.10
Peak Acceleration (in/s/s)	340.06	390.10	375.80	334.39	323.58	377.23	363.69	330.96	451.76	493.55	474.09	383.54
Hysteretic Energy (lb-in)	9.63E+06	1.39E+07	1.44E+07	7.17E+06	9.52E+06	1.29E+07	1.27E+07	5.61E+06	1.46E+07	2.17E+07	2.68E+07	1.39E+07

The uncontrolled response for the SAC3 structure due to the medium earthquake suite is shown in Table 5.2. The average geometric-mean peak drifts and permanent drifts are 3.3in and 0.5in respectively, which despite still being the response to near-field seismic events, are substantially smaller than for the high suite response. The average geometric-mean hysteretic energy is 2.96e6 lb-in, which is less than 1% of the corresponding value for the high suite. This large difference is due to the selected probability of excedance levels, with the high suite designed to represent a mean return period of approximately 2,475 years, while the medium suite represents a 474-year mean return period event.

TABLE 5.2: SAC3 UNCONTROLLED RESULTS FOR MEDIUM SUITE

	Numerical Average				Geometric-mean/50th Percentile				84th Percentile			
	Gr	**F1**	**F2**	**F3**	**Gr**	**F1**	**F2**	**F3**	**Gr**	**F1**	**F2**	**F3**
Peak Drift (in)		2.85	3.58	3.67		2.69	3.42	3.48		3.83	4.65	4.91
Permanent Drift (in)		0.81	0.82	0.87		0.50	0.44	0.50		1.58	1.91	1.90
Peak Acceleration (in/s/s)	226.98	306.85	303.48	283.55	211.49	288.31	291.73	280.14	313.06	417.08	390.10	328.89
Hysteretic Energy (lb-in)	1.79E+06	4.55E+06	3.81E+06	1.53E+06	1.56E+06	4.89E+06	3.56E+06	1.83E+06	3.95E+06	8.08E+06	7.06E+06	2.84E+06

Table 5.3 presents the uncontrolled response of the SAC3 building due to the low earthquake suite. It is interesting to note that even in this suite, which represents a 100-year return period event and does not include near-field effects, permanent drifts are not negligible at the 84th

percentile level with an average value of 0.42in, while hysteretic energy values are comparable to those for the medium suite. This result highlights the point that although this set of earthquakes is called the "low suite", their magnitudes are still appreciable and potentially damaging to structural elements, with a mean return period of 72 years.

TABLE 5.3: SAC3 UNCONTROLLED RESULTS FOR LOW SUITE.

	Numerical Average				Geometric-mean/50th Percentile				84th Percentile			
	Gr	**F1**	**F2**	**F3**	**Gr**	**F1**	**F2**	**F3**	**Gr**	**F1**	**F2**	**F3**
Peak Drift (in)		1.76	2.23	2.32		1.60	2.07	2.11		2.48	3.08	3.23
Permanent Drift (in)		0.22	0.20	0.17		0.02	0.04	0.03		0.37	0.50	0.40
Peak Acceleration (in/s/s)	164.39	268.40	275.22	247.87	139.74	236.94	253.72	237.90	259.32	406.50	392.75	324.73
Hysteretic Energy (lb-in)	3.81E+05	1.60E+06	1.11E+06	5.39E+05	1.10E+04	1.11E+06	4.09E+05	1.24E+05	8.33E+05	4.41E+06	2.61E+06	1.25E+06

5.4 SINGLE FLOOR ACTUATOR ARCHITECTURE – SAC3-A1

The main assessment of controller performance for the SAC3 building simulations is undertaken using the SAC3-A1 actuator architecture. The architecture, shown in Figure 4.1(a), has actuators placed between the ground and first floor only. Total actuator authority is limited to 450kips for each of the five controllers, which is equivalent to 13.8% of the structural weight. The lateral actuator forces applied to the structure are trigonometrically reduced according to the actuator angle, reducing the maximum actuator authority by approximately 10%. The responses using each controller are presented as percentage changes from the uncontrolled case presented in Section 5.3, with negative values implying a desired response reduction.

5.4.1 Clipped Quasi-bang-bang Control

The control law for the clipped quasi-bang-bang controller is presented in Chapter 4.3.4. Specifically, the displacement and velocity dead-bands are set at 0.2in and 1.0in/s respectively, while the displacement at which maximum actuator authority is commanded is set at 1.5in. Using scaled experimental damping plots, the velocity at the bi-linear damping transition was set at 5.0in/s.

The response of the SAC3 structure to the high earthquake suite using the quasi-bang-bang controller is presented in Table 5.4 in terms of percentage change from the uncontrolled case. The effect of the actuator placed between the ground and first floor only is clearly seen, with the largest energy reductions seen at the actuator location. Although the hysteretic energy is not as greatly reduced on the second and third floors, 84^{th} percentile values are still reduced by 12.5% on average, showing that actuators placed between the ground and first floor only are effective in reducing the overall structural energy on all three floors. The geometric-mean peak drift response of the first floor is reduced by 12.2%, while the permanent drift and peak acceleration increase by 16.8% and 19.2% respectively. The increase in the permanent drift and accelerations is due to the quasi-bang-bang control law, which applies active resistance forces that are proportional to transient drifts, hence the increased acceleration and the impact nature of control forces, that may cause permanent deformation, are not accounted for. The general trend of the controlled response at the 84^{th} percentile level is that of percentage reductions, implying that the skewed distribution has effectively been shifted further to the left. The data shows reductions at the 65^{th} and 84^{th} percentiles but not for the geometric-mean for the first two floors. This observation shows the impact of this controller, for this suite, is to shift the extremum down significantly while not affecting lower response as much, this being an example of Case 2 distribution shifting. The numerical average permanent drifts are

decreased on each floor with an average reductions of 6.1%, while peak drifts are reduced on floors 1 and 2, with an increase on floor 3 corresponding to 0.05in.

TABLE 5.4: SAC3-A1-1 RESULTS FOR HIGH SUITE WITH QUASI-BANG-BANG CONTROLLER.

	Numerical Average				Geometric-mean/50th Percentile				84th Percentile			
	Gr	**F1**	**F2**	**F3**	**Gr**	**F1**	**F2**	**F3**	**Gr**	**F1**	**F2**	**F3**
Peak Drift (%)		-11.91	-3.70	0.62		-12.15	-3.08	1.28		-11.62	-3.45	2.11
Permanent Drift (%)		-9.12	-5.40	-3.87		16.84	6.86	-8.26		-28.38	-8.54	13.18
Peak Acceleration (%)		18.30	-0.30	-0.95		19.24	0.60	-1.03	0	15.30	-3.44	-0.59
Hysteretic Energy (%)	-24.96	-12.24	-1.31	-1.43	-31.52	-12.48	-4.15	-1.96	-25.23	-11.45	-10.92	-14.08

As shown in Table 5.5, an average reduction in geometric-mean hysteretic energy for the quasi-bang-bang controller with the medium earthquake suite is 33.2%, showing the ability of the controller to reduce overall structural energy despite being placed between the ground and first floors only. Peak drifts are reduced on each floor, with the floor 2 and 3 reductions greater than for the high suite. The first floor geometric-mean permanent drift is reduced by over 43%, while the values for the upper two floors increase. As the 65th and 84th percentile permanent drifts all decrease while some of the geometric-mean values increase, it is clear that the shape of the lognormal distribution is different between the controlled and uncontrolled cases, with extreme values most significantly shifted.

TABLE 5.5: SAC3-A1-1 RESULTS FOR MEDIUM SUITE WITH QUASI-BANG-BANG CONTROLLER.

	Numerical Average				Geometric-mean/50th Percentile				84th Percentile			
	Gr	**F1**	**F2**	**F3**	**Gr**	**F1**	**F2**	**F3**	**Gr**	**F1**	**F2**	**F3**
Peak Drift (%)		-12.01	-7.74	-5.95		-12.08	-7.93	-5.74		-11.49	-7.06	-7.62
Permanent Drift (%)		-19.20	-1.52	5.94		-43.28	22.37	31.47		-10.65	-19.88	-8.98
Peak Acceleration (%)		20.47	4.89	-0.10		25.38	5.41	0.30		7.80	2.57	-2.74
Hysteretic Energy (%)	-39.48	-33.19	-24.40	-17.85	-42.78	-28.15	-27.80	-33.92	-33.54	-36.86	-17.20	-4.36

The results for the low earthquake suite are shown in Table 5.6, with substantial reductions seen in almost all of the performance measures. Both peak and permanent drifts at the 50th and 84th percentile levels are reduced for each floor level, with average geometric-mean peak and permanent drift reductions of 15.2% and 55.2% respectively. Geometric-mean hysteretic energy is reduced by over 90% on all floors, while peak accelerations show only small changes.

TABLE 5.6: SAC3-A1-1 RESULTS FOR LOW SUITE WITH QUASI-BANG-BANG CONTROLLER.

	Numerical Average				Geometric-mean/50th Percentile				84th Percentile			
	Gr	**F1**	**F2**	**F3**	**Gr**	**F1**	**F2**	**F3**	**Gr**	**F1**	**F2**	**F3**
Peak Drift (%)		-22.26	-13.81	-6.80		-23.54	-15.31	-6.72		-20.99	-12.98	-8.50
Permanent Drift (%)		-29.57	-23.48	-27.02		-48.72	-57.85	-59.13		-49.01	-45.21	-57.04
Peak Acceleration (%)		7.49	-6.04	-3.53		15.20	-4.30	-2.33		-4.50	-10.07	-7.46
Hysteretic Energy (%)	-55.51	-69.87	-41.91	-36.15	-99.38	-99.97	-93.85	-91.90	-75.56	-59.80	-44.63	-45.95

5.4.2 LQR Clipped Optimal Control

The LQR clipped optimal control law described in Section 4.4 was implemented using displacement performance weightings of 100 and velocity performance weightings of 10. These weightings were combined into a diagonal performance weighting matrix, **Q**, and used with a control effort weighting of $R = 3x10^{-8}$. With these weighting factors the controller's primary focus is on the design of state feedback gains to attenuate displacements. It should be noted that the LQR controller is designed using a linear model and implemented using the lateral degrees-of-freedom only. Hence, the LQR controller does not directly account for permanent deformations, however, indirect benefits result through the control of transient drifts.

The response of the SAC3 structure for the high earthquake suite using the LQR controller is shown in Table 5.7. The geometric-mean of the peak drift shows a reduction on all floors as might be expected from the emphasis placed on displacement within the control law. An important point to note is the centralised nature of the LQR controller, with gains selected through consideration of the entire building's response, not solely from the response of the floor to which the actuator is attached. Hence, a side effect of controlling the transient drift is to also reduce the permanent drift on all floors, with an average reduction in geometric-mean of 19.6%. While hysteretic energy is reduced on all floors, the geometric-mean peak accelerations increase on all floors, although the increase on floor 3 is insignificant. Thus, applying the control forces to reduce displacements clearly results in increased acceleration, highlighting the trade-off between displacement reduction and the resulting floor accelerations.

TABLE 5.7: SAC 3-A1-1 RESULTS FOR HIGH SUITE WITH LQR CONTROLLER.

	Numerical Average				**Geometric-mean/50th Percentile**				**84th Percentile**			
	Gr	**F1**	**F2**	**F3**	**Gr**	**F1**	**F2**	**F3**	**Gr**	**F1**	**F2**	**F3**
Peak Drift (%)		-23.13	-9.90	-3.69		-23.40	-8.95	-2.44		-23.63	-10.78	-4.10
Permanent Drift (%)		-14.83	-11.24	-11.50		-23.01	-24.00	-11.80		-8.68	15.99	-7.30
Peak Acceleration (%)	0	19.05	3.02	0.84	0	21.48	4.06	0.95	0	9.97	-0.03	0.15
Hysteretic Energy (%)	-53.10	-34.88	-13.68	-7.15	-62.53	-36.81	-15.28	-9.62	-50.74	-33.40	-18.94	-15.08

The structural response of the SAC3 building under excitation from the medium earthquake suite is mixed, with assessment of control effectiveness dependent on which performance statistic is used. Looking at the geometric-mean in Table 5.8, reductions on all floors are observed in peak drift, permanent drifts, and hysteretic energy, while the peak acceleration increases by 39.5% on the first floor and decreases slightly on floors 2 and 3. However, looking at the 84th percentile, the peak drift increases on floor 3 while the permanent drifts

increase on all three floors. This again implies a shift in the lognormal distribution, with a reduction in the majority of the responses, but with a longer tail due to increased response of an extreme event resulting in an increased variance, $\hat{\sigma}$. A hint of this trend is seen in the numerical average where the third floor shows increased permanent drift. Overall, actuators only on the first floor can result in increased higher floor results. Note also that the magnitude of the increases correspond to only a few tenths of inches compared to the uncontrolled case.

TABLE 5.8: SAC3-A1-1 RESULTS FOR MED SUITE WITH LQR CONTROLLER.

	Numerical Average				Geometric-mean/50th Percentile				84th Percentile			
	Gr	**F1**	**F2**	**F3**	**Gr**	**F1**	**F2**	**F3**	**Gr**	**F1**	**F2**	**F3**
Peak Drift (%)		-28.64	-12.83	-3.16		-28.76	-14.46	-5.69		-28.91	-8.62	1.58
Permanent Drift (%)		-36.84	-5.68	7.55		-68.28	-22.57	-4.93		11.66	41.56	67.07
Peak Acceleration (%)	0	33.55	-3.21	-2.37	0	39.54	-3.06	-2.30	0	17.95	-3.24	-2.58
Hysteretic Energy (%)	-76.46	-59.58	-31.72	-20.90	-92.40	-69.59	-33.63	-38.48	-68.29	-54.13	-18.83	-3.35

The results for the low earthquake suite with the LQR controller are shown in Table 5.9. The reduction of each of the performance measures is large, highlighting the large bandwidth of the LQR controller, effectively reducing structural demands from the 72-year events in the low suite right up to 2,475-year events in the high suite. The geometric-mean hysteretic energy is reduced by 100% for each floor, while the permanent drifts are reduced by an average of 88%.

TABLE 5.9: SAC3-A1-1 RESULTS FOR LOW SUITE WITH LQR CONTROLLER.

	Numerical Average				Geometric-mean/50th Percentile				84th Percentile			
	Gr	**F1**	**F2**	**F3**	**Gr**	**F1**	**F2**	**F3**	**Gr**	**F1**	**F2**	**F3**
Peak Drift (%)		-32.40	-23.65	-16.65		-34.33	-28.09	-22.18		-30.42	-19.72	-12.72
Permanent Drift (%)		-42.06	-29.52	-8.51		-86.60	-90.93	-86.67		-86.08	-84.50	-75.06
Peak Acceleration (%)		-7.71	-16.80	-14.33		-16.57	-22.45	-17.37		2.21	-9.19	-8.23
Hysteretic Energy (%)	-74.32	-78.55	-52.05	-42.02	-99.91	-100.00	-100.00	-100.00	-99.71	-70.70	-52.93	-54.01

5.4.3 LQRy Clipped Optimal Control

The LQRy clipped optimal controller, presented in Section 4.5, produces state feedback gains designed to minimise the total structural acceleration. The specific controller uses an equal performance weighting of $Q = 5$ on each of the three floors, while the control cost weighting was set at $R = 1.6x10^{-6}$. As with the LQR controller, control design was undertaken using a reduced order lumped mass model, with optimal gains operating on lateral degrees-of-freedom only.

From Table 5.10, which presents results for the high earthquake suite, the impact of designing for structural accelerations is striking. Regardless of which statistical measure of performance is assessed, the peak and permanent drift demands are significantly reduced for the first floor, showing an overall Case 3 distribution shift. For floors 2 and 3, a Case 1 distribution shift is observed, with reductions seen at the 50^{th} and 65^{th} percentiles. Looking at the geometric-mean, the average reductions in peak and permanent drifts are 13.0% and 23.8% respectively, while the average peak acceleration is reduced by 15.8%, with a reduction observed even on the first floor to which the actuator is attached.

TABLE 5.10: SAC3-A1-1 RESULTS FOR HIGH SUITE WITH LQRY CONTROLLER.

	Numerical Average				Geometric-mean/50th Percentile				84th Percentile			
	Gr	**F1**	**F2**	**F3**	**Gr**	**F1**	**F2**	**F3**	**Gr**	**F1**	**F2**	**F3**
Peak Drift (%)		-22.35	-9.40	-7.18		-22.62	-8.66	-7.58		-22.99	-10.02	-5.10
Permanent Drift (%)		-17.68	-14.02	-12.42		-15.79	-26.83	-28.87		-23.38	18.10	14.07
Peak Acceleration (%)		-15.90	-21.12	-9.71		-16.31	-21.66	-9.54		-14.32	-19.79	-10.88
Hysteretic Energy (%)	-47.79	-23.11	-10.31	-20.78	-56.75	-20.38	-9.65	-21.65	-47.88	-20.16	-16.69	-22.02

The results for the medium earthquake suite, presented in Table 5.11, show the same general trend as those for the high suite, with differences attributable to the different characteristics of the earthquakes within each suite. Each of the performance measures show decreased structural demand on all three floors, other than the 84th percentile permanent drifts for floors 2 and 3. It should be noted that the absolute value of these increases are relatively small when compared to the uncontrolled case. Average acceleration reductions are approximately 23% across each of the statistical levels and floors.

TABLE 5.11: SAC3-A1-1 RESULTS FOR MEDIUM SUITE WITH LQRY CONTROLLER.

	Numerical Average				Geometric-mean/50th Percentile				84th Percentile			
	Gr	**F1**	**F2**	**F3**	**Gr**	**F1**	**F2**	**F3**	**Gr**	**F1**	**F2**	**F3**
Peak Drift (%)		-22.01	-7.59	-7.83		-20.81	-7.97	-9.55		-24.65	-6.32	-5.24
Permanent Drift (%)		-42.44	-16.03	-5.53		-64.19	-19.01	-24.87		-21.81	8.82	94.19
Peak Acceleration (%)		-23.24	-30.21	-13.32		-25.04	-30.28	-13.07		-20.77	-30.67	-14.85
Hysteretic Energy (%)	-69.37	-38.34	-24.76	-40.42	-76.21	-40.85	-30.00	-57.61	-62.47	-36.25	-21.41	-26.07

The results for the low earthquake suite, shown in Table 5.12, clearly show reductions in each of the measures of structural demand. For the high and medium suites an increase in the 84th percentile was observed for the permanent drifts of floors 2 and 3, however for the low suite large reductions of over 80% are seen, indicating a Case 3 distribution shift of all performance

measures. The average geometric-mean peak acceleration is reduced by 38.8%, while hysteretic energy is reduced by 99.3%. The average geometric-mean peak and permanent drifts are reduced by 21.7% and 81.7% respectively.

TABLE 5.12: SAC3-A1-1 RESULTS FOR LOW SUITE WITH LQRY CONTROLLER

	Numerical Average				Geometric-mean/50th Percentile				84th Percentile			
	Gr	**F1**	**F2**	**F3**	**Gr**	**F1**	**F2**	**F3**	**Gr**	**F1**	**F2**	**F3**
Peak Drift (%)		-23.48	-14.94	-18.78		-24.22	-18.30	-22.22		-21.93	-10.92	-17.36
Permanent Drift (%)		-44.81	-39.42	-38.79		-73.37	-84.02	-87.76		-72.45	-81.55	-85.63
Peak Acceleration (%)		-41.09	-45.00	-24.91		-45.48	-45.70	-25.25		-38.93	-45.21	-25.05
Hysteretic Energy (%)	-71.91	-61.14	-45.25	-57.77	-99.25	-98.13	-99.96	-100.00	-93.24	-54.25	-44.77	-77.30

5.4.4 Clipped Resetable Control

The clipped resetable controller acts as a hydraulic spring with a controllable free length to dissipate energy from the structural system, as detailed in Section 4.6. In order to provide maximum actuator authority at 1.5in consistent with other controllers, a combined total spring stiffness of 300,000lb/in is used. The displacement dead band is set at 0.1in, effectively stopping the actuator resetting close to the time-varying equilibrium position.

The focus of the resetable controller is the storage and dissipation of energy at an optimised rate, and as can be seen in Table 5.13, hysteretic energy is reduced on all floors during the high earthquake suite. The peak drift is reduced on all floors for all three statistical measures, with a reduction of approximately 16% at the actuator location. Geometric-mean permanent drift is increased slightly at the first floor, but is decreased on floors 2 and 3, while the 65th and 84th percentile points are reduced on all three floors. This reduction of the 84th percentile floor 1 permanent drift is a Case 2 distribution shift, showing how the upper half is

compressed towards the geometric-mean. Peak acceleration is increased at the actuator location, but is reduced slightly on floors 2 and 3.

TABLE 5.13: SAC3-A1-1 RESULTS FOR HIGH SUITE WITH RESETABLE CONTROLLER.

	Numerical Average				Geometric-mean/50th Percentile				84th Percentile			
	Gr	**F1**	**F2**	**F3**	**Gr**	**F1**	**F2**	**F3**	**Gr**	**F1**	**F2**	**F3**
Peak Drift (%)		-15.86	-7.94	-4.16		-16.26	-6.94	-2.96		-15.92	-9.01	-4.66
Permanent Drift (%)		-13.26	-10.31	-10.41		6.91	-8.13	-18.38		-33.38	-8.15	-1.21
Peak Acceleration (%)		18.80	-1.35	-2.29		20.43	-0.04	-2.25		12.79	-5.90	-2.51
Hysteretic Energy (%)	-30.71	-19.29	-10.24	-11.43	-31.10	-19.08	-14.04	-19.22	-31.82	-15.43	-17.39	-19.91

The results for the medium earthquake suite, shown in Table 5.14, show larger peak acceleration increases than for the high suite, however, average geometric-mean hysteretic energy is reduced by over 43%, implying an overall reduction in structural damage. Permanent drifts either decrease or show little change, while the peak drift is decreased on all floors.

TABLE 5.14: SAC3-A1-1 RESULTS FOR MEDIUM SUITE WITH RESETABLE CONTROLLER.

	Numerical Average				Geometric-mean/50th Percentile				84th Percentile			
	Gr	**F1**	**F2**	**F3**	**Gr**	**F1**	**F2**	**F3**	**Gr**	**F1**	**F2**	**F3**
Peak Drift (%)		-11.71	-8.26	-6.06		-11.54	-8.86	-6.79		-11.95	-6.54	-5.58
Permanent Drift (%)		-23.05	-9.31	-3.71		-32.94	0.40	-2.92		-22.53	-22.73	2.51
Peak Acceleration (%)		40.66	5.28	-1.38		46.26	5.11	-1.06		26.27	4.50	-3.38
Hysteretic Energy (%)	-35.89	-37.17	-28.29	-24.71	-40.71	-43.83	-34.06	-56.66	-28.79	-37.32	-20.57	-8.30

The peak accelerations for the low suite follow the same trend as those for the high suite, with increased acceleration at the actuator location, but decreased elsewhere. As shown in Table 5.15, the peak drifts, permanent drift, and hysteretic energy are reduced substantially on all

floors for each of the statistical measures. The average geometric-mean hysteretic energy is reduced by 99.6%, while the average geometric-mean permanent drift is reduced by over 73%.

TABLE 5.15: SAC3-A1-1 RESULTS FOR LOW SUITE WITH RESETABLE CONTROLLER

	Numerical Average				Geometric-mean/50th Percentile				84th Percentile			
	Gr	**F1**	**F2**	**F3**	**Gr**	**F1**	**F2**	**F3**	**Gr**	**F1**	**F2**	**F3**
Peak Drift (%)		-16.72	-16.42	-12.98		-20.68	-19.88	-15.98		-11.58	-13.47	-12.39
Permanent Drift (%)		-0.80	-14.80	-28.32		-56.99	-83.50	-79.01		-32.01	-66.36	-69.39
Peak Acceleration (%)		25.70	-11.89	-10.35		33.34	-11.17	-10.29		13.87	-13.92	-11.32
Hysteretic Energy (%)	-27.79	-65.66	-47.25	-44.85	-99.45	-98.88	-99.93	-99.96	-6.12	-58.07	-43.69	-44.93

5.4.5 JQR Clipped Optimal Control

As discussed in Section 4.7, the JQR clipped optimal controller assesses overall structural performance in terms of the structural jerk, or the rate of change of acceleration. For the high and medium suites, the displacement and velocity dead bands are set at 0.4in and 1.0in/s respectively, while for the low suite values of 0.5in and 1.2in/s were used. The use of slightly larger dead bands for the suite was necessary due to instability of the MATLAB numerical solver for the JQR controller, but should not have any significant impact on the results as the differences are small.

As the effect of the JQR controller is to reduce structural jerk, the increased accelerations shown in Table 5.16 for the high suite are expected, as the controller applies control forces to smooth the acceleration, reducing its rate of change. The decreased structural jerk leads to decreased floor drifts, with geometric-mean peak and permanent drifts decreased on all three floors. Excluding the 84th percentile permanent drift value, which increases slightly, the reductions seen at each of the statistical levels are large for all floors, highlighting the

potential benefits of JQR control. The reductions in hysteretic energy are not as extensive as those commonly seen for the other controllers. This result is not surprising, as structural jerk is potentially linked to the magnitude of internal damage to people and equipment within a building, and not necessarily to the amount of yielding that occurs within the structural connections. Hence, the performance evaluation of the JQR controller for the high earthquake suite is dependent on whether external or internal damage is the primary concern.

TABLE 5.16: SAC3-A1-1 RESULTS FOR HIGH SUITE WITH JQR CONTROLLER.

	Numerical Average				Geometric-mean/50th Percentile				84th Percentile			
	Gr	**F1**	**F2**	**F3**	**Gr**	**F1**	**F2**	**F3**	**Gr**	**F1**	**F2**	**F3**
Peak Drift (%)		-12.27	-7.57	-4.68		-10.80	-6.70	-4.42		-14.04	-8.60	-3.70
Permanent Drift (%)		-16.05	-12.29	-10.33		-17.44	-17.30	-10.75		-26.22	7.60	-10.32
Peak Acceleration (%)		33.86	11.98	4.05		35.46	11.64	3.85		28.80	13.65	5.42
Hysteretic Energy (%)	-15.98	-11.66	-2.78	-2.01	-14.26	-7.80	0.07	5.58	-10.07	-8.86	-5.92	-8.68

The results for the medium earthquake suite are shown in Table 5.17. Again, an increase in peak accelerations is observed, while there is a decrease in peak and permanent drifts on all three floors. In contrast to the high suite, the hysteretic energy reductions are comparable to other controllers, with an average geometric-mean reduction of 27.4%, but are not consistently distributed across the floors.

TABLE 5.17: SAC3-A1-1 RESULTS FOR MEDIUM SUITE WITH JQR CONTROLLER.

	Numerical Average				Geometric-mean/50th Percentile				84th Percentile			
	Gr	**F1**	**F2**	**F3**	**Gr**	**F1**	**F2**	**F3**	**Gr**	**F1**	**F2**	**F3**
Peak Drift (%)		-9.45	-3.35	-1.86		-9.47	-3.69	-1.27		-9.45	-2.19	-3.82
Permanent Drift (%)		-19.88	-16.01	-14.94		-50.11	-14.51	-21.74		-7.40	-31.36	-11.76
Peak Acceleration (%)		42.33	10.51	1.76		42.63	6.05	1.49		41.98	20.65	3.08
Hysteretic Energy (%)	-30.06	-20.31	-7.19	-3.78	-43.12	-25.63	-3.74	-36.97	-33.49	-24.87	-7.03	-1.02

The trends of the results for the low suite, shown in Table 5.18, differ to those for the high and medium suites, with peak and permanent drift increases on floor 3 and generally smaller drift reductions for floors 1 and 2. This difference highlights the impact of the dead band size, with a small increase in dead band resulting in diminished demand reductions. The increases observed in the permanent drift numerical average represent absolute changes on the order of a few hundredths of an inch.

TABLE 5.18: SAC3-A1-1 RESULTS FOR LOW SUITE WITH JQR CONTROLLER.

	Numerical Average				Geometric-mean/50th Percentile				84th Percentile			
	Gr	**F1**	**F2**	**F3**	**Gr**	**F1**	**F2**	**F3**	**Gr**	**F1**	**F2**	**F3**
Peak Drift (%)		-8.52	-3.83	1.12		-8.74	-3.92	1.88		-8.67	-3.81	0.90
Permanent Drift (%)		6.10	19.03	48.90		-26.50	-29.97	15.11		-12.62	-9.19	47.67
Peak Acceleration (%)		29.03	-1.51	0.59		34.49	-2.86	0.24		20.21	-0.73	0.85
Hysteretic Energy (%)	-27.47	-40.69	-3.94	-3.39	-93.54	-68.77	-2.87	-48.32	-62.66	-43.83	-10.56	-20.87

5.5 MULTI-FLOOR ACTUATOR ARCHITECTURES – SAC3-A2 & SAC3-A3

The effect of actuator placement subject to a uniform maximum actuator authority is an area of structural control that has not been widely investigated. In this investigation, three actuator architectures are used with the SAC3 building, with actuators on the first, first and second, and all three floors, as discussed in Section 4.2.1. The control architectures SAC3-A2 and SAC3-A3 are repeated in Figure 5.2 for clarity, with the distribution of actuator forces for each architecture repeated in Table 5.19.

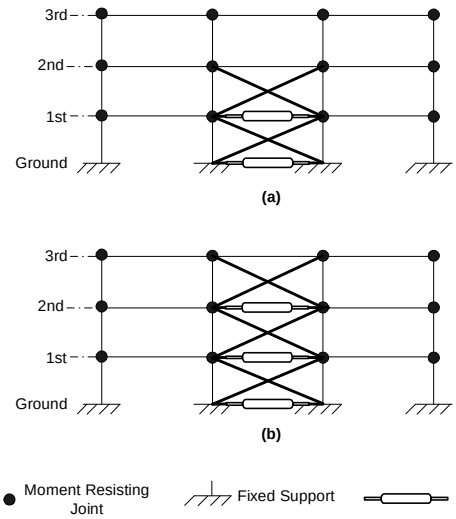

Figure 5.2: SAC3 actuator architectures: (a) SAC3-A2 (b) SAC3-A3.

TABLE 5.19: SAC3 DISTRIBUTIONS OF MAXIMUM ACTUATOR FORCES.

	Maximum Actuator Force Distribution (kips)			
Architecture	**Floor 1**	**Floor 2**	**Floor 3**	**Total Force (kips)**
SAC3-A1-1	450	0	0	***450***
SAC3-A2-1	315	135	0	***450***
SAC3-A2-2	225	225	0	***450***
SAC3-A2-3	135	315	0	***450***
SAC3-A3-1	270	135	45	***450***
SAC3-A3-2	150	150	150	***450***
SAC3-A3-3	45	135	270	***450***

This section presents the results of the actuator architecture study, with initial assessment undertaken using the resetable controller and high earthquake suite only. The results using the selected architectures with the full three earthquake suites and the resetable, LQRy, and JQR controllers are also presented, allowing detailed comparisons to be made with the SAC3-A1 architecture in Chapter 7. As discussed previously, as each actuator architecture has the same total maximum actuator authority, it is the distribution of this total force throughout the structure that is of importance. By using a uniform maximum actuator authority, direct comparison of the impact of different force distributions may be explicitly delineated.

5.5.1 Initial Actuator Architecture Assessment

The initial actuator architecture assessment was undertaken using the resetable controller with the high earthquake suite only. The high suite was selected as it represents extreme near-field seismic excitation for which the most variation in controller effectiveness was observed in the first floor actuator cases, allowing the effect of the architectures to be clearly distinguished. The initial assessment was carried out using the resetable controller due to its relative simplicity, as this approach eliminates the influence of the control law, which may obscure the impact of actuator location and force distribution.

The resetable control law used in this initial architecture assessment is the same as that used for the single floor case presented in Section 5.4.4. The actuators placed on the first, second, and third floors have individually designed stiffnesses, providing their required maximum actuator authority at 1.5in, 3.0in, and 5.0in of displacement respectively, representing drifts of 1.5, 1.5, and 2.0in for each floor. These values were selected to ensure an appropriate distribution of actuator clipping during strong motions. The results for the seven trial actuator architectures are presented in Table 5.20.

Looking at the sheer volume of data presented in Table 5.20, it is difficult to determine which of the overall responses are better than others. In order to simplify the comparisons, average response values over all three floors are compared using the numerical average, which, as the approximate 65^{th} percentile, will represent some of the trends of both the geometric-mean and the 84^{th} percentile. Although the resetable controller is decentralised, by using average performance over the entire structure, the global response may be approximately assessed. The averaged 65^{th} percentile values are shown in Table 5.21.

TABLE 5.20: SAC3 RESULTS FOR HIGH SUITE USING RESETABLE CONTROLLER WITH SAC3-A1, SAC3-A2, & SAC3-A3 ACTUATOR ARCHITECTURES.

	Numerical Average				Geometric-mean/50th Percentile				84th Percentile			
	Gr	**F1**	**F2**	**F3**	**Gr**	**F1**	**F2**	**F3**	**Gr**	**F1**	**F2**	**F3**
SAC3-A1-1 (10:0:0)												
Peak Drift (%)		-15.86	-7.94	-4.16		-16.26	-6.94	-2.96		-15.92	-9.01	-4.66
Permanent Drift (%)		-13.26	-10.31	-10.41		6.91	-8.13	-18.38		-33.38	-8.15	-1.21
Peak Acceleration (%)		18.80	-1.35	-2.29		20.43	-0.04	-2.25		12.79	-5.90	-2.51
Hysteretic Energy (%)	-30.71	-19.29	-10.24	-11.43	-31.10	-19.08	-14.04	-19.22	-31.82	-15.43	-17.39	-19.91
SAC3-A2-1 (7:3:0)												
Peak Drift (%)		-12.55	-6.62	-5.36		-11.37	-5.54	-4.69		-15.05	-7.95	-5.10
Permanent Drift (%)		-10.96	-10.36	-11.59		4.24	-29.99	-29.59		-26.17	22.05	8.29
Peak Acceleration (%)		5.30	1.82	-4.15		6.34	3.30	-4.19		2.13	-3.24	-3.86
Hysteretic Energy (%)	-26.39	-19.01	-11.48	-13.66	-24.55	-20.64	-15.50	-29.22	-27.99	-15.64	-14.72	-18.99
SAC3-A2-2 (5:5:0)												
Peak Drift (%)		-10.61	-6.83	-6.91		-10.59	-5.96	-5.94		-10.97	-7.58	-7.43
Permanent Drift (%)		-8.25	-6.35	-8.06		9.36	11.87	-1.44		-24.32	-14.14	-11.57
Peak Acceleration (%)		6.84	11.36	-2.84		7.32	13.26	-2.62		5.17	4.72	-4.31
Hysteretic Energy (%)	-20.35	-18.39	-11.96	-14.44	-17.72	-19.18	-12.22	-25.27	-20.50	-13.92	-15.09	-17.91
SAC3-A2-3 (3:7:0)												
Peak Drift (%)		-7.20	-6.42	-6.60		-7.26	-6.04	-5.53		-7.12	-6.59	-7.78
Permanent Drift (%)		-5.12	-2.70	-3.72		6.51	6.27	-8.19		-21.67	-5.98	2.07
Peak Acceleration (%)		15.99	21.94	-1.41		16.99	24.06	-1.05		12.34	14.70	-3.93
Hysteretic Energy (%)	-13.60	-16.20	-12.31	-14.28	-12.16	-15.48	-13.85	-23.08	-13.91	-11.94	-12.90	-14.70
SAC3-A3-1 (6:3:1)												
Peak Drift (%)		-10.79	-6.49	-5.80		-10.41	-5.48	-4.80		-11.62	-7.59	-6.17
Permanent Drift (%)		-6.07	-2.88	-3.89		9.64	12.82	-5.21		-20.39	-7.05	1.24
Peak Acceleration (%)		3.63	1.88	-1.41		4.25	2.98	-1.31		1.51	-1.56	-1.91
Hysteretic Energy (%)	-23.36	-17.83	-11.13	-13.48	-21.94	-18.88	-13.90	-21.33	-25.19	-12.59	-15.19	-18.33
SAC3-A3-2 (3.33x3)												
Peak Drift (%)		-6.29	-5.66	-6.69		-6.46	-4.92	-5.57		-6.24	-6.30	-7.82
Permanent Drift (%)		-3.77	-1.79	-3.62		-5.61	10.85	-7.22		-10.87	-8.45	-0.90
Peak Acceleration (%)		2.33	1.44	8.14		3.30	2.34	8.48		-1.02	-1.44	5.79
Hysteretic Energy (%)	-14.21	-12.80	-10.90	-14.05	-11.47	-10.26	-10.86	-21.09	-16.75	-9.85	-15.26	-16.23
SAC3-A3-3 (1:3:6)												
Peak Drift (%)		-1.68	-4.38	-7.73		-1.96	-3.44	-6.66		-1.22	-5.58	-9.13
Permanent Drift (%)		-2.44	-0.77	-0.75		-22.97	-2.42	-10.49		5.78	-0.29	11.14
Peak Acceleration (%)		0.81	2.99	18.14		1.54	3.59	18.68		-1.73	1.08	14.28
Hysteretic Energy (%)	-3.07	-6.44	-10.24	-14.24	-1.92	-6.10	-9.14	-13.29	-4.77	-6.22	-14.05	-15.85

TABLE 5.21: AVERAGE 65TH PERCENTILE RESULTS FOR DIFFERENT ACTUATOR AUTHORITY DISTRIBUTIONS.

	Maximum Actuator Force Distribution:						
	10:0:0	**7:3:0**	**5:5:5**	**3:7:0**	**6:3:1**	**3.33x3**	**1:3:6**
Peak Drift (%)	-9.32	-8.18	-8.12	-6.74	-7.69	-6.21	-4.60
Permanent Drift (%)	-11.33	-10.97	-7.55	-3.85	-4.28	-3.06	-1.32
Peak Acceleration (%)	5.05	0.99	5.12	12.17	1.37	3.97	7.32
Hysteretic Energy (%)	-17.92	-17.63	-16.28	-14.10	-16.45	-12.99	-8.50

From the data shown in Table 5.21 definite trends may be observed:

- *Peak Drift:* The average reduction in peak drift decreases as more of the maximum actuator authority is distributed up the structure. The largest average reduction in peak drift is 9.32%, which occurs when all 450kips of actuator force is placed between the ground and the first floor only. However, each of the seven architectures result in an average decrease in peak drift.

- *Permanent Drift:* Permanent drifts follow the same trend as the peak drifts, with greatest reductions occurring when the maximum actuator authority is placed between the ground and first floors. The contrast in performance may be clearly seen through comparison of the 7:3:0 and 3:7:0 distributions, as well as the 6:3:1 and 1:3:6 distributions, which have the opposite arrangement of actuator forces. The reductions in average permanent drifts for the 7:3:0 and 6:3:1 distributions are approximately three times greater than their opposite distributions.

- *Peak Accelerations:* Average peak acceleration increases are observed for each of the seven control force distributions, with increases ranging from 0.99% to 12.17%. The trend in the peak accelerations differs to that observed for the average drifts, with the 10:0:0 distribution no longer providing the best controlled performance. The smallest increase is observed with the 7:3:0 distribution, with an increase of 0.99%, while the next smallest increase of 1.37% obtained with the 6:3:1 distribution. This trend implies that for control of acceleration, an actuator architecture with the majority of the actuator authority placed at the base of the structure is beneficial, provided a small amount of actuator authority is assigned higher up the structure.

- *Hysteretic Energy:* The largest reduction in average structural hysteretic energy is observed when maximum actuator authority is maintained at the base of the structure, with an average reduction of 17.92% obtained. Little difference is observed between the 10:0:0 and 7:3:0 distributions, while the 1:3:6 architecture has the lowest average reduction of only 8.50%.

If maximum drift demands and reduction in structural hysteretic energy are the primary concerns when assessing structural integrity, then placing the maximum actuator authority lower in the structure is clearly worthwhile. However, as there is evidently a trade-off between displacements and accelerations, with accelerations associated with internal damage to cladding, equipment and occupants, it may be beneficial to assign a small amount of actuator authority on the second and third floors. To investigate this further, the SAC3-A2-1 (7:3:0) and SAC3-A3-1 (6:3:1) actuator architectures were selected for investigation with the full three earthquake suites using the resetable, LQRy, and JQR controllers.

5.5.2 SAC3-A2-1 (7:3:0) Architecture

5.5.2.1 LQRY CLIPPED OPTIMAL CONTROL

The LQRy clipped optimal controller used for the SAC3-A2-1 actuator architecture uses equal performance weightings of $Q = 8$ for each floor acceleration, and equal control cost weighting factors of $R = 3.62x10^{-4}$. The optimal state feedback gains are weighted in the design according to the distribution of the maximum actuator authority, which is maintained at 450kips, by weighting the terms in the control input matrix, $\mathbf{B_1}$.

The performance of the LQRy controller using the high earthquake suite is very good, with reductions in each of the performance measures for each of the response levels as shown in

Table 5.22. The largest reductions in peak drift occur at floor 1, with geometric-mean and 84th percentile response levels both reduced by 16%. Average geometric-mean acceleration is reduced by 17.3%, while average geometric-mean hysteretic energy is reduced by 25.6%.

TABLE 5.22: SAC3-A2-1 RESULTS FOR HIGH SUITE WITH LQRY CONTROLLER.

	Numerical Average				Geometric-mean/50th Percentile				84th Percentile			
	Gr	**F1**	**F2**	**F3**	**Gr**	**F1**	**F2**	**F3**	**Gr**	**F1**	**F2**	**F3**
Peak Drift (%)		-15.92	-9.54	-10.37		-15.91	-9.14	-10.54		-16.14	-9.74	-9.27
Permanent Drift (%)		-12.73	-12.09	-12.55		-1.91	-15.47	-29.12		-19.07	-2.84	-2.92
Peak Acceleration (%)		-13.07	-24.51	-12.40		-14.88	-24.73	-12.37		-7.56	-24.03	-12.68
Hysteretic Energy (%)	-33.66	-16.84	-14.15	-28.63	-35.94	-16.02	-16.66	-33.86	-35.34	-13.37	-16.97	-24.86

The performance of the LQRy controller for the medium and low suites follows the same trends as for the high suite, however, as the average magnitude of the earthquake suite decreases the reductions in structural demands increase. The results for the medium suite, shown in Table 5.23, show average reductions in geometric-mean peak and permanent drifts of 11.9% and 24.7% respectively. Average peak accelerations are reduced by 24.7% and 25.0% at the 50th and 84th percentile levels respectively, with an average geometric-mean hysteretic energy reduction of 44.3%.

TABLE 5.23: SAC3-A2-1 RESULTS FOR MEDIUM SUITE WITH LQRY CONTROLLER.

	Numerical Average				Geometric-mean/50th Percentile				84th Percentile			
	Gr	**F1**	**F2**	**F3**	**Gr**	**F1**	**F2**	**F3**	**Gr**	**F1**	**F2**	**F3**
Peak Drift (%)		-16.54	-7.57	-11.32		-15.95	-7.65	-11.97		-17.90	-7.22	-10.66
Permanent Drift (%)		-31.22	-15.36	-8.69		-46.80	-7.42	-19.95		-23.31	-18.30	35.66
Peak Acceleration (%)		-30.43	-29.50	-13.67		-31.38	-29.27	-13.41		-28.88	-30.69	-15.31
Hysteretic Energy (%)	-54.81	-31.65	-25.80	-46.92	-59.70	-33.15	-24.65	-59.77	-45.68	-29.58	-22.23	-35.96

The results for the low earthquake suite, presented in Table 5.24, show large percentage reductions for all response metrics at each of the response levels. Average peak and permanent drifts are reduced, at the 50th percentile level, by 18.7% and 69.6% respectively, with similar reductions observed for the peak accelerations and hysteretic energies.

TABLE 5.24: SAC3-A2-1 RESULTS FOR LOW SUITE WITH LQRY CONTROLLER.

	Numerical Average				Geometric-mean/50th Percentile				84th Percentile			
	Gr	**F1**	**F2**	**F3**	**Gr**	**F1**	**F2**	**F3**	**Gr**	**F1**	**F2**	**F3**
Peak Drift (%)		-18.56	-12.80	-17.97		-20.11	-15.72	-20.18		-16.02	-9.02	-16.94
Permanent Drift (%)		-31.59	-34.82	-41.33		-53.89	-74.74	-80.28		-59.98	-72.51	-82.15
Peak Acceleration (%)		-43.09	-41.14	-23.18		-45.40	-41.18	-23.30		-42.22	-42.20	-23.61
Hysteretic Energy (%)	-57.47	-53.72	-45.03	-58.78	-99.02	-83.70	-95.58	-100.00	-82.77	-44.48	-51.22	-70.47

5.5.2.2 CLIPPED RESETABLE CONTROL

The specific details of the resetable controller for these architectures are described in Section 5.5.1, where the initial actuator architecture investigation is presented. The results for the SAC3-A2-1 architecture for the high earthquake suite are presented in Table 5.25. Peak drifts are reduced on all floors for each of the response levels, with average reductions of 7.2%, 11.0%, and 9.4% at the 50th, 65th, and 84th percentile levels, respectively. The numerical average values for permanent drifts are reduced on all floors with an average reduction of 11.0%, while values for the 50th and 84th percentile show a mixture of Case 1 and 2 distribution shifts. The absolute increase in geometric-mean floor 1 permanent drift relative to the uncontrolled case is approximately 0.1in. Geometric-mean peak accelerations increase slightly on the floors where actuators are positioned, with an average increase over all floors of 1.8%.

TABLE 5.25: SAC3-A2-1 RESULTS FOR HIGH SUITE WITH RESETABLE CONTROLLER.

	Numerical Average				Geometric-mean/50th Percentile				84th Percentile			
	Gr	**F1**	**F2**	**F3**	**Gr**	**F1**	**F2**	**F3**	**Gr**	**F1**	**F2**	**F3**
Peak Drift (%)		-12.55	-6.62	-5.36		-11.37	-5.54	-4.69		-15.05	-7.95	-5.10
Permanent Drift (%)		-10.96	-10.36	-11.59		4.24	-29.99	-29.59		-26.17	22.05	8.29
Peak Acceleration (%)		5.30	1.82	-4.15		6.34	3.30	-4.19		2.13	-3.24	-3.86
Hysteretic Energy (%)	-26.39	-19.01	-11.48	-13.66	-24.55	-20.64	-15.50	-29.22	-27.99	-15.64	-14.72	-18.99

The performance of the resetable controller with the SAC3-A2-1 architecture for the medium suite is shown in Table 5.26. Average geometric-mean permanent drift is decreased by 30.6%, with the largest reduction of 63.8% observed at floor 1. Permanent drifts at the 84th percentile level show classic Case 1 distribution shifts, with the response due to extreme events causing an increase in distribution variance. Peak acceleration is seen to increase on floors 1 and 2 where actuators are placed, while average hysteretic energy is reduced on all floors with an average geometric mean of 48.0%.

TABLE 5.26: SAC3-A2-1 RESULTS FOR MEDIUM SUITE WITH RESETABLE CONTROLLER.

	Numerical Average				Geometric-mean/50th Percentile				84th Percentile			
	Gr	**F1**	**F2**	**F3**	**Gr**	**F1**	**F2**	**F3**	**Gr**	**F1**	**F2**	**F3**
Peak Drift (%)		-11.29	-8.49	-7.37		-12.07	-9.45	-7.99		-9.45	-5.77	-6.72
Permanent Drift (%)		-23.30	-5.98	1.79		-63.75	-18.20	-9.98		11.13	19.35	43.24
Peak Acceleration (%)		19.61	4.26	-3.37		22.69	4.16	-3.23		12.05	4.39	-4.31
Hysteretic Energy (%)	-33.43	-37.81	-28.66	-28.73	-62.63	-46.27	-27.90	-54.94	-16.01	-34.95	-21.68	-15.17

The results for the low suite follow the same trend as seen for the medium suite, however larger reductions are seen in each of the performance measures. Peak accelerations decrease on floors 2 and 3 for the 50th percentile and decreased on all three floors for the 84th percentile level. In contrast to the high and medium suites, the low suite now shows Case 3 distribution

shifting, rather than the Case 1. Average geometric-mean permanent drift is decreased by 77.2%, with the largest reductions observed on floors 2 and 3.

TABLE 5.27: SAC3-A2-1 RESULTS FOR LOW SUITE WITH RESETABLE CONTROLLER.

	Numerical Average				Geometric-mean/50th Percentile				84th Percentile			
	Gr	**F1**	**F2**	**F3**	**Gr**	**F1**	**F2**	**F3**	**Gr**	**F1**	**F2**	**F3**
Peak Drift (%)		-21.44	-16.83	-11.19		-23.99	-19.76	-13.31		-19.45	-14.48	-11.26
Permanent Drift (%)		-20.57	-20.08	-28.77		-66.90	-84.51	-80.32		-62.95	-72.97	-74.75
Peak Acceleration (%)		6.65	-5.99	-7.93		13.19	-5.23	-7.46		-4.13	-8.51	-9.76
Hysteretic Energy (%)	-46.37	-68.18	-45.14	-43.12	-99.75	-99.99	-99.93	-99.96	-61.13	-55.65	-42.67	-46.89

5.5.3 SAC3-A3-1 (6:3:1) Architecture

5.5.3.1 LQRY CLIPPED OPTIMAL CONTROL

The LQRy controller used for the 6:3:1 force distribution has the same performance weighting as for the 7:3:0 distribution, but with control cost weighting factors of $R = 4.1x10^{-4}$. This slight change in state feedback gain design was necessary to maintain numerical stability of the ODE solver while still providing approximately the same magnitude of actuator authority. The impact of slight design alterations on results comparisons is important to recognise, with normalisation of results according to the work done by the controller discussed in Chapter 7.

As with the previous architectures, the 6:3:1 force distribution produces reductions in all of the performance measures at each of the response levels, other than the 84th percentile permanent drift for the third floor, which increases by 12.1% as shown in Table 5.28. The largest reduction in peak drift is observed at the first floor, while the reduction in permanent drift is largest at floor 3 for the 50th percentile level. Average geometric-mean peak

acceleration is reduced by 17.9%, with average hysteretic energy at the same response level down by 23.6%.

TABLE 5.28: SAC3-A3-1 RESULTS FOR HIGH SUITE WITH LQRY CONTROLLER.

	Numerical Average				Geometric-mean/50th Percentile				84th Percentile			
	Gr	**F1**	**F2**	**F3**	**Gr**	**F1**	**F2**	**F3**	**Gr**	**F1**	**F2**	**F3**
Peak Drift (%)		-13.06	-9.04	-11.53		-12.80	-8.57	-11.65		-13.43	-9.36	-10.63
Permanent Drift (%)		-11.85	-10.64	-10.76		-11.07	-14.64	-34.24		-11.94	-1.17	12.27
Peak Acceleration (%)		-15.64	-24.62	-12.16		-16.95	-24.51	-12.13		-11.48	-25.00	-12.45
Hysteretic Energy (%)	-27.91	-14.27	-15.36	-30.87	-26.13	-14.03	-17.72	-36.38	-30.02	-11.45	-17.79	-26.06

The results for the medium earthquake suite are shown in Table 5.29, again showing significant reductions for all of the performance measures at each of the response levels, other than the 84th percentile third floor permanent drift, which increases by 14.7%. The average 84th percentile peak drift is reduced by 11.32%, while average permanent drifts are reduced by 9.0% at the same response level. Peak accelerations are reduced by similar amounts across each of the statistical levels, implying a downward shift of the entire distribution including the extreme events situated at the tail of the distribution. The average geometric-mean hysteretic energy is reduced by over 42%, representing a large structural energy reduction for this level of near-field excitation.

TABLE 5.29: SAC3-A3-1 RESULTS FOR MEDIUM SUITE WITH LQRY CONTROLLER.

	Numerical Average				Geometric-mean/50th Percentile				84th Percentile			
	Gr	**F1**	**F2**	**F3**	**Gr**	**F1**	**F2**	**F3**	**Gr**	**F1**	**F2**	**F3**
Peak Drift (%)		-14.14	-6.95	-11.85		-13.66	-6.86	-12.25		-15.29	-7.04	-11.63
Permanent Drift (%)		-27.03	-15.59	-10.15		-40.79	-12.44	-16.78		-21.30	-20.39	14.68
Peak Acceleration (%)		-30.89	-28.53	-12.60		-31.36	-28.36	-12.32		-30.10	-29.53	-14.35
Hysteretic Energy (%)	-49.37	-28.75	-26.36	-48.35	-52.93	-30.97	-23.75	-62.30	-40.05	-27.00	-23.27	-38.64

The results obtained for the low earthquake suite show 73.7% average reductions in permanent drifts as presented in Table 5.30, with an average geometric-mean hysteretic energy reduction of 92.3%. This reduction in average hysteretic energy is significant even for the low earthquake suite, as it represents an absolute energy reductions in the order of $1x10^5$ lb-in. Average peak accelerations are reduced by 35.1% and 35.2% at the 50^{th} and 84^{th} percentile levels respectively.

TABLE 5.30: SAC3-A3-1 RESULTS FOR LOW SUITE WITH LQRY CONTROLLER.

	Numerical Average				Geometric-mean/50^{th} Percentile				84^{th} Percentile			
	Gr	**F1**	**F2**	**F3**	**Gr**	**F1**	**F2**	**F3**	**Gr**	**F1**	**F2**	**F3**
Peak Drift (%)		-17.10	-11.70	-18.02		-18.49	-14.32	-19.70		-14.85	-8.21	-17.36
Permanent Drift (%)		-30.83	-35.19	-46.29		-58.31	-78.80	-84.08		-61.35	-74.11	-83.75
Peak Acceleration (%)		-42.23	-39.74	-21.98		-43.93	-39.45	-22.02		-41.79	-41.15	-22.54
Hysteretic Energy (%)	-54.85	-50.09	-44.64	-59.69	-98.81	-80.91	-91.46	-99.99	-79.29	-43.02	-52.19	-68.55

5.5.3.2 CLIPPED RESETABLE CONTROL

The specific design of the clipped resetable controller is as described in the initial actuator architecture investigation. Table 5.31 presents the results for the high earthquake suite, with reductions in peak drift and hysteretic energy observed at all statistical response levels. Permanent drifts and peak accelerations at the 50^{th} percentile level are seen to increase slightly on the first and second floors, but decrease on the third floor. At the 84^{th} percentile level, the inverse is observed for the permanent drift, with reductions observed for the first and second floors. The absolute permanent drift increase of 1.24% corresponds to an absolute increase of 0.06in. Both peak and permanent drifts are decreased for the 65^{th} percentile level, while average geometric-mean hysteretic energy is reduced by 19.0%, with greatest reductions seen at the ground and third floors.

TABLE 5.31: SAC3-A3-1 RESULTS FOR HIGH SUITE WITH RESETABLE CONTROLLER.

	Numerical Average				Geometric-mean/50th Percentile				84th Percentile			
	Gr	**F1**	**F2**	**F3**	**Gr**	**F1**	**F2**	**F3**	**Gr**	**F1**	**F2**	**F3**
Peak Drift (%)		-10.79	-6.49	-5.80		-10.41	-5.48	-4.80		-11.62	-7.59	-6.17
Permanent Drift (%)		-6.07	-2.88	-3.89		9.64	12.82	-5.21		-20.39	-7.05	1.24
Peak Acceleration (%)		3.63	1.88	-1.41		4.25	2.98	-1.31		1.51	-1.56	-1.91
Hysteretic Energy (%)	-23.36	-17.83	-11.13	-13.48	-21.94	-18.88	-13.90	-21.33	-25.19	-12.59	-15.19	-18.33

The resetable actuator produces peak drift reductions at each of the statistical measures for the medium earthquake suite, as shown in Table 5.32. Average geometric-mean peak drifts are reduced by 9.0%, with reductions approximately equally distributed across the three floors and statistical levels. Reductions in permanent drifts differ greatly between floors, with a geometric-mean reduction of 48.6% for the first floor compared with a 14.4% increase for the third floor.

TABLE 5.32: SAC3-A3-1 RESULTS FOR MEDIUM SUITE WITH RESETABLE CONTROLLER.

	Numerical Average				Geometric-mean/50th Percentile				84th Percentile			
	Gr	**F1**	**F2**	**F3**	**Gr**	**F1**	**F2**	**F3**	**Gr**	**F1**	**F2**	**F3**
Peak Drift (%)		-10.96	-7.42	-6.74		-11.51	-8.16	-7.21		-9.60	-5.30	-6.20
Permanent Drift (%)		-20.97	-0.66	7.43		-48.55	-2.31	14.36		3.05	30.93	21.07
Peak Acceleration (%)		9.22	1.98	-2.02		11.69	1.34	-2.16		2.16	3.38	-1.29
Hysteretic Energy (%)	-34.86	-35.67	-25.68	-25.62	-60.14	-42.41	-23.11	-48.80	-19.38	-32.77	-16.89	-15.73

The structural response percentage reductions for the low earthquake suite are shown in Table 5.33. Reductions in all performance measures are observed, with almost 100% reductions in hysteretic energy at the 50th percentile level. Average geometric-mean and 84th percentile peak drift levels are both reduced by approximately 15%, showing a general reduction across

the entire distribution. Peak acceleration reductions are generally larger at the 84th percentile level than for the 50th percentile, with an average reduction of 7.7%.

TABLE 5.33: SAC3-A3-1 RESULTS FOR LOW SUITE WITH RESETABLE CONTROLLER.

	Numerical Average				Geometric-mean/50th Percentile				84th Percentile			
	Gr	**F1**	**F2**	**F3**	**Gr**	**F1**	**F2**	**F3**	**Gr**	**F1**	**F2**	**F3**
Peak Drift (%)		-19.19	-16.49	-11.99		-20.81	-18.38	-12.57		-17.49	-15.14	-13.38
Permanent Drift (%)		-22.61	-30.94	-50.42		-59.82	-79.99	-78.79		-41.11	-67.84	-78.07
Peak Acceleration (%)		2.39	-7.44	-6.11		7.74	-7.89	-5.31		-7.04	-7.08	-9.10
Hysteretic Energy (%)	-47.49	-64.02	-48.24	-43.84	-99.56	-99.98	-99.91	-99.95	-66.71	-54.29	-42.57	-44.77

5.5.3.3 JQR CLIPPED OPTIMAL CONTROL

The JQR controller used for the three-actuator architecture has uniform structural jerk performance weightings of $Q = 4$, with control cost weighting factors of $R = 1x10^{-3}$. The results for the high earthquake suite, shown in Table 5.34, indicate the effectiveness of the JQR controller with this architecture in reducing peak drifts, however, the geometric-mean permanent drift increases by 16% on the second floor. Average geometric-mean hysteretic energy is decreased by 22.2%, with similar reductions observed across all floors and statistical levels.

TABLE 5.34: SAC3-A3-1 RESULTS FOR HIGH SUITE WITH JQR CONTROLLER.

	Numerical Average				Geometric-mean/50th Percentile				84th Percentile			
	Gr	**F1**	**F2**	**F3**	**Gr**	**F1**	**F2**	**F3**	**Gr**	**F1**	**F2**	**F3**
Peak Drift (%)		-8.13	-9.15	-8.93		-7.59	-8.36	-7.70		-9.22	-10.04	-10.10
Permanent Drift (%)		-3.92	0.75	0.55		-12.51	16.27	-2.23		31.22	-1.27	23.99
Peak Acceleration (%)		11.40	-1.85	0.76		13.02	-0.58	1.30		5.49	-6.44	-3.16
Hysteretic Energy (%)	-20.11	-20.21	-21.82	-23.54	-17.61	-21.17	-23.05	-27.12	-22.08	-16.19	-25.90	-24.53

The permanent drift performance of the JQR controller for the medium suite is improved compared to the high suite, with geometric-mean reductions observed on all floors with an average reduction of 20.5% as shown in Table 5.35. The numerical average shows reductions in both peak and permanent drifts, with average reductions of 13.7% and 14.0% respectively. Though peak accelerations are increased slightly on each floor, the average geometric-mean hysteretic energy is decreased by over 50%.

TABLE 5.35: SAC3-A3-1 RESULTS FOR MEDIUM SUITE WITH JQR CONTROLLER.

	Numerical Average				Geometric-mean/50th Percentile				84th Percentile			
	Gr	**F1**	**F2**	**F3**	**Gr**	**F1**	**F2**	**F3**	**Gr**	**F1**	**F2**	**F3**
Peak Drift (%)		-16.45	-12.72	-11.81		-16.02	-13.17	-10.86		-17.38	-11.37	-14.47
Permanent Drift (%)		-23.88	-10.72	-7.48		-44.94	-4.53	-12.03		-2.71	0.20	44.99
Peak Acceleration (%)		19.67	6.91	4.32		24.73	8.43	4.79		6.06	1.79	1.14
Hysteretic Energy (%)	-47.49	-42.95	-36.45	-35.34	-52.94	-50.20	-46.27	-58.65	-38.00	-39.01	-24.11	-32.05

As shown in Table 5.36, the JQR controller produces reductions in peak and permanent drifts for the low suite across all floors and statistical measures. Average geometric-mean peak and permanent drifts are reduced by 19.6% and 78.3% respectively, while geometric-mean hysteretic energy is decreased by almost 100% on each floor level. As has been noted previously for displacement controllers, geometric-mean peak accelerations increase on each floor where an actuator is attached, with the increases corresponding to the distribution of the maximum actuator authority.

TABLE 5.36: SAC3-A3-1 RESULTS FOR LOW SUITE WITH JQR CONTROLLER.

	Numerical Average				Geometric-mean/50th Percentile				84th Percentile			
	Gr	**F1**	**F2**	**F3**	**Gr**	**F1**	**F2**	**F3**	**Gr**	**F1**	**F2**	**F3**
Peak Drift (%)		-19.08	-17.31	-14.24		-19.37	-18.76	-14.53		-19.28	-16.39	-15.58
Permanent Drift (%)		-23.16	-34.78	-54.11		-72.81	-80.73	-81.27		-72.90	-74.42	-78.58
Peak Acceleration (%)		22.10	4.46	-1.05		34.86	8.42	0.41		-1.36	-5.49	-6.53
Hysteretic Energy (%)	-53.74	-72.15	-55.42	-46.47	-99.30	-99.98	-99.95	-99.96	-42.35	-65.94	-53.69	-42.12

5.6 HYBRID CONTROL

This section briefly details the simulation of a simple base isolation system used in conjunction with the MR damper quasi-bang-bang controller for the SAC3 structure. As described in Section 4.8, the base isolator alters the response of the building by introducing an additional lower fundamental mode to the isolated structural system. The effect of this new isolator fundamental mode is to dramatically reduce the magnitude of the building's fundamental frequency. A 4:1 frequency reduction system was selected, giving a new fundamental frequency of 0.26Hz. As the simulation of base isolation is essentially a side issue of interest, the simulations were undertaken using a reduced high suite only. The five earthquakes in the reduced suite are Kobe (1995), Loma Prieta (1989), Northridge (1994), Tabas (1974), and Elysian Park (simulated).

The response of the uncontrolled passively isolated structure is presented in Table 5.37 as the percentage change from the uncontrolled, un-isolated reduced high suite response. Each of the performance measurements show very large reductions across all floors and statistical levels, with all reductions greater than 58%. The permanent drift and hysteretic energy reductions are consistently reduced by almost 100%, while average peak drifts are reduced by approximately 70% across the three statistical levels. In previous simulations the peak ground acceleration is unaffected by the controller, however, the effect of the base isolation pre-filtering is to reduced the peak ground acceleration by approximately 67%.

TABLE 5.37: SAC3 UNCONTROLLED RESULTS WITH BASE ISOLATION – REDUCED HIGH SUITE.

	Numerical Average				Geometric-mean/50th Percentile				84th Percentile			
	Gr	**F1**	**F2**	**F3**	**Gr**	**F1**	**F2**	**F3**	**Gr**	**F1**	**F2**	**F3**
Peak Drift (%)		-66.61	-65.86	-76.99		-67.22	-65.75	-76.64		-67.05	-66.80	-78.56
Permanent Drift (%)		-98.33	-98.91	-99.58		-99.06	-99.24	-99.59		-97.67	-98.99	-99.60
Peak Acceleration (%)	-67.95	-69.86	-67.64	-58.92	-67.44	-69.82	-67.21	-59.04	-69.82	-70.26	-70.08	-57.93
Hysteretic Energy (%)	-94.37	-93.55	-98.50	-100.00	-100.00	-99.99	-100.00	-100.00	-95.25	-93.85	-98.78	-100.00

The results for the hybrid base isolated semi-active control system are shown in Table 5.38. As was generally observed for the un-isolated quasi-bang-bang control simulation results, peak and permanent drifts are reduced while floor peak accelerations increase. Comparing the isolated controlled and uncontrolled results, the additional demand reductions due to the semi-active controller are relatively small compared to those attained through base isolation alone.

TABLE 5.38: SAC3 QUASI-BANG-BANG CONTROLLED RESULTS WITH BASE ISOLATION – REDUCED HIGH SUITE.

	Numerical Average				Geometric-mean/50th Percentile				84th Percentile			
	Gr	**F1**	**F2**	**F3**	**Gr**	**F1**	**F2**	**F3**	**Gr**	**F1**	**F2**	**F3**
Peak Drift (%)		-70.14	-68.50	-77.29		-71.11	-68.89	-77.17		-70.02	-68.52	-78.34
Permanent Drift (%)		-99.21	-99.58	-98.53		-99.77	-99.75	-99.70		-99.28	-99.67	-98.69
Peak Acceleration (%)	-67.95	-37.48	-60.32	-57.23	-67.44	-38.18	-60.26	-57.50	-69.82	-34.65	-61.23	-55.52
Hysteretic Energy (%)	-95.56	-95.73	-98.59	-99.95	-100.00	-100.00	-100.00	-100.00	-96.26	-96.32	-98.86	-99.95

Despite the fact that base isolators are designed to attenuate response over a specific small frequency range, the results in this section show their benefit in the control of squat shear buildings, whose response is predominantly first mode. It is expected that the benefits of the base isolation and semi-active control systems would be reversed for taller structures, as

multi-mode response becomes significant, and a small design frequency range may be insufficient.

5.7 CHAPTER SUMMARY

This chapter has presented the results for the SAC3 building using controllers and actuator architectures presented in Chapter 4. As three suites of earthquakes were used, the statistical tools utilised are important to ensure the true trends of the data are represented. Section 5.2 presented an explanation of the statistical tools used, with an explanation of why the skewed structural response is well represented by a lognormal distribution. Using the lognormal distribution, peak drift, permanent drift, peak acceleration, and hysteretic energy responses were presented as percentages of the uncontrolled response, using the 50^{th}, 65^{th}, and 84^{th} percentile levels.

Initial evaluation of the quasi-bang-bang, LQR, LQRy, resetable, and JQR controllers was undertaken using the SAC3-A1 architecture with a maximum actuator authority of 450kips, which is equivalent to 13.8% of the building weight, placed entirely between the ground and first floor. The quasi-bang-bang controller was found to generally decrease the peak and permanent drifts at each of the statistical levels, while increasing the peak floor accelerations for the high and medium suites. The LQR results followed trends similar to those observed for the quasi-bang-bang controller, with reductions in peak drift, permanent drift, and hysteretic energy, and slight increases in peak acceleration. The LQRy controller, which uses acceleration performance to design state feedback gains, was the only controller to show reductions in all of the performance measures, including acceleration. For the resetable controller, accelerations were generally found to increase only on the floor to which the actuator was attached, while reductions in peak and permanent drifts were generally seen

across all floors. Hysteretic energy reductions were lower for the JQR during the high earthquake suite, while the reductions in peak and permanent drifts were accompanied again by slight acceleration increases across all floors.

The effect of actuator architecture was presented, with the initial investigation undertaken using the resetable controller with the high earthquake suite only. This method of assessment eliminated the impact of actuator-actuator interaction on different floors. It was observed that for the SAC3 structure, which is a squat shear building with a predominantly first mode response, peak and permanent drifts reductions were larger as more actuator authority was placed at the base of the structure. In addition, it was seen that peak accelerations were reduced more when most of the actuator authority was placed at the base, with a small amount distributed onto the second and/or third floors. Hence, the SAC3-A2-1 and SAC3-A3-1 architectures were assessed using the three earthquake suites.

As was seen with the SAC3-A1 architecture, the LQRy controller reduced all of the performance measures across each floor and statistical level for both the SAC3-A2-1 and SAC3-A3-1 architectures, with the size of the reduction increasing as the earthquake magnitude decreased. The resetable actuator results showed general reductions in peak drift, permanent drift, and hysteretic energy, while the peak acceleration increased on floors 2 and 3 with the addition of actuators. The results for the JQR controller with the SAC3-A3-1 architecture showed smaller increases in peak acceleration and higher energy dissipation than for the SAC3-A1 architecture, but with smaller reductions in peak and permanent drifts.

Reduction in the numerical average, or 65^{th} percentile, were observed almost consistently across each of the performance metrics for each of the different controllers and architectures, while the 50^{th} and 84^{th} percentiles showed variety indicative of a change in distribution shape.

It is important to note that it is not so much the percentage reductions that are the critical result, but rather the characteristics of each controller and architecture with respect to the different performance measurements.

Chapter 6 presents the results for the SAC9 building simulations, using the architectures presented in Section 4.2.2, with the LQR, LQRy, and resetable actuators described in Chapter 4. The results presented in Chapters 5 and 6 are normalised and compared in Chapter 7, with conclusions made in Chapter 8.

6. SAC9 SIMULATION RESULTS

6.1 INTRODUCTION

This chapter presents the results for the SAC9 structural simulations using the clipped optimal LQR and LQRy controllers, and decentralised resetable actuators. Two actuator architectures are used in each set of simulations, the SAC9-A3 architecture with actuators attached to floors 2, 3, and 9, and the SAC9-A8 architecture, which has actuators attached to floors 2 through 9. As it is only possible to control the actuator saturation level and not the total transient work done by each of the controllers, this chapter presents the results with brief discussion of the characteristics of each individual control system only. Comparisons of control design, actuator architecture, and structural characteristics are presented in Chapter 7, where specialised normalisation techniques are utilised to provide effective means of comparison.

Due to the computational intensity of the SAC9 simulations, with the moment-resisting steel frame structure represented by 327 degrees-of-freedom, reduced odd-half (OH) earthquake suites are used. As each set of earthquakes are orthogonal pairs at 45^{o} to the fault strike, the use of one earthquake from each pair should still give an accurate representation of the different excitation characteristics within each of the three earthquake suites. As described in Section 5.2, a lognormal distribution is used to characterise the results obtained for the ten earthquakes in each suite, with the geometric-mean (50^{th} percentile), numerical average (65^{th} percentile), and the 84^{th} percentile (one standard deviation) used to identify the general trends of the distribution. All controlled system results are presented as percentages of the uncontrolled response, as detailed in Section 6.2. As the results for each suite are presented for all nine floors at the 50^{th}, 65^{th}, and 84^{th} percentile levels, the size of the tables require that they be presented at the end of this chapter, in Section 6.7, rather than within the text.

Following the presentation of the SAC9 uncontrolled structural response, details of the preliminary investigation are presented, in which general actuator architecture is assessed using the Kobe time-history record from the high, or 2% in 50 year event, suite. The results for the SAC9-A3 and SAC9-A8 architectures are then detailed, using the clipped optimal LQR and LQRy controllers, and resetable actuators.

6.2 SAC9 UNCONTROLLED RESPONSE

The uncontrolled response of the SAC9 structure was determined using the same time-history analysis as the controlled simulations, with the control input set to zero. The SAC9 controlled responses are shown as percentage changes from the absolute values presented in this section, with negative percentages representing desired response reductions.

The results for the uncontrolled SAC9 response to the OH high earthquake suite are shown in Table 6.2. Interestingly, the average response values for the SAC9 structure are somewhat lower than those for the uncontrolled SAC3 structure. This result is potentially an indication of the different response characteristics of tall buildings compared to squat shear buildings, with decreased structural constraint leading to smaller inter-story drifts and accelerations. Additionally, this effect may be exaggerated by the use of OH earthquake suites, with potential for the exclusion of a large event with a response at the tail of the lognormal distribution. However, this effect is expected to be minimal due to the presence of orthogonal pairs within each suite, although, as shown in Figure 2.3, the OH high suite has higher median spectral acceleration with slightly lower median spectral displacement over the frequency range of the SAC3 and SAC9 models. At each of the statistical levels, the peak and permanent drifts of the first floor are the largest of the nine floors. This trend is attributed to the soft first story, which is essentially used as built-in base isolation, with increased story

height acting to reduce stiffness. A reduction in story stiffness clearly explains the increase in relative displacement magnitude between the ground and the first floor.

The results for the uncontrolled OH medium and low earthquake suites are presented in Tables 6.3 and 6.4. As with the high suite, the peak drift at the first floor is the largest of all the floors, however, the permanent drifts no longer follow this trend, with maximum values seen at the top story. This trend may be indicative of the tuning of the soft first story, with maximum isolation designed for extreme near-field events, with smaller events results in significant "top-whip". This hypothesis is supported by the trend in peak accelerations, with peak first story accelerations lower than the ground acceleration for the high suite, but not for the medium and low suites.

As expected, the magnitude of the structural responses decreases as the magnitude of the earthquakes is reduced, with the largest differences observed between the high and medium suites. For the low suite, the average 65^{th} percentile structural hysteretic energy is approximately 13% of that for the medium suite, however, the average magnitude of $5.34x10^5$lb-in for this suite is still considerable. This trend is best illustrated by the 65^{th} percentile peak ground acceleration, for which the value is reduced by 35% from the high to the medium suite, but only another 13% to the low suite. Hence, this trend follows the roughly exponential decrease in input for each of the suites.

6.3 PRELIMINARY INVESTIGATION

The preliminary investigation was undertaken following initial problems encountered when control laws and actuators were in the form used for the SAC3 structure. This initial study

was undertaken using the first 30 seconds of the Kobe earthquake record, during which all of the strong motion occurs. The purpose of this initial investigation was:

i) To assess the effect of actuator-actuator interaction on different floors due to actuator reaction forces.

ii) To determine the effect of retaining the soft first story.

6.3.1 Actuator-Actuator Interaction

Simulations were first undertaken for the SAC9 structure where actuators were positioned on floors 1, 2 and 9, with LQR and resetable controllers used with the OH suites. The results obtained were marginal at best, with increases in all story drifts and small hysteretic energy reductions, or even increases, common. With the potential of these controllers already identified using the SAC3 structure, it was recognised that the different, and potentially multi-mode, response characteristics of the SAC9 structure may have a significant impact on control performance.

The residual permanently deformed shape of the uncontrolled structure gives an indication of the predominant modes within the dynamic response. As the majority of permanent deformation for each floor in the high earthquake suite occurs during a single large jolt during the strong motion of the earthquake, the deformed shape shown in Figure 6.1(b) represents the final equilibrium position about which the structure oscillates. Figure 6.1(a) shows the relative permanent story drifts, which clearly reduce above floor 3. If the response was solely first mode, one would expect the drifts to be approximately constant, as was observed for the SAC3 structure.

An interpretation of the uncontrolled response may be obtained using Figure 6.2, which shows the first four mode shapes of the SAC9 structure, using the nine degree-of-freedom lumped mass model. The permanently deformed shape shown in Figure 6.1(b) clearly does not match the first mode solely, with significant influences of second, third, and fourth modes present. To quantify the relative contributions of each mode to the overall uncontrolled response, the permanently deformed response was decomposed into its respective modal participations, and relative percentage contributions of each were calculated and presented in Table 6.1.

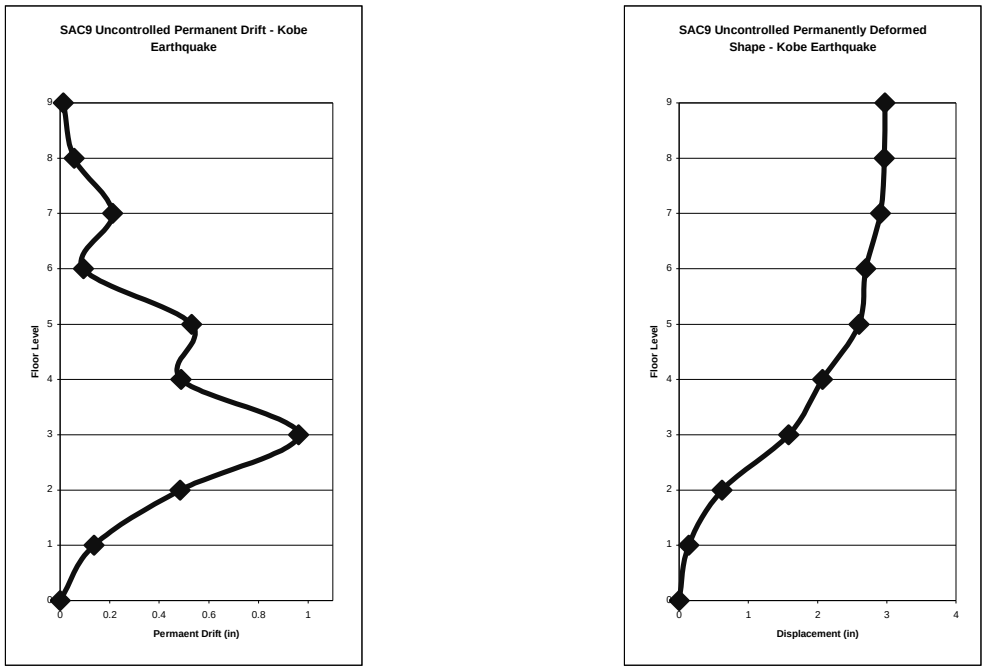

(a) (b)

Figure 6.1: SAC9 uncontrolled yielded response. (a) Permanent drifts. (b) Permanently deformed shape.

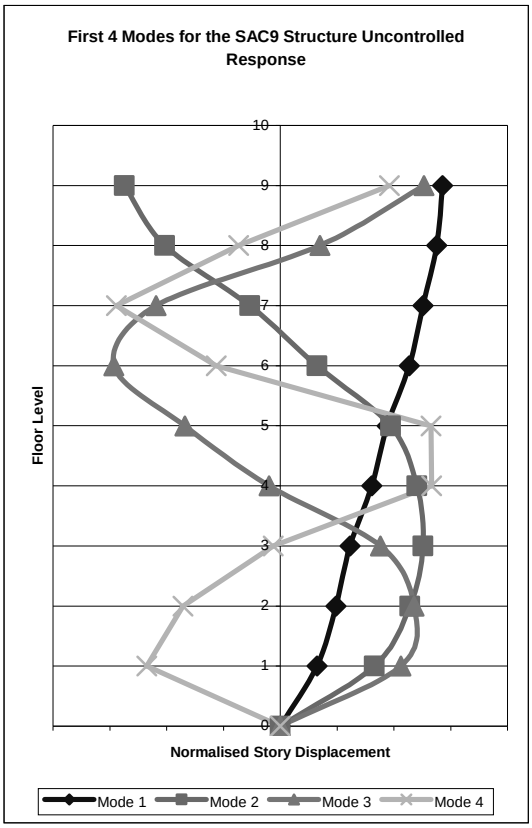

Figure 6.2: First four modes for SAC9 uncontrolled response.

TABLE 6.1: MODAL CONTRIBUTIONS TO SAC9 UNCONTROLLED PERMANENTLY DEFORMED SHAPE – KOBE EARTHQUAKE.

Mode	Contribution to Deformed Shape (%)
1	74.6
2	1.8
3	-7.7
4	6.1
5	-2.8
6	2.5
7	-0.3
8	-1.4
9	-2.8

Although the modal contributions shown in Table 6.1 are predominantly first mode, the contributions of the 2nd and particularly 3rd and 4th modes are significant, with the influence of

the third mode clearly visible in the lower stories of Figure 6.1. This influence of higher modes is the primary difference between the SAC3 and SAC9 structural responses, and requires adjustment of how the control laws are designed and implemented for the SAC9 structure.

When higher modes are present, actuators placed on adjacent floors may in fact have a negative impact due to the equal and opposite reaction forces applied to the floors on which they are placed. For example, for the resetable actuator, with higher modes present the velocity of the floors may be slightly out of phase. Hence, the decentralised controller may actually apply forces for which the reaction forces augment the response of some floors while attempting to restrict others. This effect is shown schematically in Figure 6.3, where forces F_1 and F_3 are acting to restore floors 2 and 3 back to the equilibrium position based on the relative velocities and displacements employed. However, the combination of these forces, F_2, is tending to push the second floor away from the equilibrium position. This interaction can easily occur if higher modes cause the relative velocity of floor 1 and 2 to be less than or near zero, or if their displacements are nearly equal as shown in the figure. Similar actuator-actuator interactions are expected using the LQR and LQRy controllers, as the oscillation about the higher mode deformed shape is not accounted for by the linear control design methods. In addition, with actuators on each floor reaction loads can, at best, cancel out the effect of the actuator below, and, at worst, accelerate certain floors away from their equilibrium position.

Hence, for the SAC9 structure, actuators are not placed between individual floors due to this coupling and cancelling of actuator forces through higher modal contributions. Instead, actuator authority is applied via tendons between the ground and the respective upper floors. This approach is more effective as it removes the possibility of actuator-actuator interaction,

as all measurements and reaction forces are relative to the ground. The approach eliminates the interaction, or "cross-talk", between actuators and stories that can occur, without care, when dealing with higher order modes – resulting in reduced control efficacy. This effect was seen in the SAC9 responses using both resetable and LQR controllers designed using linear models, however, the effect was minimal for the SAC3 structure due to the greater predominance of the first mode in the response.

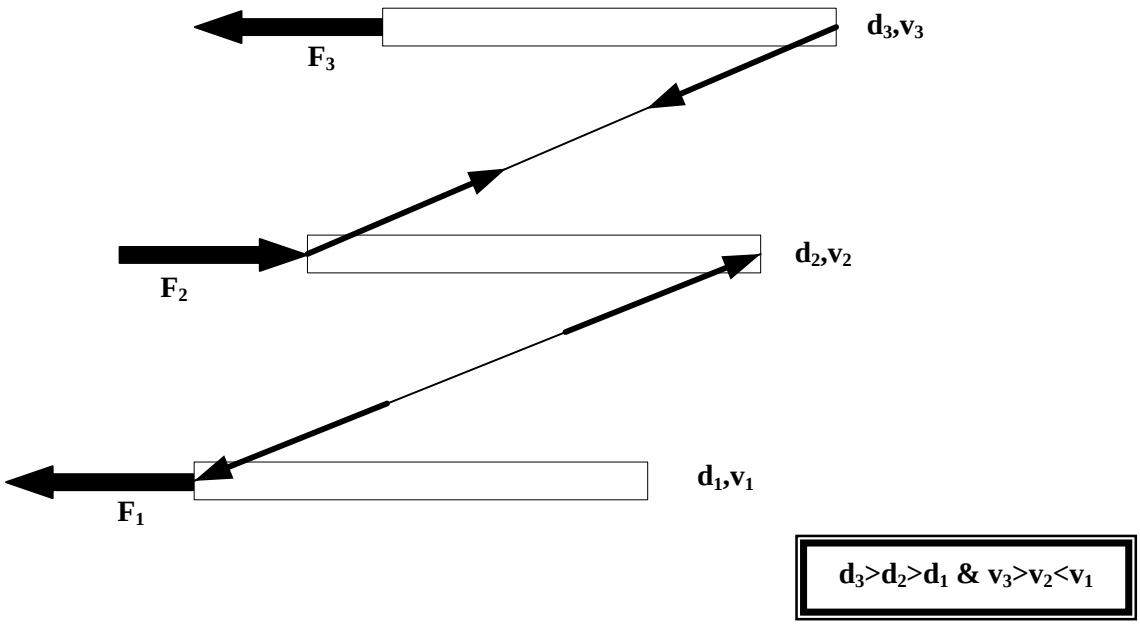

Figure 6.3: Schematic of actuator-actuator interaction for resetable controller.

6.3.2 Actuator Placement

The height of the first floor in the SAC9 structure is larger than subsequent floors, effectively reducing the first floor stiffness. Using the first 30 seconds of the Kobe earthquake record from the high earthquake suite, the effect of retaining the soft first story was briefly investigated. This was undertaken by comparing the results for actuators placed on floors 1, 3, and 9; and 2, 3 and 9, using the same actuator authority distribution for each, effectively testing the isolation ability of the soft first story verses a stiffer first story response. It was

found that the percentage changes for drifts, accelerations, and hysteretic energy were all improved when the flexibility of the soft first story was retained, hence the SAC9-A3 and SAC9-A8 actuator architectures do not directly apply control forces to the first story.

As actuator forces are applied to each story via tendons connected to actuators on the ground floor, the reduction in forces due to the tendon angle is large above the third story. The large force reduction was minimised by positioning the tendons so that they span two of the horizontal bays, effectively decreasing the force application angle. In addition, control forces and actuator authority are more effectively utilised in all architectures by employing an active tuned mass damper (ATMD) for control of the top floor of the building (floor 9), rather than using tendons.

6.4 SAC9-A3 ACTUATOR ARCHITECTURE

The SAC9-A3 control architecture has tendons attached between the ground and floors 2 and 3, with an ATMD placed on the ninth floor. To increase the effective lateral actuator authority on floors 2 and 3 the tendons span two horizontal bays, rather than just the central bay used for the SAC3 simulations. Figure 6.4 shows the architecture schematic originally presented in Chapter 4 and repeated here for clarity. The total actuator authority for each of the control architectures is 1,500kips, which represents 13.6% of the structural weight. The maximum actuator authority is distributed with 750, 450, and 200kips on the 2^{nd}, 3^{rd}, and 9^{th} floors respectively. The maximum actuator authority on floors 2 and 3 is reduced through transformation to lateral degrees-of-freedom due to the tendon angle, by factors of 0.89 and 0.81 respectively. The results for each controller are presented as percentage changes from the uncontrolled cases presented in Section 6.2, with tables located at the end of the chapter in Section 6.7.2 for clarity, due to their large size.

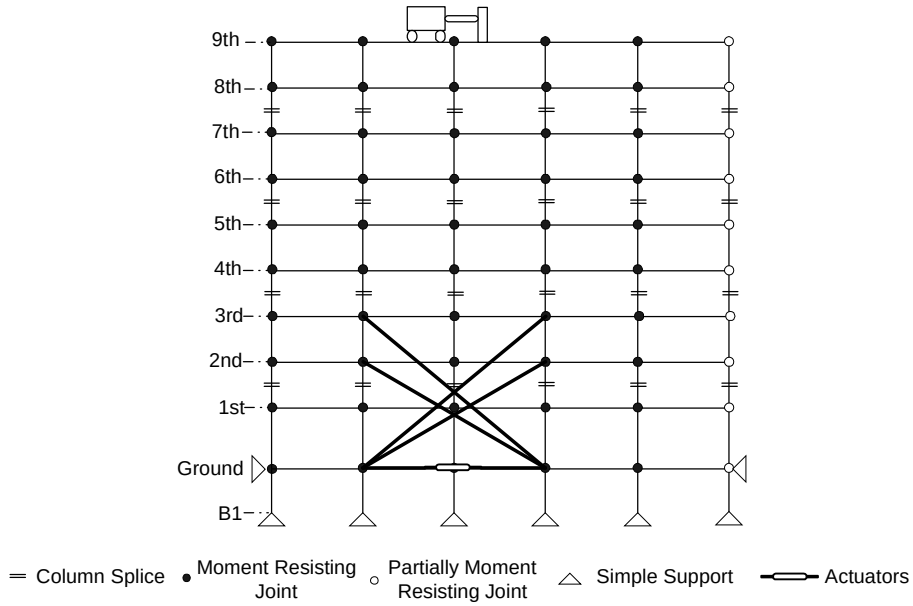

Figure 6.4: Schematic of SAC9-A3 actuator architecture.

6.4.1 LQR Clipped Optimal Control

The LQR clipped optimal controller used with this actuator architecture employs state feedback gains based on the displacements and velocities of the lateral degrees of freedom as described in Section 4.4. Displacement and velocity performance weighting factors were set at 10 and 1 respectively, with equal values for each of the lateral degrees-of-freedom. The control-cost weighting factors were uniformly set at $R = 1x10^{-3}$. These weighting factors were selected through observation of the control performance for single earthquake simulations, which was necessary due to the computational intensity of running multiple earthquake suites. As for the SAC3 structure, the LQR control design was undertaken using a reduced-order lumped mass linear model.

The results for the LQR controller with the OH high earthquake suite are shown in Table 6.5. At each of the statistical levels, peak drifts are reduced significantly on floors 1 to 4, with each reduction greater than 20%. Peak drifts increase slightly on floors 6 and 7, with

reductions seen on floors 8 and 9. This trend may relate to the influence of the third mode, which has an extremum at floor 6, at shown in Figure 6.2. Geometric-mean permanent drifts are reduced significantly on floors 1 through 4, with increases seen on the floors above. Similar trends are seen at the 65th and 84th percentile levels, perhaps indicating the presence of top-whip, despite the force applied through the ATMD. This may in part be due to the smaller ATMD force of only 200kips, or the fact that the large actuator authority on floors 2 and 3 effectively clamps the structure, causing increased motion further up the structure where no actuators are connected. Without the ATMD however, top floor permanent drifts for single earthquake simulations were seen to be much larger. Geometric-mean peak accelerations are reduced on all floors, excluding floors 1 and 9, with an average reduction of 4.3%. Average geometric-mean and 84th percentile of the hysteretic energy are reduced by 35.4% and 41.7% respectively. Overall, hysteretic energy is reduced on all floors, with floors 4 through 6 seeing less than the average reductions in specific cases. Each of the percentile levels show similar reduction trends, indicating little change in the lognormal distribution shape.

The peak drifts for the medium suite show reductions at each of the statistical levels on all nine floors, as shown in Table 6.6. Average reductions at the 50th, 65th, and 84th percentiles are 24.7%, 24.9%, and 25.4% respectively. Permanent drifts tend to increase slightly for floors 5 to 8 for the 65th and 84th percentile levels, while reductions are observed on all floors for the geometric-mean, with an average reduction of 38.2%. This result indicates an increase in the distribution variance due to relative movement of the mean and distribution tail, showing Case 1 distribution shifting as described in Section 5.2. Peak accelerations are reduced slightly on most floors for each of the statistical levels, with less than 1% increases on floors 1 and 2 for the 65th percentile, and floor 2 for the geometric-mean. Average

hysteretic energy is reduced by 81.6%, 73.9%, and 71.2% at the 50^{th}, 65^{th}, and 84^{th} percentiles levels, respectively.

The geometric-mean response values for the low suite, presented in Table 6.7, show large reductions in each of the four performance measures, with average reductions in peak drift, permanent drift, peak acceleration, and hysteretic energy of 38.9%, 90.6%, 18.8%, and 98.7% respectively. Minor increases in floor 7 and 8 permanent drifts are observed at the 65^{th} percentile level, however, the magnitude of these increases are much smaller than the reductions on other floors, and represent less than 0.02in in absolute terms. Peak accelerations are reduced for all floors at each statistical level other than the 84^{th} percentile value for floor 1, which has a 0.9% increase (2.5in/s/s). Hysteretic energy is reduced on all floors, with average reductions of 80.0%, 98.7%, and 92.1% at the 50^{th}, 65^{th} and 84^{th} percentile levels, respectively.

6.4.2 LQRy Clipped Optimal Control

The clipped optimal LQRy controller designs state feedback gains based on the acceleration performance of the lateral degrees of freedom for each floor. Control design is undertaken on a nine degree-of-freedom linear lumped mass model. Specifically, the control design has equal acceleration performance weighting factors of 1.0, with control-cost weighting factors of $R = 1x10^{-2}$. As with the optimal control implementations discussed previously, the state feedback gains employ lateral displacement and velocity degrees-of-freedom as feedback during the time-history analysis.

The results for the LQRy controller using the high earthquake suite are shown in Table 6.8. Peak drifts are reduced on all floors across the distribution, with slightly smaller reductions

observed at the 84th percentile compared to the 50th and 65th percentiles, indicating a slight Case 1 distribution shift. Average peak drifts are reduced by 19.5%, 18.4% and 14.8% at the 50th, 65th and 84th percentile levels respectively. Permanent drifts are substantially reduced in the top half of the building, however, it is at the cost of increases in the lower half for the geometric-mean values. Peak accelerations show a similar trend as the permanent drifts, with increases observed on floors 1 to 3 across the distribution, but with substantial reductions seen for floors 4 to 9. Hysteretic energy is reduced across all floors and statistical levels, with average reductions of 60.6%, 47.3%, and 41.9% seen at the 50th, 65th, and 84th percentile levels respectively.

The trends in permanent drifts and peak accelerations, observed for the high earthquake suite, can be understood through consideration of both the control law intent, and the positioning of actuators. The LQRy optimal control law is a centralised control system, in that gains are designed to minimise the global response using a global model, and not just the response of the floors to which the actuators are attached, as is the case with decentralised control using resetable devices. Initially, one might assume that this control law would then give maximum acceleration reductions where maximum actuator force is applied, as is typically the case for a decentralised controller. However, as it is the global response that is the focus of the control law, a trade-off occurs to minimise total acceleration energy of the structure. With 87% of the total actuator authority applied to floors 2 and 3, the controller applies force to these floors so that the overall response may be improved, which may result in augmented accelerations and permanent drifts on these floors due to the more complex multi-mode response of the structure. In addition, the controller minimises acceleration energy equally for each floor, therefore, the top-whip of this structure may lead to greater reductions in the objective function, J, being found in these floors at the expense of lower floors. A re-design with higher performance weighting factors, Q_{ii}, for the lower floors may help alleviate this

situation. Clearly, there is a trade-off between local and global performance, with the very difficult decision required as to which is of the most importance.

The SAC9-A3 results for the medium earthquake suite, presented in Table 6.9, show reductions in peak drifts for each floor across the response distribution. Average reductions in peak drift at the 50^{th}, 65^{th}, and 84^{th} percentile levels are 27.1%, 26.9%, and 25.9% respectively, indicating a Case 3 distribution shift, where the entire distribution is shifted to the left. Peak accelerations show the same trend as those for the high suites, with acceleration reductions observed above the third floor only. As discussed previously, this effect is potentially due the impact of applying large control forces of floors 2 and 3 only, in an attempt to control the global response using a centralised controller. Geometric-mean permanent drifts are reduced across all floors, with the largest reduction of 82.9% observed for floor 9, showing the positive effect of the ATMD positioned on the roof of the building. Large reductions in hysteretic energy are seen on all floors, with reductions of 83.9%, 77.8%, and 71.4% at the 50^{th}, 65^{th}, and 84^{th} percentile levels respectively.

The SAC9-A3 response for the low earthquake suite is presented in Table 6.10. The most significant reductions across the entire response distribution are seen in permanent deformations and hysteretic energy. Average geometric-mean permanent drift and hysteretic energy reductions are 93.9% and 99.4% respectively, with values at the 84^{th} percentile of 93.4% and 99.4% respectively. Peak drifts are reduced at all floors, with average reductions of 41.2%, 44.7% and 35.3% respectively. Peak accelerations show trends similar to those for the high suite, with reductions of over 45% seen above floor 3, and lower, or smaller positive, values on the lower floors. The contrast in permanent drifts between the high and low suites is due to the reduced excitation magnitude, with the magnitude of the low suite generally insufficient to cause large scale yielding.

6.4.3 Clipped Resetable Control

In preliminary investigations the resetable actuator controllers were most affected by actuator-actuator interactions, due to their dependence on relative floor velocities. These effects were mitigated through the use of tendons attached between the ground and controlled floors, as described in Section 6.3.1. In order to reduce the effect of top-whip, while maintaining practical applicability of tendon use, an ATMD is placed on the top floor, as has already been implemented in existing structures [Chase and Smith 1995(a), Housner et al. 1997]. The ATMD is controlled using the LQR clipped optimal control method, which is effective in mitigating peak drifts through to its focus on displacement performance, as was proven for the SAC3 structure, creating a hybrid control system architecture. Specifically, the resetable controller for the second and third floors has displacement dead bands of 0.1 and 0.2in respectively, with spring stiffness of 750,000lb/in and 367,000lb/in giving maximum actuator authority at 1.0 and 1.5in respectively. These actuators are clipped at 750kips and 550kips, respectively, to ensure a total maximum actuator authority of 1,500kips with the 200kip ATMD. The ATMD LQR controller has displacement and velocity performance weightings of 10 and 1 respectively for each lateral degree-of-freedom, with a control-cost weighting factor of $R = 1x10^{-8}$.

The results for the high earthquake suite, shown in Table 6.11, show reductions in peak drift for all floors at each of the three statistical levels, with the exception of the 84th percentile for floor 6, which shows a 1.8% (0.05in) increase. The geometric-mean permanent drifts show reductions at each floor other than floor 3, with an average reduction across all floors of 27.0%. Permanent drifts at the 65th and 84th percentile levels show increases at each of the floors, excluding floors 2 and 9, which reduce by more than 10%. This reduced geometric-mean with increased upper percentiles is Case 1 distribution shifting, with an increase in

distribution variance due to the combination of a decreased geometric-mean and low reductions for responses at the tail of the lognormal distribution. Peak accelerations show a general increase across the distribution, with significantly greater increases on floors 2 and 3 where the resetable actuators are attached. The hysteretic energy is reduced on all floors, with average reductions of 52.8%, 49.3%, and 42.8% at the 50^{th}, 65^{th} and 84^{th} percentile levels.

The response of this structure to the medium earthquake suite is much improved over that for the high suite, with general reductions in both peak and permanent drifts observed across all levels of the distribution. As shown in Table 6.12, average geometric-mean peak and permanent drifts are reduced by 33.5% and 76.6% respectively, while average hysteretic energy is reduced by 86.7%. Similar reductions are observed at the higher levels of the distribution, other than for floor 1 permanent drifts, which increase by 54.5% (0.1in) and 168.5% (1.1in) at the 65^{th} and 84^{th} percentile levels respectively. Although the soft first story adds isolation advantages, a problem is created when the floors directly above it are controlled with decentralised actuator forces, as the soft first story may have very large drifts due to the high stiffness of the controlled floors above, and lack of centralised design to account for this effect. As this effect is only observed above the 65^{th} percentile of the distribution, it appears that this first floor drift augmentation only occurs during the extreme events within the suite, with the majority of responses resulting in first floor permanent drift reductions. This effect was not as predominant in the high earthquake suite, as the other reductions within the distribution were smaller, so the stretching of the distribution is less clear. Peak accelerations are generally increased, with greatest increases on the resetable actuated floors, while hysteretic energy is reduced by an average of 50% across all floors and distribution levels.

The results for the low earthquake suite are presented in Table 6.13. The peak and permanent drifts show significant reductions across all floors, with similar reductions obtained at the

50th, 65th, and 84th percentile levels, indicating a Case 3 distribution shift where the response is improved for both small and large events within the earthquake suite. Average geometric-mean peak and permanent drifts are reduced by 55.2% and 92.4% respectively. As was observed with the high and medium suites, peak accelerations show a general increase across the distribution, with the largest increases seen at the second and third floors where actuator tendons are attached. This increase in accelerations appears to be the primary deficiency with the combination of the resetable actuator decentralised controller and ATMD architecture with actuators attached to floors 2, 3, and 9 only. Hysteretic energy reductions are observed on each floor, despite having actuators attached to only floors 2, 3, and 9. Hysteretic energy is reduced by an average of 99.7%, 89.5%, and 92.8% at the 50th, 65th, and 84th percentiles respectively, showing the effective energy dissipation ability of the resetable actuator.

6.5 SAC9-A8 ACTUATOR ARCHITECTURE

The SAC9-A8 actuator architecture has actuator forces applied to the structure on floors 2 through 9. Actuators are placed on the ground floor and connected to floors 2 through 8 via tendons, while an ATMD is placed on floor 9. As with the SAC9-A3 architecture, the actuator tendons span two horizontal bays, effectively reducing the angle at which actuator forces are applied. However, the maximum actuator authority applied to the structure is still dependent on the actuator angle, with reductions increasing as the floor height and resulting angle increase. A schematic of the SAC9-A8 actuator architecture is repeated in Figure 6.5 for clarity. The maximum actuator authority is maintained at 1500kips, which is equivalent to 13.6% of the structural weight. Actuator forces are distributed with maximum forces of 450kips and 350kips applied on floors 2 and 3 respectively, with 100kips allotted to floors 4 to 8, and 200kips reserved for the ATMD on the ninth floor. Each of these values will be

reduced by the cosine of the tendon angle for the specific floor. Result tables for the SAC9-A8 architecture are presented in Section 6.7.3.

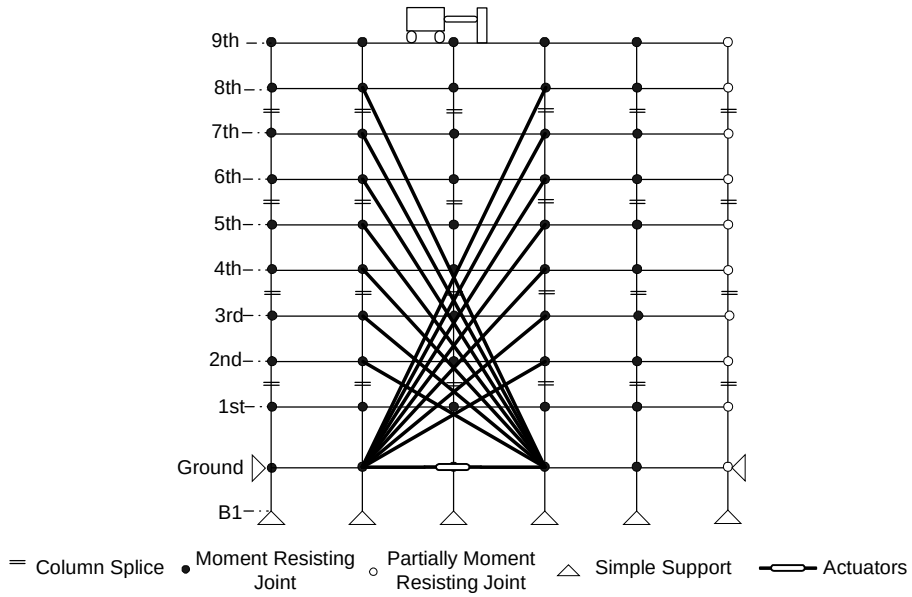

Figure 6.5: Schematic of SAC9-A8 actuator architecture.

6.5.1 LQR Clipped Optimal Control

The LQR clipped optimal controller used for the SAC9-A8 actuator architecture has the same performance and control-cost weighting factors as that for the SAC9-A3 architecture presented in Section 6.4.1. Different weighting are included in the $\mathbf{B_1}$ control input matrix, to account for the distribution of actuator authority up the height of the structure in the control design. Control design was undertaken using a nine degree-of-freedom lumped model, with state feedback gains applied to the lateral degrees-of-freedom in the time-history analysis.

The results for the high earthquake suite are presented in Table 6.14. Peak drift reductions are observed on all floors other than floor 6 at the 84th percentile level, which has a 1.43% (0.04in) increase. Average peak drift reductions are 12.3% at the 50th and 65th percentile

levels, and 11.8% for the 84th percentile. Results for the permanent drifts are mixed, with largest reductions observed for the smaller earthquakes within the suite. Peak accelerations are reduced slightly on floors 2 to 8 across the distribution, except for floor 2 at the 84th percentile level, which has a small increase of 2.2% (8.3in/s/s). Hysteretic energy is reduced on all floors for each of the statistical levels, with average reductions of 31.7%, 32.1%, and 35.5% at the 50th, 65th and 84th percentiles, respectively.

Trends similar to those observed for the high suite are seen for the medium earthquake suite, as shown in Table 6.15. Average peak drifts are reduced across all floors and statistical levels, with largest reductions observed on floors 2 and 3 where actuator authority is greatest. The geometric-mean permanent drifts are reduced on all floors except floor 5, with an average reduction of 19.6%, while the 84th percentile shows Case 1 distribution shifting. Peak accelerations are reduced on floors 1 through 8, while floor 9 shows an average increase of 2.0% across the distribution. Again, hysteretic energy is reduced at all levels of the distribution, with average reductions of 67.0%, 64.4% and 61.4% at the 50th, 65th and 84th percentiles respectively.

As shown in Table 6.16, the results for the low earthquake suite show significant reductions in peak drift, peak accelerations, and hysteretic energy at all levels, while permanent drift is significantly reduced for all measures, other than for floors 8 and 9 at the 65th percentile level. Average geometric-mean peak and permanent drifts are reduced by 31.4% and 83.8% respectively, while average accelerations and hysteretic energy are reduced by 14.1% and 96.4% at the same statistical level. At the 84th percentile, average permanent drifts are reduced by 76.3%, while hysteretic energy is reduced by 86.3% on average.

6.5.2 LQRy Clipped Optimal Control

The centralised clipped optimal LQRy controller designs state feedback gains based on the acceleration performance of the lateral degrees of freedom for each floor. Control design is undertaken on a nine degree-of-freedom linear lumped mass model. Due to numerical difficulties experienced with MATLAB's differential equation solver, small gain adjustments were required to obtain solutions for each of the three suites. Although the gains for each suite are still within the same order of magnitude, comparison of the percentage reductions for each suite presented in Tables 6.17 to 6.19 should not be undertaken in absolute terms, however, the normalised results presented in Chapter 7 do allow performance comparisons of average responses to be made. For each of the suites, equal acceleration performance weighting factors of 1 were used, with control cost weighting factors of $9x10^{-3}$, $1x10^{-3}$, and $2x10^{-3}$, used for the high, medium, and low suites respectively. As with the optimal control implementations discussed previously, the state feedback gains employ lateral displacement and velocity degrees-of-freedom as feedback during the time-history analysis.

The structural response for the high earthquake suite is presented in Table 6.17. Peak drifts are reduced on all floors for each of the statistical levels, with average reductions of 17.7%, 16.7%, and 13.5% for the 50^{th}, 65^{th}, and 84^{th} percentiles respectively. Permanent drifts show a Case 1 distribution shift, with reductions observed for floors 2 to 9 at the 50^{th} percentile, but increases for floors 3 to 8 at the 84^{th} percentile. It should be noted that through the tracking of the time-varying equilibrium position, increases in permanent drift for the most extreme excitations might be expected, as control forces are not applied to re-yield the structure back to the equilibrium position. However, the average geometric-mean permanent drift is still reduced by over 14%. Peak accelerations are reduced on all floors except floor 2, where the largest actuator authority is assigned. Average peak accelerations are reduced by 12.6%,

11.2%, and 6.4% at the 50th, 65th, and 84th percentile levels, respectively. Hysteretic energy is substantially reduced on all floors across the response distribution, indicating a reduction in total yielding energy, despite the increased permanent drifts at the tail of the distribution. Hysteretic energy reductions at the 50th, 65th, and 84th percentile are, on average, 53.6%, 44.6%, and 42.5%, respectively.

The results for the medium earthquake suite, presented in Table 6.18, show large reductions in peak and permanent drifts for all floors, across the entire response distribution. Average geometric-mean reductions for peak and permanent drifts are 40.4% and 80.3% respectively, with largest peak drift reductions observed at positions of largest actuator authority. Peak accelerations at the 50th and 65th percentile levels show similar trends to those observed previously, with increased peak acceleration on floors 2 and 3, where over 50% of the actuator authority is assigned. Potentially, this effect may be reduced by a more even distribution of actuator authority onto the upper floors of the building. The peak accelerations at the 84th percentile increase slightly for the upper floors, indicating a Case 1 distribution shift due to a very large event within the suite. Hysteretic energy is substantially reduced across all floors at each of the statistical levels, with all reductions greater than 84%. Hence, despite the difficulty with acceleration reductions for this structure, from both the drift and hysteretic energy values it can be seen that the structural damage reduction is extensive using the LQRy controller.

Reductions in peak drift, permanent drift, and hysteretic energy are extensive for the SAC9-A8 control architecture with the low earthquake suite, as presented in Table 6.19. Average reductions in permanent drifts at the 50th, 65th, and 84th percentiles are 93.9%, 77.6%, and 92.9% respectively, with the largest reductions generally seen in the lower half of the structure. Peak accelerations follow the same trend as previously discussed, with reductions

observed away from floors 2 and 3. Reductions in hysteretic energy are in excess of 90% on average, indicating appreciable reductions in hysteretic yielding energy within the structure.

6.5.3 Clipped Resetable Control

The decentralised clipped resetable controller has tendons connecting floors 2 through 8 to the actuators placed on the ground, with an ATMD placed on the roof of the building in an attempt to control the effect of top-whip, which is especially prevalent when actuators effectively increase the stiffness of floors below. The ATMD is controlled using the clipped optimal LQR control law, which designs state feedback gains to primarily mitigate floor displacements. Specifically, the resetable controller has displacement dead bands of 0.1in and 0.2in for floors 2 and 3, and 0.3in and 0.4in for floors 4 through 6 and 7 through 9, respectively. Spring stiffnesses were adjusted to provide maximum actuator authority at appropriate displacements during strong earthquake motion. The ATMD LQR controller has displacement and velocity performance weightings of 100 and 10 respectively for each lateral degree-of-freedom, with a control-cost weighting factor of $R = 1x10^{-8}$. Hence, this control architecture is a hybrid system of decentralised resetable actuators and a single ATMD on the roof.

The results for the high earthquake suite are presented in Table 6.20, showing significant reductions in peak drift, with average reductions of 23.0%, 20.3% and 13.8% at the 50^{th}, 65^{th} and 84^{th} percentile levels respectively. Geometric-mean permanent drifts are reduced for all floors, with an average reduction of over 46%. Peak accelerations for floors 5, 7, and 8 are reduced across the distribution, while the other floors experienced increased peak accelerations. Hysteretic energy is reduced on all floors across the distribution, with average reductions of 46.4%, 43.0% and 43.1% at the 50^{th}, 65^{th} and 84^{th} percentile levels. This Case 3

energy distribution shift indicates a reduction in total structural energy for all levels and characteristics of seismic events within the suite.

For the medium suite, peak and permanent drifts are reduced on all floors across the response distribution, as presented in Table 6.21. Reductions in peak drifts are approximately uniform across the distribution, with average reductions of 38.6% across the floors. The reductions in permanent drifts are largest at the 50^{th} percentile level, with an average reduction of 90.1%, however, reductions at the 65^{th} and 84^{th} percentiles as still significant, at 48.1% and 60.9% respectively. As has been observed previously for the high suite, peak accelerations show a general increase across the distribution, while hysteretic energy is reduced by 97.9%, 91.0% and 88.3% at the 50^{th}, 65^{th} and 84^{th} percentiles respectively.

The results for the low earthquake suite, presented in Table 6.22, show reductions in each of the performance measures. Average geometric-mean peak and permanent drifts are reduced by 56.4% and 91.9% respectively, with similar reductions observed at the 65^{th} and 84^{th} percentile levels. Peak accelerations are increased slightly for floors 1, 2 and 3, while reductions are observed for each of the floors above. Averaging across the floors, the geometric-mean peak acceleration is reduced by 2.2%, while slightly smaller reductions are observed at the 65^{th} and 84^{th} percentile levels. Reductions in hysteretic energy are extensive across the response distribution, with average reductions of 99.8%, 84.1% and 92.9% at the 50^{th}, 65^{th}, and 84^{th} percentiles respectively.

6.6 CHAPTER SUMMARY

This chapter has presented the results for the SAC9 structure, using the centralised LQR and LQRy clipped optimal controllers, and the decentralised resetable actuator. Two control

architectures were used in the SAC9 simulations, the SAC9-A3 architecture, with actuator authority applied to floors 2, 3, and 9, and the SAC9-A8 architecture, with actuator authority applied to floors 2 through 9. The maximum actuator authority was maintained at 1500kips for each of the different controllers and architectures, which represents 13.6% of the structural weight. This limitation helps maintains the practical applicability of the controllers developed.

An initial investigation into actuator architectures was presented, with the effect of actuator-actuator interaction and the retainment of the soft first story investigated. Due to the contributions of higher modes within the SAC9 structural response, the interaction of adjacent actuators may in fact act to augment the response of the common story, as was illustrated for the decentralised resetable actuator. This type of interaction was eliminated through the use of tendons connected between actuators on the ground floor, and the upper stories to which control forces are applied. In order to reduce the tendon angle and the subsequent reduction in lateral actuator forces, tendons span two horizontal bays. Also, rather than using long tendons connected to the 9^{th} floor, an ATMD is positioned on the roof of the structure, and controlled using clipped optimal control. Investigations using the Kobe earthquake record from the high suite showed that the retainment of the soft first story was beneficial to the global response through the base isolation characteristics of the story, however, subsequent full simulations found that the response of the first story was at times increased due to the control of the stories above.

The SAC9-A3 control architecture was assessed using the LQR and LQRy clipped optimal controllers, and the decentralised resetable actuator. The results presented for each controller showed reductions in peak drifts across the response distributions for all three earthquake suites. For the LQR clipped optimal controller, permanent drifts were seen to increases

slightly on uncontrolled floors for the high suites, while slight reductions in peak accelerations were generally observed across all three suites. High and medium suite peak accelerations were seen to increase on floors 2 and 3 for the LQRy clipped optimal controller, where the majority of the actuator authority was assigned. Although the LQRy control design is intended to reduce the global accelerations, a trade off exists between the accelerations of the floors where the actuator authority is located, and those for the structure as a whole. The decentralised resetable actuator was effective in reducing both peak and permanent drifts across the response distributions for all three earthquake suites, with the exception of the first floor, which is potentially due to the retainment of the soft first story. Peak accelerations were seen to increase across all floors using the resetable actuator. Extensive reductions in hysteretic energy were observed for each of the controllers across the three earthquake suites, indicating the effective energy dissipation ability of each of the controllers.

Results were presented for the SAC9-A8 control architecture using the LQR and LQRy clipped optimal controllers, and the decentralised resetable controllers. As with the SAC9-A3 control architecture, reductions in peak drifts were observed for each of the controllers for all three earthquake suites. For the LQR controller high suite response, a mix of increased and decreased permanent drifts were observed at each of the statistical levels, while reductions were generally observed for the medium and low suites. Small reductions in acceleration were observed for most floors for the LQR controller, with any increases occurring at either floor 1 or floor 9. The LQRy controller produced reductions in permanent drifts for the medium and low suites, while a Case 1 distribution shift was observed for the high suite. Peak accelerations are reduced at each of the floors for the LQRy controller, with the exception of floors 2 and 3, where the largest proportion of actuator authority is assigned. Permanent drifts for the resetable controller show Case 1 distribution shifts for the high suite, while universal reductions are observed for the medium and low suites. For the high and

medium suites, the resetable actuator produced small increases in peak accelerations, as was observed for the SAC9-A3 control architecture. Large hysteretic energy reductions are observed for each of the controllers, approximately independent of the location of maximum actuator authority.

The results presented in Chapters 5 and 6 are normalised and discussed in the following chapter. In order to obtain valid comparisons between controllers and control architectures, normalisation of the results is required, as although maximum actuator authority was identical for each controller, the controllers do not operate at this level continuously. Two normalising techniques are presented in Chapter 7, the first using the change in hysteretic energy between controlled and uncontrolled responses as a representation of actuator effort, and the second using the $\mathbf{L_2}$-norm of the control input, u(t).

6.7 SAC9 RESULT TABLES

This section presents the results for the SAC9 control simulations as referred to previously within the Chapter 6. This sections is divided into three primary sections: SAC9 uncontrolled results, SAC9-A3 results, and SAC9-A8 results.

6.7.1 SAC9 Uncontrolled Result Tables

TABLE 6.2: SAC9 UNCONTROLLED RESPONSE FOR ODD-HALF HIGH SUITE.

	GR	F1	F2	F3	F4	F5	F6	F7	F8	F9
Numerical Average/65th percentile										
Peak Drift (in)		5.95	2.63	5.07	2.67	4.43	2.02	4.11	2.69	4.31
Permanent Drift (in)		1.27	0.56	0.96	0.53	1.10	0.62	0.98	0.59	1.12
Peak Acceleration (in/s/s)	331.57	306.47	293.04	289.84	279.91	307.32	300.11	315.47	295.47	308.50
Hysteretic Energy (lb-in)	3.7E+06	1.6E+07	1.5E+07	1.6E+07	1.1E+07	7.9E+06	4.2E+06	9.7E+06	7.8E+06	2.2E+06
Geometric-Mean/50th percentile										
Peak Drift (in)		5.38	2.34	4.50	2.38	4.04	1.90	4.04	2.64	4.18
Permanent Drift (in)		0.61	0.37	0.55	0.34	0.58	0.39	0.71	0.39	0.59
Peak Acceleration (in/s/s)	313.62	298.98	286.08	280.70	272.94	303.98	295.38	306.95	286.08	304.91
Hysteretic Energy (lb-in)	2.0E+06	1.3E+07	9.6E+06	1.0E+07	6.7E+06	5.8E+06	3.5E+06	7.9E+06	5.2E+06	1.1E+06
84th Percentile										
Peak Drift (in)		8.38	3.85	7.42	3.92	6.31	2.72	4.91	3.21	5.44
Permanent Drift (in)		2.85	1.28	2.19	1.08	2.37	1.17	1.73	1.23	3.18
Peak Acceleration (in/s/s)	450.77	376.62	360.00	368.77	346.67	355.16	356.20	393.51	374.49	357.45
Hysteretic Energy (lb-in)	3.9E+06	2.5E+07	2.5E+07	2.8E+07	2.1E+07	1.3E+07	6.3E+06	1.5E+07	1.1E+07	3.2E+06

TABLE 6.3: SAC9 UNCONTROLLED RESPONSE FOR ODD-HALF MEDIUM SUITE.

	GR	F1	F2	F3	F4	F5	F6	F7	F8	F9
Numerical Average/65th percentile										
Peak Drift (in)		3.70	1.52	2.85	1.57	2.67	1.33	2.99	2.02	3.24
Permanent Drift (in)		0.20	0.15	0.31	0.17	0.27	0.21	0.48	0.32	0.58
Peak Acceleration (in/s/s)	214.76	219.07	223.84	204.89	204.82	205.76	221.37	221.34	226.47	271.99
Hysteretic Energy (lb-in)	9.6E+05	9.6E+06	6.3E+06	8.3E+06	5.1E+06	3.1E+06	1.0E+06	3.7E+06	2.5E+06	4.3E+05
Geometric-Mean/50th percentile										
Peak Drift (in)		3.52	1.44	2.72	1.50	2.56	1.28	2.90	1.97	3.14
Permanent Drift (in)		0.08	0.06	0.13	0.07	0.10	0.07	0.25	0.21	0.32
Peak Acceleration (in/s/s)	203.72	210.84	216.23	201.29	199.89	202.91	217.18	215.20	220.23	269.73
Hysteretic Energy (lb-in)	5.5E+03	9.7E+06	6.6E+06	9.5E+06	4.9E+06	2.1E+06	6.3E+05	3.5E+06	2.0E+06	4.0E+05
84th Percentile										
Peak Drift (in)		4.86	2.09	3.79	2.07	3.46	1.72	3.77	2.50	4.12
Permanent Drift (in)		0.64	0.56	1.39	0.82	0.69	0.47	1.01	0.56	1.10
Peak Acceleration (in/s/s)	285.46	279.82	283.97	246.15	250.79	240.91	267.33	276.05	284.38	308.60
Hysteretic Energy (lb-in)	4.0E+05	1.5E+07	1.0E+07	1.6E+07	8.5E+06	5.8E+06	2.3E+06	5.0E+06	3.5E+06	8.3E+05

TABLE 6.4: SAC9 UNCONTROLLED RESPONSE FOR ODD-HALF LOW SUITE

	GR	F1	F2	F3	F4	F5	F6	F7	F8	F9
Numerical Average/65th percentile										
Peak Drift (in)		2.54	0.86	1.59	0.89	1.57	0.90	2.03	1.35	2.28
Permanent Drift (in)		0.10	0.06	0.13	0.07	0.09	0.05	0.10	0.08	0.17
Peak Acceleration (in/s/s)	175.56	163.90	178.86	167.60	168.41	176.97	172.98	184.62	172.37	237.28
Hysteretic Energy (lb-in)	1.4E+03	1.3E+06	1.5E+05	4.1E+05	1.5E+05	9.6E+04	1.6E+05	1.3E+06	1.4E+06	4.4E+05
Geometric-Mean/50th percentile										
Peak Drift (in)		2.49	0.84	1.55	0.87	1.53	0.88	1.95	1.26	2.09
Permanent Drift (in)		0.04	0.02	0.04	0.02	0.03	0.01	0.01	0.01	0.02
Peak Acceleration (in/s/s)	148.65	149.86	166.17	159.08	158.86	164.32	165.19	173.03	164.11	229.85
Hysteretic Energy (lb-in)	8.4E+02	3.3E+05	3.3E+04	5.2E+05	1.2E+04	1.9E+03	6.6E+02	3.4E+05	7.4E+04	8.4E+01
84th Percentile										
Peak Drift (in)		3.03	1.06	1.96	1.10	1.91	1.11	2.62	1.85	3.17
Permanent Drift (in)		0.18	0.13	0.34	0.17	0.18	0.04	0.17	0.18	0.24
Peak Acceleration (in/s/s)	283.72	232.74	247.28	222.42	225.50	242.80	223.96	251.13	227.25	299.52
Hysteretic Energy (lb-in)	2.5E+03	3.0E+06	3.1E+05	7.5E+05	3.3E+05	1.7E+05	5.9E+04	3.0E+06	1.9E+06	1.2E+05

6.7.2 SAC9-A3 Result Tables

TABLE 6.5: SAC9-A3 RESULTS FOR ODD-HALF HIGH SUITE WITH LQR CONTROLLER.

	GR	F1	F2	F3	F4	F5	F6	F7	F8	F9
Numerical Average/65th percentile										
Peak Drift (%)		-36.55	-29.66	-21.31	-12.88	-2.55	9.24	0.25	-9.41	-7.80
Permanent Drift (%)		-51.42	-34.67	-2.82	24.98	28.38	45.18	36.72	33.62	15.15
Peak Acceleration (%)		5.89	-3.41	-9.65	-7.49	-9.55	-0.08	-9.50	-3.63	5.88
Hysteretic Energy (%)	-85.57	-63.30	-52.08	-36.98	-28.64	-11.47	-1.43	-35.13	-35.85	-22.74
Geometric-Mean/50th percentile										
Peak Drift (%)		-33.82	-27.18	-19.68	-12.39	-6.22	1.10	-2.12	-10.03	-8.92
Permanent Drift (%)		-41.20	-35.34	-29.44	-40.05	10.15	-12.24	29.82	52.80	45.81
Peak Acceleration (%)		4.91	-4.69	-10.89	-8.35	-10.49	-0.80	-10.31	-3.82	6.12
Hysteretic Energy (%)	-96.37	-67.78	-46.79	-21.52	-0.59	-8.79	-15.85	-33.04	-37.07	-26.44
84th Percentile										
Peak Drift (%)		-39.97	-32.01	-22.25	-12.50	2.78	22.51	10.48	-5.73	-4.51
Permanent Drift (%)		-55.54	-45.25	36.53	83.55	20.79	138.71	63.17	22.89	-12.44
Peak Acceleration (%)		10.35	0.98	-7.03	-4.15	-4.83	3.23	-6.66	-3.39	4.79
Hysteretic Energy (%)	-92.05	-58.26	-52.08	-42.49	-36.62	-23.65	-7.47	-41.86	-38.37	-23.69

TABLE 6.6: SAC9-A3 RESULTS FOR ODD-HALF MEDIUM SUITE WITH LQR CONTROLLER.

	GR	F1	F2	F3	F4	F5	F6	F7	F8	F9
Numerical Average/65th percentile										
Peak Drift (%)		-29.08	-37.25	-33.36	-26.81	-22.67	-17.52	-13.92	-19.78	-23.43
Permanent Drift (%)		-42.47	-42.23	-24.26	-14.72	6.73	-8.54	2.36	3.72	-18.70
Peak Acceleration (%)		0.60	0.18	-5.77	-8.21	-2.30	-7.01	-12.09	-8.55	-0.38
Hysteretic Energy (%)	-97.90	-81.24	-88.22	-79.19	-76.29	-74.07	-47.82	-56.02	-63.58	-74.11
Geometric-Mean/50th percentile										
Peak Drift (%)		-27.54	-36.09	-32.31	-25.95	-22.60	-18.66	-15.33	-20.42	-23.12
Permanent Drift (%)		-63.04	-57.91	-47.91	-73.15	-16.07	-29.37	-10.82	-18.42	-26.89
Peak Acceleration (%)		-0.69	0.28	-6.19	-7.88	-2.78	-6.16	-11.69	-8.38	-0.31
Hysteretic Energy (%)	-84.08	-88.54	-96.40	-85.22	-85.40	-90.45	-85.83	-46.14	-54.10	-99.69
84th Percentile										
Peak Drift (%)		-32.38	-40.11	-36.84	-29.86	-23.02	-14.48	-9.28	-17.78	-24.68
Permanent Drift (%)		-17.99	-42.94	-33.49	-22.71	43.65	3.53	7.58	16.81	-10.90
Peak Acceleration (%)		2.93	-0.48	-4.84	-9.61	-0.20	-11.74	-13.63	-9.27	-0.63
Hysteretic Energy (%)	-99.36	-76.94	-90.82	-76.53	-71.86	-67.32	-46.17	-54.08	-60.41	-68.01

TABLE 6.7: SAC9-A3 RESULTS FOR ODD-HALF LOW SUITE WITH LQR CONTROLLER.

	GR	F1	F2	F3	F4	F5	F6	F7	F8	F9
Numerical Average/65th percentile										
Peak Drift (%)		-43.02	-43.90	-39.00	-36.46	-37.06	-34.63	-32.13	-29.70	-25.36
Permanent Drift (%)		-97.50	-98.04	-92.97	-95.40	-95.52	-64.90	-8.65	18.04	2.87
Peak Acceleration (%)		-2.55	-13.77	-14.91	-20.32	-19.02	-12.98	-19.84	-20.03	-22.86
Hysteretic Energy (%)	-96.36	-99.79	-99.85	-93.24	-99.88	-99.74	-69.06	-65.20	-53.72	-23.29
Geometric-Mean/50th percentile										
Peak Drift (%)		-45.37	-45.13	-41.03	-38.15	-38.62	-37.72	-36.94	-35.12	-32.01
Permanent Drift (%)		-97.51	-97.57	-96.35	-96.41	-95.45	-85.64	-75.88	-85.69	-85.12
Peak Acceleration (%)		-3.86	-15.51	-18.33	-23.28	-20.38	-16.90	-23.12	-21.64	-26.06
Hysteretic Energy (%)	-97.65	-99.97	-99.88	-99.98	-99.56	-98.33	-96.76	-99.98	-99.95	-94.68
84th Percentile										
Peak Drift (%)		-34.76	-39.99	-33.12	-31.34	-31.93	-26.13	-23.40	-23.91	-20.01
Permanent Drift (%)		-97.13	-98.28	-96.77	-97.51	-96.54	-87.07	-77.29	-81.34	-76.76
Peak Acceleration (%)		0.89	-10.18	-8.73	-15.03	-15.82	-4.67	-13.93	-15.59	-15.06
Hysteretic Energy (%)	-97.16	-99.99	-99.94	-96.39	-99.94	-99.72	-68.39	-86.50	-89.45	-83.53

TABLE 6.8: SAC9-A3 RESULTS FOR ODD-HALF HIGH SUITE WITH LQRY CONTROLLER.

	GR	F1	F2	F3	F4	F5	F6	F7	F8	F9
Numerical Average/65th percentile										
Peak Drift (%)		-10.22	-10.45	-11.61	-15.58	-16.50	-19.38	-22.34	-28.10	-31.67
Permanent Drift (%)		-12.39	12.04	36.34	32.90	8.83	-19.18	-6.04	-4.26	-27.77
Peak Acceleration (%)		9.81	79.38	13.80	-23.00	-26.83	-26.18	-28.34	-26.85	-6.88
Hysteretic Energy (%)	-14.28	-29.05	-28.29	-35.63	-38.85	-47.33	-57.94	-67.35	-74.34	-80.25
Geometric-Mean/50th percentile										
Peak Drift (%)		-11.40	-10.37	-11.56	-15.03	-17.35	-21.38	-23.93	-30.05	-34.07
Permanent Drift (%)		12.51	15.67	73.06	34.59	-2.67	-68.49	-18.56	-13.84	-29.67
Peak Acceleration (%)		4.36	79.09	13.61	-28.11	-33.79	-31.21	-31.22	-27.04	-7.54
Hysteretic Energy (%)	-76.47	-53.38	-46.02	-43.62	-43.21	-54.07	-54.73	-66.33	-76.14	-91.78
84th Percentile										
Peak Drift (%)		-7.99	-9.84	-10.42	-15.29	-14.44	-15.14	-14.97	-19.68	-25.02
Permanent Drift (%)		-27.55	-4.71	10.97	27.53	24.41	-1.13	37.75	33.72	-20.18
Peak Acceleration (%)		27.60	80.97	12.81	-10.80	-7.64	-11.88	-20.97	-26.76	-3.13
Hysteretic Energy (%)	-13.90	-11.71	-22.64	-32.73	-40.02	-46.49	-54.61	-69.39	-71.96	-83.74

TABLE 6.9: SAC9-A3 RESULTS FOR ODD-HALF MEDIUM SUITE WITH LQRY CONTROLLER.

	GR	F1	F2	F3	F4	F5	F6	F7	F8	F9
Numerical Average/65th percentile										
Peak Drift (%)		-20.85	-20.80	-20.12	-20.46	-20.76	-23.91	-31.33	-42.17	-41.56
Permanent Drift (%)		12.24	28.36	21.55	20.54	20.05	-44.94	-53.51	-60.82	-69.51
Peak Acceleration (%)		7.26	102.64	51.42	-17.25	-16.25	-20.82	-17.22	-11.30	-4.88
Hysteretic Energy (%)	-97.08	-60.24	-57.79	-65.31	-71.47	-78.65	-82.98	-83.77	-91.10	-89.71
Geometric-Mean/50th percentile										
Peak Drift (%)		-19.85	-21.11	-21.63	-20.90	-21.14	-23.49	-31.57	-42.49	-42.07
Permanent Drift (%)		-24.53	-10.57	-42.02	-45.49	-31.28	-51.92	-63.86	-78.56	-82.91
Peak Acceleration (%)		-2.59	89.27	45.36	-27.66	-26.19	-28.51	-24.65	-15.88	-8.78
Hysteretic Energy (%)	-68.55	-72.67	-79.47	-77.20	-80.99	-88.84	-98.34	-80.78	-92.42	-100.00
84th Percentile										
Peak Drift (%)		-21.58	-20.17	-16.95	-19.84	-19.67	-24.73	-29.91	-40.62	-39.89
Permanent Drift (%)		60.36	39.06	19.07	-11.01	49.99	-38.37	-41.48	-45.48	-60.50
Peak Acceleration (%)		23.77	141.74	67.51	0.58	5.21	-4.66	-3.57	-0.18	12.09
Hysteretic Energy (%)	-94.72	-45.26	-38.97	-55.88	-58.83	-76.76	-79.18	-80.45	-88.52	-95.87

TABLE 6.10: SAC9-A3 RESULTS FOR ODD-HALF LOW SUITE WITH LQRY CONTROLLER.

	GR	F1	F2	F3	F4	F5	F6	F7	F8	F9
Numerical Average/65th percentile										
Peak Drift (%)		-42.17	-39.65	-43.20	-40.16	-36.32	-37.63	-41.87	-45.06	-44.94
Permanent Drift (%)		-91.07	-96.81	-98.92	-98.45	-91.12	-76.38	-66.32	-61.98	-48.03
Peak Acceleration (%)		0.54	-0.14	-12.70	-46.98	-51.07	-43.95	-46.95	-39.48	-39.04
Hysteretic Energy (%)	-96.53	-98.20	-99.90	-99.90	-99.89	-80.96	-85.70	-78.62	-77.24	-63.36
Geometric-Mean/50th percentile										
Peak Drift (%)		-43.85	-41.02	-44.46	-41.96	-38.78	-41.19	-45.78	-51.11	-54.27
Permanent Drift (%)		-97.62	-98.15	-98.29	-97.99	-96.15	-89.01	-86.21	-90.60	-91.10
Peak Acceleration (%)		-10.14	-14.93	-20.32	-56.48	-57.34	-54.07	-53.52	-46.15	-47.55
Hysteretic Energy (%)	-98.07	-99.96	-99.84	-99.99	-99.63	-98.27	-98.08	-100.00	-99.99	-99.81
84th Percentile										
Peak Drift (%)		-36.05	-35.48	-39.23	-34.87	-29.18	-28.64	-34.95	-39.60	-39.73
Permanent Drift (%)		-95.29	-98.37	-99.27	-99.06	-96.88	-83.62	-86.50	-91.93	-89.59
Peak Acceleration (%)		13.76	12.41	-4.29	-39.51	-45.57	-35.12	-41.18	-30.91	-26.69
Hysteretic Energy (%)	-97.82	-99.98	-99.95	-99.98	-99.96	-99.84	-99.62	-97.38	-99.28	-100.00

TABLE 6.11: SAC9-A3 RESULTS FOR ODD-HALF HIGH SUITE WITH RESETABLE CONTROLLER.

	GR	F1	F2	F3	F4	F5	F6	F7	F8	F9
Numerical Average/65th percentile										
Peak Drift (%)		-16.90	-21.85	-23.81	-23.70	-18.99	-9.15	-14.80	-18.79	-17.14
Permanent Drift (%)		0.43	-10.67	10.79	21.55	15.13	13.32	11.94	3.57	-14.62
Peak Acceleration (%)		19.92	99.66	46.60	17.65	4.37	11.98	7.38	5.82	17.16
Hysteretic Energy (%)	-43.61	-48.75	-48.02	-47.98	-51.05	-45.71	-38.18	-54.73	-57.20	-57.45
Geometric-Mean/50th percentile										
Peak Drift (%)		-18.47	-24.60	-27.44	-25.34	-22.27	-15.55	-17.82	-21.58	-19.51
Permanent Drift (%)		-30.97	-27.78	7.73	-10.47	-24.13	-70.69	-34.22	-18.20	-33.66
Peak Acceleration (%)		21.82	102.61	50.77	19.33	4.09	12.16	9.24	7.41	17.88
Hysteretic Energy (%)	-74.58	-54.47	-53.80	-35.03	-55.27	-60.47	-37.60	-53.43	-49.51	-54.21
84th Percentile										
Peak Drift (%)		-12.13	-17.17	-19.42	-22.41	-16.29	1.76	-2.41	-7.94	-10.84
Permanent Drift (%)		20.88	-14.03	3.02	21.55	17.81	309.13	97.47	13.99	-21.14
Peak Acceleration (%)		11.46	86.53	26.20	10.15	6.05	11.16	-1.02	-0.38	12.29
Hysteretic Energy (%)	28.11	-39.13	-47.27	-51.66	-58.70	-47.90	-35.58	-53.43	-54.62	-68.20

TABLE 6.12: SAC9-A3 RESULTS FOR ODD-HALF MEDIUM SUITE WITH RESETABLE CONTROLLER.

	GR	F1	F2	F3	F4	F5	F6	F7	F8	F9
Numerical Average/65th percentile										
Peak Drift (%)		-13.62	-33.61	-41.37	-38.51	-37.07	-30.12	-31.38	-38.50	-34.06
Permanent Drift (%)		76.23	-29.92	-51.89	-49.45	-39.82	-58.27	-46.68	-47.10	-58.67
Peak Acceleration (%)		54.52	182.78	103.61	34.87	31.20	23.12	41.13	14.81	17.01
Hysteretic Energy (%)	-67.83	-74.90	-93.03	-91.79	-93.26	-93.44	-83.16	-86.70	-79.23	-90.98
Geometric-Mean/50th percentile										
Peak Drift (%)		-14.95	-33.12	-40.90	-38.86	-37.97	-30.17	-32.68	-39.41	-33.25
Permanent Drift (%)		-61.79	-74.81	-70.40	-75.81	-74.78	-80.74	-83.48	-85.06	-82.68
Peak Acceleration (%)		56.05	191.11	104.01	36.91	31.35	20.41	42.26	17.52	17.16
Hysteretic Energy (%)	-24.15	-73.63	-99.82	-98.58	-99.40	-99.93	-99.82	-89.79	-81.81	-99.96
84th Percentile										
Peak Drift (%)		-9.32	-35.30	-43.23	-37.87	-34.26	-30.29	-27.88	-35.01	-37.16
Permanent Drift (%)		168.45	-36.53	-61.10	-78.55	-59.30	-70.40	-43.33	-8.46	-24.19
Peak Acceleration (%)		50.99	147.60	101.55	25.92	30.78	31.89	37.51	0.62	15.98
Hysteretic Energy (%)	-39.21	-73.94	-90.85	-90.40	-88.24	-92.82	-91.81	-82.41	-75.23	-90.72

TABLE 6.13: SAC9-A3 RESULTS FOR ODD-HALF LOW SUITE WITH RESETABLE CONTROLLER.

	GR	F1	F2	F3	F4	F5	F6	F7	F8	F9
Numerical Average/65th percentile										
Peak Drift (%)		-59.52	-57.13	-55.84	-51.55	-50.80	-51.69	-55.53	-42.55	-32.23
Permanent Drift (%)		-97.54	-99.36	-99.45	-99.36	-97.03	-88.96	-83.34	-56.95	-58.25
Peak Acceleration (%)		39.99	130.23	64.48	24.15	1.62	6.16	0.86	-3.43	6.93
Hysteretic Energy (%)	-98.50	-99.61	-99.88	-99.94	-99.96	-94.32	-94.58	-84.27	-71.45	-52.66
Geometric-Mean/50th percentile										
Peak Drift (%)		-62.41	-61.65	-59.45	-53.82	-53.79	-58.77	-61.82	-47.73	-37.67
Permanent Drift (%)		-98.16	-98.76	-98.79	-98.80	-97.48	-87.49	-84.98	-86.24	-80.43
Peak Acceleration (%)		42.90	145.70	69.52	18.89	3.73	5.81	0.74	-5.83	6.46
Hysteretic Energy (%)	-99.86	-100.00	-100.00	-100.00	-99.97	-99.92	-99.92	-100.00	-99.99	-96.83
84th Percentile										
Peak Drift (%)		-51.82	-49.00	-49.12	-46.01	-43.19	-39.83	-47.75	-37.88	-27.79
Permanent Drift (%)		-98.30	-99.52	-99.66	-99.58	-98.58	-90.26	-93.27	-89.71	-83.76
Peak Acceleration (%)		36.04	89.54	50.85	32.18	-0.13	7.98	2.00	1.35	7.76
Hysteretic Energy (%)	-99.73	-100.00	-99.95	-99.96	-99.99	-99.86	-93.90	-97.74	-89.04	-47.86

6.7.3 SAC9-A8 Result Tables

TABLE 6.14: SAC9-A8 RESULTS FOR ODD-HALF HIGH SUITE WITH LQR CONTROLLER.

	GR	F1	F2	F3	F4	F5	F6	F7	F8	F9
Numerical Average/65th percentile										
Peak Drift (%)		-22.22	-18.93	-15.41	-13.27	-9.15	-3.18	-6.25	-11.66	-10.94
Permanent Drift (%)		-25.75	-20.00	3.78	11.29	6.45	12.44	7.49	3.95	-8.81
Peak Acceleration (%)		1.13	-1.59	-2.78	-3.92	-5.35	-0.72	-4.55	-4.97	7.34
Hysteretic Energy (%)	-58.87	-40.45	-35.76	-28.85	-28.07	-24.62	-25.94	-29.86	-28.41	-20.03
Geometric-Mean/50th percentile										
Peak Drift (%)		-20.81	-17.61	-14.52	-12.28	-10.62	-5.56	-6.32	-11.44	-11.26
Permanent Drift (%)		-10.98	-13.41	15.36	-35.22	-30.80	6.77	2.70	26.39	29.01
Peak Acceleration (%)		0.46	-2.70	-3.77	-4.55	-6.14	-0.83	-5.11	-5.26	7.84
Hysteretic Energy (%)	-61.21	-41.43	-23.12	-13.64	-11.37	-21.16	-32.54	-30.50	-38.35	-43.34
84th Percentile										
Peak Drift (%)		-23.57	-19.78	-15.58	-14.00	-6.58	1.43	-5.02	-12.34	-10.49
Permanent Drift (%)		-32.66	-38.35	-10.38	50.80	35.95	15.00	31.31	-12.58	-39.92
Peak Acceleration (%)		3.89	2.22	-0.60	-1.53	-1.00	-0.15	-2.52	-4.13	4.49
Hysteretic Energy (%)	-67.10	-35.50	-38.22	-34.57	-32.81	-32.57	-30.09	-37.70	-30.25	-16.11

TABLE 6.15: SAC9-A8 RESULTS FOR ODD-HALF MEDIUM SUITE WITH LQR CONTROLLER.

	GR	F1	F2	F3	F4	F5	F6	F7	F8	F9
Numerical Average/65th percentile										
Peak Drift (%)		-20.45	-28.67	-26.63	-20.99	-18.35	-15.66	-11.86	-16.66	-19.44
Permanent Drift (%)		-17.84	0.66	3.03	13.35	31.86	-4.78	-5.62	0.89	-14.24
Peak Acceleration (%)		-3.69	-2.10	-2.05	-4.49	-2.24	-5.31	-8.38	-5.41	2.56
Hysteretic Energy (%)	-90.13	-68.07	-75.45	-69.55	-67.95	-64.37	-44.97	-47.34	-51.73	-64.42
Geometric-Mean/50th percentile										
Peak Drift (%)		-18.61	-27.60	-25.94	-20.55	-18.56	-16.44	-12.69	-17.08	-19.40
Permanent Drift (%)		-52.42	-15.40	-27.72	-34.17	13.14	-15.58	-20.62	-6.55	-16.69
Peak Acceleration (%)		-3.94	-1.93	-1.84	-3.96	-2.89	-4.97	-8.06	-5.82	2.83
Hysteretic Energy (%)	-63.76	-74.70	-87.34	-75.65	-77.80	-74.58	-81.30	-33.63	-37.75	-93.19
84th Percentile										
Peak Drift (%)		-24.82	-31.42	-28.95	-22.74	-18.20	-13.28	-8.91	-15.31	-19.82
Permanent Drift (%)		74.64	21.82	6.04	42.13	122.57	3.52	4.60	14.34	4.58
Peak Acceleration (%)		-3.22	-2.74	-3.39	-6.89	0.96	-6.90	-9.53	-3.92	0.73
Hysteretic Energy (%)	-98.29	-64.25	-74.46	-67.09	-58.78	-55.63	-41.83	-46.12	-50.05	-57.08

TABLE 6.16: SAC9-A8 RESULTS FOR ODD-HALF LOW SUITE WITH LQR CONTROLLER.

	GR	F1	F2	F3	F4	F5	F6	F7	F8	F9
Numerical Average/65th percentile										
Peak Drift (%)		-32.95	-33.81	-32.74	-30.89	-31.26	-27.14	-26.44	-23.60	-18.77
Permanent Drift (%)		-78.46	-88.30	-85.04	-90.05	-92.90	-53.17	-2.31	24.21	11.94
Peak Acceleration (%)		-8.22	-10.00	-10.63	-13.97	-14.34	-9.59	-13.06	-14.70	-17.41
Hysteretic Energy (%)	-88.25	-89.75	-97.92	-86.84	-99.53	-99.64	-56.52	-61.46	-47.23	-20.00
Geometric-Mean/50th percentile										
Peak Drift (%)		-35.14	-34.93	-34.39	-32.62	-32.31	-29.73	-30.53	-28.64	-24.70
Permanent Drift (%)		-94.68	-95.99	-94.99	-94.62	-93.47	-82.06	-64.70	-71.75	-61.73
Peak Acceleration (%)		-8.35	-10.13	-12.98	-16.15	-15.38	-12.26	-15.96	-15.66	-19.86
Hysteretic Energy (%)	-89.57	-99.86	-99.62	-99.96	-99.14	-96.27	-91.26	-99.97	-99.91	-88.43
84th Percentile										
Peak Drift (%)		-24.95	-30.21	-27.73	-25.53	-27.31	-19.10	-18.16	-17.96	-13.15
Permanent Drift (%)		-91.58	-94.67	-94.25	-95.50	-95.53	-82.18	-65.16	-41.41	-26.83
Peak Acceleration (%)		-7.21	-9.49	-6.12	-9.97	-11.64	-3.56	-7.52	-11.44	-10.74
Hysteretic Energy (%)	-92.36	-99.91	-99.83	-86.60	-99.88	-99.66	-72.77	-83.63	-82.52	-45.59

TABLE 6.17: SAC9-A8 RESULTS FOR ODD-HALF HIGH SUITE WITH LQRY CONTROLLER.

	GR	F1	F2	F3	F4	F5	F6	F7	F8	F9
Numerical Average/65th percentile										
Peak Drift (%)		-10.19	-10.26	-10.78	-13.23	-13.84	-15.64	-19.83	-26.81	-30.07
Permanent Drift (%)		-8.78	-10.74	15.42	20.96	8.22	-6.52	4.36	1.77	-24.78
Peak Acceleration (%)		-2.61	35.96	-6.45	-21.48	-27.86	-21.03	-27.28	-25.81	-4.36
Hysteretic Energy (%)	-24.08	-26.05	-24.82	-30.79	-35.69	-43.62	-55.37	-64.24	-70.29	-71.01
Geometric-Mean/50th percentile										
Peak Drift (%)		-10.88	-9.71	-10.23	-12.58	-15.30	-18.47	-21.25	-28.40	-32.21
Permanent Drift (%)		0.74	-30.34	20.37	-14.03	-15.47	-57.48	-5.13	-2.70	-22.36
Peak Acceleration (%)		-5.83	36.03	-7.41	-23.05	-30.64	-23.34	-28.68	-25.10	-5.03
Hysteretic Energy (%)	-63.61	-44.19	-38.29	-32.28	-29.32	-43.28	-54.88	-66.43	-78.26	-85.90
84th Percentile										
Peak Drift (%)		-8.85	-10.67	-10.85	-13.61	-11.40	-10.40	-12.79	-19.28	-23.83
Permanent Drift (%)		-6.36	-12.68	16.42	82.83	37.28	32.00	38.73	24.19	-24.20
Peak Acceleration (%)		8.79	36.55	-4.05	-16.66	-17.04	-12.69	-22.93	-28.41	-0.70
Hysteretic Energy (%)	-5.96	-12.17	-18.50	-29.65	-39.13	-44.15	-54.18	-64.79	-70.84	-85.86

TABLE 6.18: SAC9-A8 RESULTS FOR ODD-HALF MEDIUM SUITE WITH LQRY CONTROLLER.

	GR	F1	F2	F3	F4	F5	F6	F7	F8	F9
Numerical Average/65th percentile										
Peak Drift (%)		-37.12	-44.56	-42.53	-36.80	-32.85	-30.30	-36.60	-48.84	-48.13
Permanent Drift (%)		-40.18	-55.58	-47.95	-31.46	-26.04	-62.75	-59.76	-65.46	-76.93
Peak Acceleration (%)		17.34	66.62	39.23	0.52	-0.63	-11.79	-10.49	-9.91	-4.38
Hysteretic Energy (%)	-99.93	-91.44	-96.28	-92.56	-92.57	-91.00	-90.29	-91.38	-92.98	-93.70
Geometric-Mean/50th percentile										
Peak Drift (%)		-35.68	-43.52	-42.74	-37.21	-33.63	-30.73	-38.22	-51.00	-51.02
Permanent Drift (%)		-77.02	-81.81	-74.89	-70.55	-68.49	-80.74	-88.95	-89.43	-90.92
Peak Acceleration (%)		11.88	69.49	37.90	-6.94	-9.97	-19.97	-19.47	-13.44	-8.46
Hysteretic Energy (%)	-87.06	-92.72	-98.09	-96.31	-97.11	-97.44	-99.87	-96.13	-98.75	-100.00
84th Percentile										
Peak Drift (%)		-39.63	-46.98	-41.78	-35.02	-29.70	-27.48	-30.72	-41.32	-39.63
Permanent Drift (%)		-43.94	-67.83	-63.23	-57.33	-25.14	-64.80	-41.01	-43.70	-69.62
Peak Acceleration (%)		31.17	57.42	44.13	23.65	29.03	10.36	7.90	1.44	13.41
Hysteretic Energy (%)	-99.70	-88.11	-95.15	-90.98	-91.26	-89.40	-91.44	-86.43	-89.25	-93.69

TABLE 6.19: SAC9-A8 RESULTS FOR ODD-HALF LOW SUITE WITH LQRY CONTROLLER.

	GR	F1	F2	F3	F4	F5	F6	F7	F8	F9
Numerical Average/65th percentile										
Peak Drift (%)		-54.83	-52.68	-52.57	-50.77	-48.87	-48.77	-49.78	-54.43	-53.07
Permanent Drift (%)		-98.87	-99.54	-99.51	-99.33	-98.10	-78.19	-41.67	-41.86	-41.63
Peak Acceleration (%)		6.43	18.72	19.83	-15.57	-30.94	-31.59	-29.43	-32.06	-31.54
Hysteretic Energy (%)	-98.41	-99.90	-99.95	-99.76	-99.96	-99.88	-89.83	-77.59	-72.10	-73.44
Geometric-Mean/50th percentile										
Peak Drift (%)		-57.13	-54.91	-55.75	-53.25	-51.35	-53.63	-57.82	-64.71	-66.28
Permanent Drift (%)		-98.46	-99.04	-99.12	-98.12	-96.41	-85.66	-85.37	-95.54	-87.01
Peak Acceleration (%)		-4.72	-1.91	0.66	-38.98	-44.92	-46.17	-44.80	-40.39	-44.51
Hysteretic Energy (%)	-99.65	-100.00	-99.98	-100.00	-99.95	-99.77	-99.69	-100.00	-100.00	-99.99
84th Percentile										
Peak Drift (%)		-47.80	-46.90	-45.48	-44.51	-41.94	-38.56	-39.69	-47.48	-46.25
Permanent Drift (%)		-98.78	-99.66	-99.62	-99.58	-98.55	-83.45	-83.93	-87.22	-85.24
Peak Acceleration (%)		22.44	46.84	49.49	11.39	-13.66	-11.00	-13.61	-19.10	-11.96
Hysteretic Energy (%)	-99.33	-100.00	-99.97	-99.95	-99.97	-99.89	-87.76	-90.37	-95.99	-99.96

TABLE 6.20: SAC9-A8 RESULTS FOR ODD-HALF HIGH SUITE WITH RESETABLE CONTROLLER.

	GR	F1	F2	F3	F4	F5	F6	F7	F8	F9
Numerical Average/65th percentile										
Peak Drift (%)		-21.24	-24.92	-24.16	-23.46	-20.70	-12.69	-14.98	-20.51	-20.01
Permanent Drift (%)		-31.66	-16.17	-1.26	17.56	15.49	5.74	5.64	-6.92	-23.25
Peak Acceleration (%)		2.02	41.56	19.21	1.42	-6.42	2.95	-2.04	-1.72	16.28
Hysteretic Energy (%)	-39.40	-43.51	-46.11	-50.59	-52.57	-48.79	-41.99	-51.28	-55.58	-55.29
Geometric-Mean/50th percentile										
Peak Drift (%)		-22.25	-28.47	-27.95	-25.75	-23.24	-16.12	-18.92	-22.73	-21.29
Permanent Drift (%)		-47.63	-56.85	-50.41	-46.54	-41.95	-72.10	-41.41	-38.87	-23.74
Peak Acceleration (%)		1.13	43.59	20.49	2.75	-7.12	2.63	-1.73	-1.83	17.07
Hysteretic Energy (%)	-66.53	-38.08	-41.14	-36.67	-41.34	-49.48	-31.80	-51.04	-54.14	-55.83
84th Percentile										
Peak Drift (%)		-17.59	-18.85	-18.73	-20.16	-16.69	-4.80	0.07	-11.02	-16.36
Permanent Drift (%)		33.71	54.17	42.04	62.36	52.65	365.05	106.76	13.96	-36.10
Peak Acceleration (%)		5.95	32.10	14.39	-4.66	-1.89	5.01	-3.00	-0.24	10.90
Hysteretic Energy (%)	-21.83	-40.52	-52.31	-57.37	-63.44	-54.23	-40.43	-47.44	-46.84	-6.12

TABLE 6.21: SAC9-A8 RESULTS FOR ODD-HALF MEDIUM SUITE WITH RESETABLE CONTROLLER.

	GR	F1	F2	F3	F4	F5	F6	F7	F8	F9
Numerical Average/65th percentile										
Peak Drift (%)		-36.03	-46.61	-47.68	-44.43	-40.75	-32.04	-30.80	-36.92	-33.44
Permanent Drift (%)		-29.31	-53.95	-61.33	-63.54	-51.56	-51.24	-35.73	-33.93	-52.50
Peak Acceleration (%)		16.91	61.53	18.71	11.29	11.95	2.69	4.15	0.41	13.71
Hysteretic Energy (%)	-99.88	-91.94	-97.11	-95.39	-96.13	-93.31	-77.70	-83.74	-82.83	-91.83
Geometric-Mean/50th percentile										
Peak Drift (%)		-35.06	-45.93	-47.60	-44.14	-40.98	-33.57	-33.32	-39.03	-32.87
Permanent Drift (%)		-87.05	-92.13	-91.92	-94.02	-88.55	-86.42	-91.40	-90.47	-88.79
Peak Acceleration (%)		17.86	65.85	18.47	11.92	11.28	3.13	4.34	1.84	14.26
Hysteretic Energy (%)	-95.83	-98.41	-99.98	-99.76	-99.98	-99.97	-99.86	-94.59	-90.43	-99.96
84th Percentile										
Peak Drift (%)		-37.93	-49.12	-48.58	-45.49	-39.61	-28.17	-24.32	-31.15	-35.84
Permanent Drift (%)		-54.11	-79.37	-83.12	-86.18	-69.78	-64.20	-41.01	-23.36	-46.87
Peak Acceleration (%)		14.21	44.75	18.88	8.68	15.48	0.10	2.70	-6.15	9.02
Hysteretic Energy (%)	-99.43	-88.56	-97.68	-94.35	-94.05	-92.11	-77.00	-75.67	-72.51	-91.65

TABLE 6.22: SAC9-A8 RESULTS FOR ODD-HALF LOW SUITE WITH RESETABLE CONTROLLER.

	GR	F1	F2	F3	F4	F5	F6	F7	F8	F9
Numerical Average/65th percentile										
Peak Drift (%)		-53.87	-53.27	-53.40	-56.10	-55.04	-54.55	-52.59	-44.91	-34.20
Permanent Drift (%)		-90.36	-93.51	-98.14	-98.42	-90.96	-71.25	-64.41	-59.35	-62.79
Peak Acceleration (%)		3.27	36.47	1.32	-4.34	-10.04	-8.10	-10.10	-17.93	-5.65
Hysteretic Energy (%)	-95.55	-94.88	-98.54	-99.61	-99.93	-79.90	-82.76	-77.74	-67.54	-44.15
Geometric-Mean/50th percentile										
Peak Drift (%)		-57.36	-57.52	-57.12	-59.52	-59.13	-62.52	-60.83	-52.38	-41.48
Permanent Drift (%)		-98.02	-98.79	-98.46	-98.91	-97.09	-86.09	-82.43	-85.95	-81.10
Peak Acceleration (%)		3.51	42.77	-3.47	-5.43	-9.70	-9.62	-10.68	-18.91	-8.45
Hysteretic Energy (%)	-99.86	-100.00	-100.00	-100.00	-99.99	-99.97	-99.94	-100.00	-99.99	-98.05
84th Percentile										
Peak Drift (%)		-45.53	-45.50	-46.46	-49.07	-46.35	-43.36	-43.93	-39.69	-29.38
Permanent Drift (%)		-97.12	-98.40	-99.29	-99.05	-97.30	-81.39	-87.50	-89.50	-83.61
Peak Acceleration (%)		4.34	23.18	7.77	-2.47	-10.09	-3.70	-9.26	-16.10	0.50
Hysteretic Energy (%)	-98.72	-99.99	-99.89	-99.82	-99.99	-99.94	-61.06	-95.36	-92.59	-81.09

7. PERFORMANCE NORMALISATION & COMPARISON

7.1 INTRODUCTION

This chapter presents a discussion of the results for the SAC3 and SAC9 structures presented in Chapters 5 and 6 respectively. While some discussion was presented within these chapters, it was limited to the characteristics and basic results of each individual controller or architecture. Although the same maximum actuator authority was used in the simulations for each controller, the total amount of control input is dependent on the specific control law, with unclipped actuator forces related to the specific displacement, velocity, acceleration, or jerk of the structure. Hence, a means of normalising the different results was developed to allow valid inter-controller and inter-architecture comparisons to be made.

Normalisation is a means of processing results relative to the same datum, allowing comparisons to be made while retaining the characteristics of the pre-normalised responses. The primary normalisation method used in this investigation was to define the percentage performance reductions in terms of the average change in geometric-mean structural hysteretic energy between the uncontrolled and controlled responses. This normalisation is based on that assumption that the reduction in hysteretic energy is representative of the amount of energy removed by the controller, and hence of the level of control input. The hysteretic energy metric is not normalised, as the result is trivial. However, as universal reductions in hysteretic energy were observed for each of the controllers, this lack of normalised comparison is not considered crucial. The second normalisation method, used for the SAC9 response only, employs the $\mathbf{L_2}$-norm of the control input u(t), $||u||_2$, to normalise the percentage performance reductions. This norm is a measure of the rms control energy, and for a given individual control input, u_i, is defined:

$$\left\|u_i(t)\right\|_2 = \sqrt{\int_0^{t_f} u_i^2(t)dt} = \sqrt{\mathbf{u}_i{}^T \mathbf{u}_i(\Delta t)} \qquad (7.1)$$

where u_i is the control input at the i^{th} time step of "n" total time steps, $\mathbf{u}_i$ is the vector of the control input u_i for all time steps, and Δt is the uniform time step between successive u_i values, with $\Delta t = 0.01$ seconds for all simulations in this investigation. Note that the final time, t_f, is essentially infinity in proper definitions, but as control input and response are assumed zero at t_f, the norm is finite.

The energy associated with the structural system is constant for semi-active controllers, as this class of controllers do not supply additional energy to the system, but act to dissipate energy from the system. While the structure is in motion there is a trade off between kinetic and potential energy depending on the points of maximum displacement and velocity, however, assuming the structure is at rest at the start and end of the excitation, the total energy into the system must equal the total energy dissipated at the end of the motion. Energy is dissipated through inherent structural damping, linear and non-linear hysteretic, and through the semi-active controllers. As linear structural damping is relatively small, it may be assumed that the most significant path of energy dissipation is through the semi-active actuators and hysteretic motion.

The structural hysteretic energy used in this investigation is a measure of the energy associated with the plasticity and yielding of the structural joints, which correlates to overall structural damage. For semi-active control systems, any difference in energy out of the structure, compared to the uncontrolled response, must have passed through the semi-active actuators. Hence, the change in structural hysteretic energy is approximately proportional to control energy. The change in hysteretic energy represents approximately the 50^{th} percentile

of the control energy distribution, whereas the $\|u\|_2$ is an rms value representing the 70.7^{th} percentile. Therefore, both normalisation methods are dependent on the shape of the control energy distribution, and may show different characteristics as the energy distribution shifts.

Despite the development of two normalisation techniques, a primary difficulty in summarising and comparing the different responses is the large number of response metrics, with drifts, accelerations, and energies assessed at each floor. To reduce the number of variables that must be compared, the average geometric-mean (50^{th} percentile) response reductions across all floors for each response metric are used in the normalisation. It is important to note that a structure can fail through the failure of a single floor only, hence, individual story response is vital when assessing the overall performance of individual controllers. As details of the individual floor responses are presented and discussed in Chapters 5 and 6, this technique is intended to simplify the comparisons in terms of a single number per metric for each controller and suite.

Section 7.2 presents the average normalised response reductions for each of the controllers and architectures used for the SAC3 and SAC9 structures, with discussion and comparisons made in Section 7.3. The remainder of this chapter details other analysis results, such as the contribution of particular extreme earthquakes within the high earthquake suites and the sensitivity of the lognormal distribution to extreme events, analysis of the SAC3 jerk distributions as means of evaluation, and the impact of tracking the time-varying equilibrium point.

7.2 NORMALISED RESULTS & COMPARISONS

This section presents the normalised results for the SAC3 and SAC9 structural responses, with comparisons made between controllers and architectures. The normalised results are average geometric-mean response measures divided by either the absolute change in counted-mean hysteretic energy between the controlled and uncontrolled cases (a negative number), or the negative of the counted-mean $\|u\|_2$ of the control input. Therefore, positive normalised responses indicate that a response reduction is obtained from the control input, whereas a negative value indicates that control expenditure results in an increase of the average response. The more positive the normalised performance value (NPV), the greater the response reductions per unit of control input energy. Hence, the normalisation technique essentially gives a cost-benefit comparison.

7.2.1 Hysteretic Energy Performance Normalisation: SAC3 & SAC9

7.2.1.1 SAC3 PERFORMANCE: HYSTERETIC ENERGY NORMALISATION

The normalised results for the SAC3-A1 structural simulations are shown in Table 7.1. The SAC3-A1 control architecture has the maximum actuator authority of 450kips placed entirely on the first floor. Interestingly, the LQRy clipped optimal controller is the only controller that shows positive NPVs across each of the performance measures for each of the three earthquake suites. For the high earthquake suite, the LQRy controller has the highest NPVs for each of the four performance measures, with the exception of the JQR clipped optimal controller, which has the highest drift NPVs. While the focus of the LQRy control design is in the minimisation of total structural accelerations in an attempt to increase occupant safety, this result highlights the benefit of acceleration control as a means of also reducing external structural damage.

TABLE 7.1: SAC3-A1 HYSTERETIC ENERGY NORMALISED AVERAGE GEOMETRIC-MEAN RESULTS.

	High Suite		Medium Suite		Low Suite	
	% Reduction	**NPV**	**% Reduction**	**NPV**	**% Reduction**	**NPV**
Quasi-bang-bang						
Average Peak Drift	-4.65	**0.35**	-8.59	**0.94**	-15.19	**3.76**
Average Permanent Drift	5.14	**-0.39**	3.52	**-0.39**	-55.23	**13.66**
Average Peak Acceleration	6.27	**-0.48**	10.37	**-1.13**	2.86	**-0.71**
LQR						
Average Peak Drift	-11.60	**0.35**	-16.30	**0.97**	-28.20	**6.83**
Average Permanent Drift	-19.61	**0.59**	-31.92	**1.89**	-88.07	**21.32**
Average Peak Acceleration	8.83	**-0.27**	11.39	**-0.68**	-18.80	**4.55**
LQRy						
Average Peak Drift	-12.95	**0.49**	-12.78	**0.96**	-21.58	**5.29**
Average Permanent Drift	-23.83	**0.91**	-36.02	**2.71**	-81.72	**20.04**
Average Peak Acceleration	-15.84	**0.60**	-22.80	**1.72**	-38.81	**9.51**
Resetable						
Average Peak Drift	-8.72	**0.42**	-9.06	**0.72**	-18.85	**4.60**
Average Permanent Drift	-6.53	**0.32**	-11.82	**0.94**	-73.17	**17.85**
Average Peak Acceleration	6.05	**-0.29**	16.77	**-1.33**	3.96	**-0.97**
JQR						
Average Peak Drift	-7.31	**1.43**	-4.81	**0.70**	-3.59	**1.70**
Average Permanent Drift	-15.16	**2.97**	-28.78	**4.21**	-13.79	**6.53**
Average Peak Acceleration	16.99	**-3.32**	16.72	**-2.44**	10.62	**-5.03**

The general trend in the NPVs across the three earthquake suites in Table 7.1 is an increasingly positive value as the magnitude of the suite decreases. This trend shows that for each unit of control input expended, the improvements in structural response increase as the magnitude of the earthquake suite decreases, as is intuitively expected when the actuator authority is saturated at a maximum level. The approximately exponential relationship between ground excitations of the three earthquake suites is mirrored by the NPVs, as shown in Figure 7.1 for the average peak drift NPVs, with the exception of the JQR controller, which does not follow this trend. As the medium and low earthquake suites represent 72- and 474-

year mean return period events, this trend is beneficial, as extremely large performance reductions are obtained for the more likely, yet still sizable, seismic events.

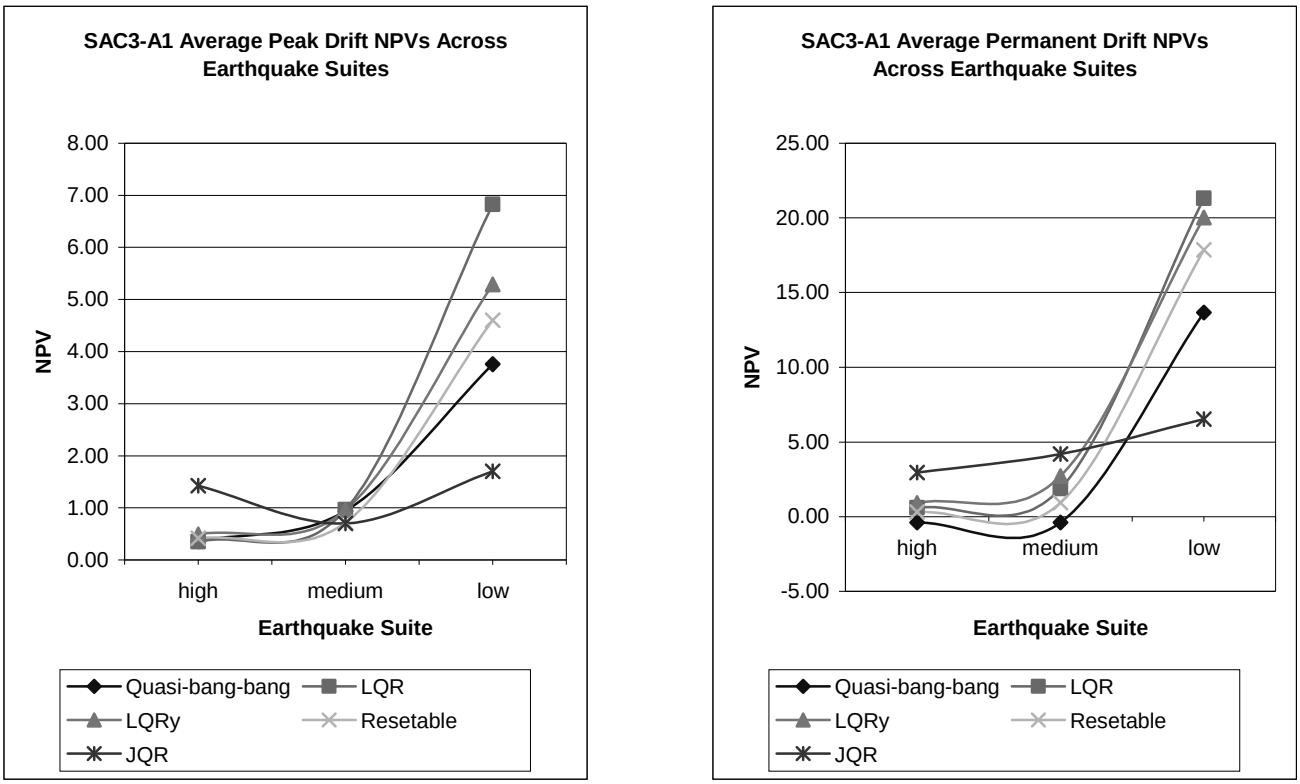

(a) (b)

Figure 7.1: SAC3-A1 average drifts across earthquake suites: (a) Peak drifts, (b) Permanent drifts.

Interestingly, the quasi-bang-bang controller is the only controller presented in Table 7.1 that shows negative permanent drift NPVs for the high and medium suites, despite showing comparable peak drift NPVs. This trend of increased permanent drifts for large magnitude events may be an indication of an important characteristic of using decentralised control in which the semi-active resisting stiffness is applied to the structure to minimise the transient displacements of the floors to which the actuators are attached. The inherent link between displacements and accelerations is highlighted by both this result and those for the LQR clipped optimal controller, with displacement regulation resulting in an increase in total structural accelerations during medium to strong earthquake motions. This relationship

between displacement regulation and acceleration increases may not have been detected if lower magnitude suites, or single earthquake records were used.

As with the quasi-bang-bang controller, the resetable controller is decentralised, in that control forces are applied to mitigate the motion of the floor to which they are directly attached using only local measurements. However, in contrast to the quasi-bang-bang controller, the permanent drift NPVs for the resetable controller are positive for each of the three earthquake suites, although peak acceleration NPVs are still negative. The primary difference between these two controllers is the focus on maximum dissipation of energy for the resetable controller, with the free length of the hydraulic spring reset such that the maximum amount of energy is stored and then dissipated before it is returned to the structure. Hence, although a semi-active resisting stiffness is applied to the structure for both controllers, a control law which considers the maximum dissipation of structural energy shows superior performance over one which determines control input based on transient displacements, when average drifts are the basis of performance assessment.

Previous investigations into resetable actuators have been undertaken using linear structural models, with either cyclic roof loads or single earthquake excitations [Bobrow et al. 1995, Bobrow and Jabbari 1997, Bobrow et al. 2000]. Within these investigations, the performance of these actuators was illustrated using roof accelerations for a three story building model with an actuator placed on the first story only. Although reductions in roof acceleration were also observed in each of the resetable controller simulations within this investigation, the increases in accelerations of the lower two floors are such that the average peak acceleration increases, giving negative acceleration NPVs in Table 7.1. This observation highlights the importance of assessing the global structural performance when evaluating the efficacy of controllers. Potentially, reductions in accelerations may have been observed on all floors in

previous investigations using the linear models, however, this result would emphasise the importance of including non-linear structural responses within structural control models.

The acceleration NPVs for the JQR controller in Table 7.1 are the largest negative values for the SAC3-A1 control architecture across all the three earthquake suites. As the JQR control design uses state feedback gains to minimise total structural jerk, this result clearly shows an acceleration smoothing effect of the controller, where peak accelerations increase in order to reduce the acceleration rate of change. However, the potential of the JQR controller in reducing external structural damage is seen through the very large permanent drift NPVs for the extreme near-field seismic events contained within the high and medium earthquake suites. The NPVs for the JQR controller also do not follow the approximately exponential trend across the earthquake suites. This result may indicate the limitation of controlling structural jerks across a large range of seismic excitations using the same state feedback gain design, with the very large range of structural jerks between near- and far-field seismic events across all three suites. Further development of the JQR controller may help widen its effective performance band, while an experimental investigation may be useful to clarify the effect of total structural jerk on occupant safety and external structural damage.

The normalised results for the SAC3-A2-1 control architecture are presented in Table 7.2 for the LQRy clipped optimal controller and decentralised resetable actuator. The SAC3-A2-1 control architecture has actuators placed on the first and second stories, with 70% of the 450kip maximum actuator authority assigned to the first story. Through comparison with the NPVs in Table 7.1 for the SAC3-A1 architecture, the efficacy of the different control architectures may be assessed.

Looking at the normalised average results for the LQRy clipped optimal controller presented in Table 7.2, the drift NPVs are generally slightly smaller than those in Table 7.1, while the peak acceleration NPVs are larger across all three suites. The largest increase in acceleration NPVs is observed for the medium suite, with an increase of over 25% in NPV from 1.72 to 2.18. This result indicates that it may beneficial to locate some actuator authority on the second floor, as this approach gives larger reductions, per unit of control effort, in the acceleration demands, which are the focus of this centralised control design. However, slight decreases in peak and permanent drift reduction may result from this control architecture compared to those obtained from the SAC3-A1 architecture. It is possible that these reductions in drifts are partially a result of a small amount of actuator-actuator interaction, however, this effect is expected to be small due to the very high proportion of the first mode in the structural response.

The NPVs for the decentralised resetable actuator, presented in Table 7.2, show increases for permanent drifts and peak accelerations, compared to those for the SAC3-A1 control architecture. This reduction in permanent drifts is in contrast to the initial architecture assessment results presented in Section 5.5.1, which used the 65^{th} percentile to imply that the largest reductions in drifts were obtained by placing the maximum actuator authority entirely on the first story. This difference highlights the importance of observing the characteristics of the response distributions that result from each earthquake suite, with the overall distribution shape change of primary concern, as was discussed in Chapters 5 and 6.

TABLE 7.2: SAC3-A2-1 HYSTERETIC ENERGY NORMALISED AVERAGE GEOMETRIC-MEAN RESULTS.

	High Suite		Medium Suite		Low Suite	
	% Reduction	**NPV**	**% Reduction**	**NPV**	**% Reduction**	**NPV**
LQRy						
Average Peak Drift	-11.86	**0.50**	-11.86	**1.05**	-18.67	**5.14**
Average Permanent Drift	-15.50	**0.65**	-24.72	**2.19**	-69.64	**19.16**
Average Peak Acceleration	-17.33	**0.73**	-24.68	**2.18**	-36.63	**10.08**
Resetable						
Average Peak Drift	-7.20	**0.33**	-9.84	**0.75**	-19.02	**4.60**
Average Permanent Drift	-18.45	**0.86**	-30.64	**2.34**	-77.24	**18.70**
Average Peak Acceleration	1.82	**-0.08**	7.87	**-0.60**	0.17	**-0.04**

The normalised results for the SAC3-A3-1 actuator architecture, for the clipped optimal LQRy and JQR controllers, and the decentralised resetable actuator, are shown in Table 7.3. This control architecture has an actuator authority distribution of 60%:30%:10% on the first, second, and third stories respectively. For the LQRy clipped optimal controller the changes in NPVs from the SAC3-A1 and SAC3-A2-1 control architectures are small. In general, NPV increases are observed, relative to the SAC3-A1 architecture, for each of the performance measures across all three earthquake suites, with the exception of the peak drift NPV, which decreases slightly.

TABLE 7.3: SAC3-A3-1 HYSTERETIC ENERGY NORMALISED AVERAGE GEOMETRIC-MEAN RESULTS.

	High Suite		Medium Suite		Low Suite	
	% Reduction	**NPV**	**% Reduction**	**NPV**	**% Reduction**	**NPV**
LQRy						
Average Peak Drift	-11.00	**0.51**	-10.92	**1.01**	-17.50	**4.98**
Average Permanent Drift	-19.98	**0.93**	-23.34	**2.16**	-73.73	**20.98**
Average Peak Acceleration	-17.87	**0.83**	-24.01	**2.22**	-35.13	**10.00**
Resetable						
Average Peak Drift	-6.89	**0.37**	-8.96	**0.76**	-17.25	**4.18**
Average Permanent Drift	5.75	**-0.31**	-12.17	**1.03**	-72.87	**17.65**
Average Peak Acceleration	1.97	**-0.11**	3.62	**-0.31**	-1.82	**0.44**
JQR						
Average Peak Drift	-7.88	**0.36**	-13.35	**0.89**	-17.56	**4.25**
Average Permanent Drift	0.51	**-0.02**	-20.50	**1.37**	-78.27	**18.95**
Average Peak Acceleration	4.58	**-0.21**	12.65	**-0.84**	14.56	**-3.53**

Compared to the NPVs for the SAC3-A2-1 architecture, peak drift NPVs are lower for the SAC3-A3-1 across all three suites, while the permanent drift NPVs increase slightly for the high and low suites, and peak acceleration NPVs are higher across all three suites. These trends indicate that for the 50^{th} percentile of the lognormal response distribution of the SAC3 structure, maximum average response reduction, per unit of control cost, is achieved through the assignment of a small amount of actuator authority on the upper two floors, with most of the actuator authority retained on the first story.

The normalised results for the decentralised resetable actuator in Table 7.3 are mixed compared to those for the SAC3-A1 and SAC-A2-1 architectures. The permanent drift NPVs are all lower compared to the SAC3-A2-1 architecture, while peak drift NPVs are higher for the high and medium suite, but reduced for the low suite. These results indicate that the reduction of global structural damage at the 50^{th} percentile level using resetable actuators is not increased by placing some of the available actuator authority on the roof of the three-story

structure, rather than just on stories 1 and 2. This conclusion is a potentially counterintuitive finding for a decentralised controller, as one might have expected larger benefits to be attained when each of the stories is controlled. However, considering the extremely high first mode contribution to the structural response, the SAC3 structural response is such that story drifts are relatively constant. Hence, the top floor would tend to follow the motion of the stories below. It should be noted that this type of behaviour should only be expected for squat shear buildings, and is not likely for taller structures, where top-whip and higher mode contributions are a major concern.

The NPVs for the JQR clipped optimal controller shown in Table 7.3 are all increased for the low earthquake suite, compared to the SAC3-A1 architecture, while permanent drift NPVs are reduced for the high and medium suites. The peak drift NPV is greatly reduced for the high suite, while that for the medium suite has a slight increase compared to the SAC3-A1 case. Peak acceleration NPVs increase across each of the three suites, however, each of the average percentage changes are still positive. This mixture of increased and decreased NPVs leads to the suggestion that the choice of control architecture for the JQR controller is dependent on the likely magnitude of seismic events, and whether story drifts or accelerations are of primary concern.

7.2.1.2 SAC9 PERFORMANCE: HYSTERETIC ENERGY NORMALISATION

The normalised results for the SAC9-A3 control architecture, using the change in structural hysteretic energy, are presented in Table 7.4. The SAC9-A3 control architecture has the maximum actuator authority of 1500kips distributed across floors 2, 3 and 9, with a ratio of 50%:37%:13%, respectively. The peak drift NPVs are comparable for each of the three control designs across the three earthquake suites, although the decentralised resetable

actuator has the largest values for each of the three earthquake suites. The resetable actuator also has the largest permanent drift NPVs for the high and medium suites, indicating the effectiveness of this control law's focus on maximum energy dissipation for reductions of structural damage in tall, slender structures using this control architecture.

As was observed for the SAC3 NPVs, the resetable actuator has negative peak acceleration NPVs, indicating potential increases in internal or occupant damage despite clear reductions in external structural damage. In contrast to this result, the peak acceleration NPVs for the LQR and LQRy clipped optimal controllers are positive for each of the earthquake suites, with the LQR controller having the largest acceleration NPV for the medium suite. In contrast to this results, for the SAC3-A1 control architecture, the LQRy controller was the only controller to produce all positive acceleration NPVs. This difference highlights the importance of considering different architectures and structural characteristics when undertaking controller comparisons, as the interaction of the control and structural systems may differ greatly. The acceleration NPVs for the high suite are substantially less for this LQRy controller compared to those for the SAC3 control architectures, while those for the LQR controller are slightly larger. This trend potentially indicates the difficulty of centralised acceleration control for tall structures subjected to extreme near-field excitations, using a limited distribution of actuator authority.

TABLE 7.4: SAC9-A3 HYSTERETIC ENERGY NORMALISED AVERAGE GEOMETRIC-MEAN RESULTS.

	High Suite		Medium Suite		Low Suite	
	% Reduction	**NPV**	**% Reduction**	**NPV**	**% Reduction**	**NPV**
LQR						
Average Peak Drift	-13.25	**0.56**	-24.67	**0.75**	-38.90	**29.68**
Average Permanent Drift	-2.19	**0.09**	-38.18	**1.16**	-90.62	**69.15**
Average Peak Acceleration	-4.26	**0.18**	-4.87	**0.15**	-18.79	**14.34**
LQRy						
Average Peak Drift	-19.46	**0.54**	-27.14	**0.87**	-44.71	**34.12**
Average Permanent Drift	0.29	**-0.01**	-47.90	**1.54**	-93.90	**71.65**
Average Peak Acceleration	-6.87	**0.19**	0.04	**0.00**	-40.06	**30.56**
Resetable						
Average Peak Drift	-21.40	**0.64**	-33.48	**0.93**	-55.23	**42.13**
Average Permanent Drift	-26.93	**0.80**	-76.62	**2.13**	-92.35	**70.44**
Average Peak Acceleration	27.26	**-0.81**	57.42	**-1.60**	31.99	**-24.40**

The normalised results for the SAC9-A8 control architecture are presented in Table 7.5, with normalisation undertaken using the scaled change in hysteretic energy between the controlled and uncontrolled responses. The SAC9-A8 control architecture has actuator tendons attached to floors 2 through 8, with an ATMD positioned on the roof of the structure, as shown in Figure 6.5. Like the SAC9-A3 architecture, this system does not actuate the soft first story to allow it to perform as designed. The maximum actuator authority is 1500kips, which represents 13.6% of the building weight, and is the same as that used for the SAC9-A3 control architecture.

Compared to the results presented in Table 7.4 for the SAC9-A3 architecture, only small changes in NPVs are observed. The effect of applying control forces on eight floors rather than only three appears detrimental to the performance of the LQR controller, with reductions seen in each of the NPVs except the peak drift for the high suite, which shows a 19.6% increase. In contrast to this result, the LQRy controller shows general increases in NPVs,

with notable increases seen for the high suite in particular. The differences between the LQR and LQRy clipped optimal controllers for the SAC9-A3 and SAC9-A8 architectures are perhaps indicative of the different characteristics of centralised displacement and acceleration controllers, with acceleration control much less effective than displacement control when the majority of floors are left uncontrolled. An additional possibility is that the particular regulator design weighting matrices, **Q** and **R**, could be modified to achieve more equivalent results for the two control architectures.

The LQRy controller has the largest permanent drift NPVs for the three controllers, and the largest peak drift NPVs for the medium and low suites. This result shows the overall benefit of centralised acceleration control, as in addition to the reduction of peak accelerations that are related to occupant damage, reductions in peak and permanent deformation indicate reductions in external structural damage. It should be noted that although the performance of the LQRy controller may be considered superior to that of the LQR controller for the SAC9-A8 control architecture, it may be seen that the performance of the LQR controller for the SAC9-A3 control architecture is generally comparable. With many fewer tendons required for the SAC9-A3 architecture, its use with the LQR controller may be more practically favourable than the LQRy controller with the SAC9-A8 architecture.

Considering the decentralised nature of the resetable actuator, one would expect the response reductions to increase as more floors are actuated due to the multi-mode structural response. This trend may be seen through comparison of resetable actuator NPVs presented in Tables 7.4 and 7.5, for the SAC9-A3 and SAC9-A8 control architectures respectively. Each of the resetable actuator NPVs shown in Table 7.5 are larger than their equivalent measures in Table 7.4, with the exception of the high suite permanent drift NPV, which shows a slight decrease for the SAC9-A8 architecture. This result differs to the similar comparison for the SAC3

control architectures, highlighting the participation of higher modes in the SAC9 structural response, and their impact on controller performance. The peak acceleration for the resetable actuator has been a major deficiency in performance. However, the SAC9-A8 peak acceleration NPVs increase by 63%, 73%, and 107% for the high, medium, and low earthquake suites respectively, compared to those in Table 7.4, greatly increasing the viability of this type of decentralised control.

TABLE 7.5: SAC9-A8 HYSTERETIC ENERGY NORMALISED AVERAGE GEOMETRIC-MEAN RESULTS.

	High Suite		**Medium Suite**		**Low Suite**	
	% Reduction	**NPV**	**% Reduction**	**NPV**	**% Reduction**	**NPV**
LQR						
Average Peak Drift	-12.27	**0.67**	-19.65	**0.69**	-31.44	**24.01**
Average Permanent Drift	-1.13	**0.06**	-19.56	**0.69**	-83.78	**63.97**
Average Peak Acceleration	-2.23	**0.12**	-3.40	**0.12**	-14.08	**10.75**
LQRy						
Average Peak Drift	-17.67	**0.57**	-40.42	**1.07**	-57.20	**43.63**
Average Permanent Drift	-14.04	**0.46**	-80.31	**2.12**	-93.86	**71.59**
Average Peak Acceleration	-12.56	**0.41**	4.56	**-0.12**	-29.53	**22.52**
Resetable						
Average Peak Drift	-22.97	**0.81**	-39.17	**1.01**	-56.43	**43.04**
Average Permanent Drift	-46.61	**1.64**	-90.08	**2.32**	-91.87	**70.08**
Average Peak Acceleration	8.55	**-0.30**	16.55	**-0.43**	-2.22	**1.69**

7.2.2 Control Energy Performance Normalisation: SAC9

This section presents the average results for the SAC9 structural simulations using the $\mathbf{L_2}$-norm normalisation method described in Section 7.1. It should be noted that this normalisation method uses the rms value of the control input energy, whereas the hysteretic energy normalisation is undertaken using the mean reduction in hysteretic energy, which is approximately proportional to control input energy for semi-active control systems. Hence,

the NPVs for the two normalisation techniques may show different trends, depending on the specific distributions. However, the NPVs obtained from each of the normalisation methods are equally valid, but are measures of different levels of control energy within the distribution, and therefore are different perspectives on overall energy management.

The normalised results for the SAC9-A3 control architecture are presented in Table 7.6 for the LQR and LQRy clipped optimal controllers, and the decentralised resetable actuator. Compared to the hysteretic energy normalised NPVs in Table 7.4, it is interesting to note that the NPVs in Table 7.6 are, relative to each other, generally higher for the centralised controllers, but lower for the decentralised resetable actuator. The LQR controller has the highest peak drift NPVs, as well as the highest permanent drift NPVs for the medium and low earthquake suites. This result is in direct contrast to the hysteretic energy normalised results, which showed the resetable actuator to have the highest peak and permanent drift NPVs. This observation highlights the difference between the rms and mean energy values employed, with the decentralised resetable actuator clearly having a larger distribution spread compared to the centralised controllers.

The LQR and LQRy clipped optimal controllers have approximately the same peak acceleration NPVs for the high suite, while for the low suite the LQRy controller has the largest acceleration NPV. The resetable actuator is the only controller to have all negative peak acceleration NPVs, following the trends obtained using the hysteretic energy normalisation.

One of the advantages of using this control energy normalisation is the ability to obtain non-trivial NPVs for the hysteretic energy performance. For the high earthquake suite, the LQRy controller has the highest hysteretic energy NPV, while the LQR controller has the highest for

the medium and low suites. These results indicate that for smaller magnitude near-field, and all far field excitations, the LQR controller is better able to reduce structural hysteretic energy than the LQRy controller. As the LQR controller is primarily displacement focused, and the hysteretic energy at the structural joints is a function of beam-column joint rotations, the higher energy NPVs are expected.

TABLE 7.6: SAC9-A3 CONTROL ENERGY NORMALISED AVERAGE GEOMETRIC-MEAN RESULTS.

	High Suite		Medium Suite		Low Suite	
	% Reduction	**Norm**	**% Reduction**	**Norm**	**% Reduction**	**Norm**
LQR						
Average Peak Drift	-13.25	**0.79**	-24.67	**1.88**	-38.90	**5.56**
Average Permanent Drift	-2.19	**0.13**	-38.18	**2.91**	-90.62	**12.96**
Average Peak Acceleration	-4.26	**0.25**	-4.87	**0.37**	-18.79	**2.69**
Average Hysteretic Energy	-35.42	**2.11**	-81.58	**6.21**	-98.67	**14.11**
LQRy						
Average Peak Drift	-19.46	**0.69**	-27.14	**0.98**	-44.71	**3.23**
Average Permanent Drift	0.29	**-0.01**	-47.90	**1.72**	-93.90	**6.79**
Average Peak Acceleration	-6.87	**0.24**	0.04	**0.00**	-40.06	**2.89**
Average Hysteretic Energy	-60.57	**2.15**	-83.93	**3.02**	-99.36	**7.18**
Resetable						
Average Peak Drift	-21.40	**0.58**	-33.48	**0.80**	-55.23	**1.91**
Average Permanent Drift	-26.93	**0.73**	-76.62	**1.83**	-92.35	**3.19**
Average Peak Acceleration	27.26	**-0.74**	57.42	**-1.37**	31.99	**-1.10**
Average Hysteretic Energy	-52.84	**1.43**	-86.69	**2.07**	-99.65	**3.44**

The control energy normalised results for the SAC9-A8 control architecture are presented in Table 7.7. The general trend observed from comparison of the SAC9-A3 and SAC9-A8 architectures suggests that the largest benefits from SAC9-A8 control architecture are obtained by the LQRy and resetable controllers, with increases observed in the majority of the NPVs. As discussed previously, this trend suggests that more effective centralised acceleration control, and decentralised energy control, is obtained when the maximum

actuator authority is distributed over a large number of floors. This conclusion is in contrast to the LQR controller, which sees most of its NPV increases for the low suite only. Hysteretic energy NPVs are generally reduced slightly compared to those for the SAC9-A3 architecture, excluding the high suite LQRy and resetable NPVs, which show small increases. This result suggests that little hysteretic energy reduction benefit is obtained from a greater distribution of actuator authority. However, a more even distribution of actuator authority up the structure may show a different trend, as the actuator authority placed on floors 4 to 9 in the SAC9-A8 control architecture may be insufficient, compared to the large forces on floors 2 and 3, to reduce the effects of top-whip that result from the increased stiffness lower in the structure.

Compared to the hysteretic energy normalisation results for the SAC9-A8 actuator architecture, presented in Table 7.5, the most significant difference with those in Table 7.7 is seen in the relative performance of the LQR controller. In Table 7.5, the LQR controller has the largest NPV for the medium suite peak acceleration only, with maximum NPVs for the other metrics shared between the LQRy and resetable controllers. However, in Table 7.7 the LQR controller has the maximum NPVs for some of the metrics for each of the three earthquake suites. This difference again highlights the different control energy distribution characteristics at the 50^{th} and 70.7^{th} (rms) percentile levels for different types of controller.

TABLE 7.7: SAC9-A8 CONTROL ENERGY NORMALISED AVERAGE GEOMETRIC-MEAN RESULTS.

	High Suite		Medium Suite		Low Suite	
	% Reduction	**Norm**	**% Reduction**	**Norm**	**% Reduction**	**Norm**
LQR						
Average Peak Drift	-12.27	**1.14**	-19.65	**2.28**	-31.44	**6.71**
Average Permanent Drift	-1.13	**0.11**	-19.56	**2.26**	-83.78	**17.88**
Average Peak Acceleration	-2.23	**0.21**	-3.40	**0.39**	-14.08	**3.00**
Average Hysteretic Energy	-31.67	**2.95**	-69.97	**8.10**	-96.40	**20.57**
LQRy						
Average Peak Drift	-17.67	**0.87**	-40.42	**1.22**	-57.20	**3.82**
Average Permanent Drift	-14.04	**0.69**	-80.31	**2.42**	-93.86	**6.26**
Average Peak Acceleration	-12.56	**0.62**	4.56	**-0.14**	-29.53	**1.97**
Average Hysteretic Energy	-53.64	**2.65**	-96.35	**2.91**	-99.90	**6.67**
Resetable						
Average Peak Drift	-22.97	**0.71**	-39.17	**1.24**	-56.43	**2.66**
Average Permanent Drift	-46.61	**1.45**	-90.08	**2.85**	-91.87	**4.33**
Average Peak Acceleration	8.55	**-0.27**	16.55	**-0.52**	-2.22	**0.10**
Average Hysteretic Energy	-46.61	**1.45**	-97.88	**3.09**	-99.78	**4.70**

7.3 PASSIVE CONTROL COMPARISON

Although semi-active controllers offer greater potential for practical implementation then fully active systems, to gain acceptance in the structural engineering community their performance must be superior to passive systems already in use. As discussed previously, passive systems perform acceptably within their specific design envelope, but unlike semi-active systems they are not always suited to wide ranges of seismic excitations and structural responses. As it is assumed that semi-active control systems have wider performance bandwidths than passive systems, this section focuses on performance comparisons for the high earthquake suite only.

Using previous research in this area, results were obtained for a passive viscous brace system using the same structures and earthquake suites employed in this investigation [Breneman 2000]. Only the peak drift and hysteretic energy were used to define the structural response in this prior research, hence comparisons are made with these metrics only. It should be noted that the lack of peak acceleration response presentation in the previous research is of concern, as large reductions in peak drifts through extremely large control forces may result in significant increases in floor accelerations.

Prior SAC3 passive system research places viscous dampers on all three floors, with unlimited actuator authority. The 84^{th} percentile of the actuator authority distribution is 3454kips, which represents approximately 106% of the building weight. This level of actuator authority may not currently be practically realisable, as the required energy dissipation would be potentially immense. The passive brace system was designed to introduce 30% critical damping into the first mode of the structural response, although it should be noted that pure damping is not completely obtainable, with some stiffness contribution inherent in most large viscous dampers.

The structural response for the passive system is shown in Table 7.8, while those for the SAC3-A3-1 semi-active LQRy and resetable control systems, with maximum actuator authorities of 450kips (13.8% of building weight), are presented in Tables 7.9 and 7.10, respectively. The LQRy and resetable control systems are presented to given an indication of both semi-active centralised and decentralised control, allowing valid comparison with the decentralised passive system. While the percentage reductions for both peak drift and hysteretic energy are larger for the passive system, the reductions for the LQRy and resetable controllers are such that it is clear that the much lower actuator authority is used much more

effectively by the semi-active systems, using both centralised and decentralised control methods.

TABLE 7.8: SAC3 RESPONSE FOR VISCOUS BRACE SYSTEM FOR HIGH EARTHQUAKE SUITES [BRENEMAN 2000].

	Gr	F1	F2	F3
Geometric-Mean/50th percentile				
Peak Drift (%)		-34.25	-45.27	-65.63
Hysteretic Energy (%)	-68.76	-64.76	-90.67	-94.81
84th Percentile				
Peak Drift (%)		-41.35	-51.94	-69.46
Hysteretic Energy (%)	-47.10	-58.43	-85.71	-95.44

TABLE 7.9: SAC3-A3-1 RESPONSE FOR HIGH EARTHQUAKE SUITE USING LQRY CONTROLLER.

	Geometric-mean/50th Percentile			
	Gr	**F1**	**F2**	**F3**
Geometric-Mean/50th percentile				
Peak Drift (%)		-13.66	-6.86	-12.25
Hysteretic Energy (%)	-52.93	-30.97	-23.75	-62.30
84th Percentile				
Peak Drift (%)		-15.29	-7.04	-11.63
Hysteretic Energy (%)	-40.05	-27.00	-23.27	-38.64

TABLE 7.10: SAC3-A3-1 RESPONSE FOR HIGH EARTHQUAKE SUITE USING DECENTRALISED RESETABLE CONTROLLER.

	Geometric-mean/50th Percentile			
	Gr	**F1**	**F2**	**F3**
Geometric-Mean/50th percentile				
Peak Drift (%)		-10.41	-5.48	-4.80
Hysteretic Energy (%)	-21.94	-18.88	-13.90	-21.33
84th Percentile				
Peak Drift (%)		-11.62	-7.59	-6.17
Hysteretic Energy (%)	-25.19	-12.59	-15.19	-18.33

The passive brace control system architecture for the SAC9 viscous brace system has actuators placed on floors 1, 3, and 9. Its maximum actuator authority is unlimited with an 84th percentile value of 4572kips distributed approximately evenly between the actuators. This peak actuator authority represents 44% of the building weight. Although this control architecture was not used in this investigation due to the desire to retain the soft first story, a performance comparison may be made with the SAC9-A3 architecture, which has a maximum actuator authority of 1500kips (13.8% of building weight) distributed across floors 2, 3, and 9.

The response for the passive viscous brace system is presented in Table 7.11. For the geometric-mean, increases in peak drift are observed on floors 4, 5, and 6, while hysteretic energy is seen to increase on floors 4 and 5. At the 84th percentile level, peak drifts also increase on floors 5 and 6. These results show the inability of the passive system to control the higher mode contributions within the structural response with this limited control architecture. Specifically, the extremum for the third mode located approximately at sixth floor.

In contrast to this response, the response for the semi-active LQRy clipped optimal controller, presented in Table 7.12 show reductions in both peak drift and hysteretic energy for all nine floors at both percentile levels. The response for the decentralised resetable controller, presented in Table 7.13, shows reductions in both peak drift and hysteretic energy, with the exception of the floor 1 hysteretic energy and the floor 6 peak drift at the 84th percentile level. The increased peak drift for floor 6 appears to be a feature of the decentralised controller with limited actuator authority distribution, while the increased floor 1 hysteretic energy is due to the combination of the retained soft first story, and the decentralised displacement regulation of the second story. The increase in floor 6 peak drift is 75% smaller than that for the passive control system. Despite the use of over three times the actuator authority in the passive

control system, the reductions from the semi-active systems are comparable to, and in some cases greater than, those for the passive system. Hence, it can be clearly seen that the global response reductions for the semi-active system, and the efficiency with which they are attained, are generally superior to the passive system.

TABLE 7.11: SAC9 RESPONSE FOR VISCOUS BRACE SYSTEM FOR HIGH EARTHQUAKE SUITES [BRENEMAN 2000].

	GR	F1	F2	F3	F4	F5	F6	F7	F8	F9
Geometric-Mean/50th percentile										
Peak Drift (%)		-30.00	-26.25	-11.95	0.00	5.67	0.00	-30.79	-57.00	-53.68
Hysteretic Energy (%)	-83.04	-78.93	-62.47	-61.03	18.12	40.11	-31.93	-90.79	-94.66	-80.00
84th Percentile										
Peak Drift (%)		-33.22	-23.93	-11.61	-3.12	4.95	7.04	-23.25	-52.61	-42.52
Hysteretic Energy (%)	-60.14	-27.04	-26.01	-17.91	-10.10	-14.99	-18.40	-77.70	-86.71	-93.65

TABLE 7.12: SAC9-A3 RESPONSE FOR HIGH EARTHQUAKE SUITE USING LQRY CONTROLLER.

	GR	F1	F2	F3	F4	F5	F6	F7	F8	F9
Geometric-Mean/50th percentile										
Peak Drift (%)		-11.40	-10.37	-11.56	-15.03	-17.35	-21.38	-23.93	-30.05	-34.07
Hysteretic Energy (%)	-76.47	-53.38	-46.02	-43.62	-43.21	-54.07	-54.73	-66.33	-76.14	-91.78
84th Percentile										
Peak Drift (%)		-7.99	-9.84	-10.42	-15.29	-14.44	-15.14	-14.97	-19.68	-25.02
Hysteretic Energy (%)	-13.90	-11.71	-22.64	-32.73	-40.02	-46.49	-54.61	-69.39	-71.96	-83.74

TABLE 7.13: SAC9-A3 RESPONSE FOR HIGH EARTHQUAKE SUITE USING DECENTRALISED RESETABLE CONTROLLER.

	GR	F1	F2	F3	F4	F5	F6	F7	F8	F9
Geometric-Mean/50th percentile										
Peak Drift (%)		-18.47	-24.60	-27.44	-25.34	-22.27	-15.55	-17.82	-21.58	-19.51
Hysteretic Energy (%)	-74.58	-54.47	-53.80	-35.03	-55.27	-60.47	-37.60	-53.43	-49.51	-54.21
84th Percentile										
Peak Drift (%)		-12.13	-17.17	-19.42	-22.41	-16.29	1.76	-2.41	-7.94	-10.84
Hysteretic Energy (%)	28.11	-39.13	-47.27	-51.66	-58.70	-47.90	-35.58	-53.43	-54.62	-68.20

7.4 EXTREME EARTHQUAKE CONTRIBUTION

As discussed in Section 2.3, the three earthquake suites consist of 10 pairs of earthquakes appropriately scaled such that the total suite fits pre-defined statistical levels of excedance. An important note about these earthquake suites is that the probabilities of excedance are representative of the geometric-mean of the entire suite. Therefore, while at any particular period the geometric-mean spectral accelerations of the entire suite may fit the desired excitation level, individual earthquakes may exceed that level. To represent the overall response trends for each suite, a lognormal distribution of response was assumed, as presented in Section 5.2. A desirable feature of the lognormal distribution is the ability to accurately represent the distribution characteristics with relative insensitivity to the responses at the extreme end of the distribution. This section briefly examines the sensitivity of the lognormal distribution to extreme events within the high earthquake suite.

The Elysian Park Earthquake is the 17^{th} record within the high earthquake suite, and represents the most extreme event in the suite, with large magnitude and rapidly changing accelerations. It was consistently, and by far, the input with the largest peak and permanent deflection results. As a simple assessment of the lognormal distribution's sensitivity to extreme events, the lognormal statistics were recalculated for the SAC3-A3-1 LQRy control system after the removal of this Elysian Park response. Table 7.14 presents the differences between the suite responses with and without the Elysian Park record. The largest differences are observed in the hysteretic energy reductions, which is indicative of the large amount of jolt within the Elysian Park response. However, the largest difference is still only 3.25%, which is small compared to the typical SAC3 hysteretic energy reductions. Hence, the sensitivity of the lognormal distribution to extreme events is appropriate for the level of detail required in this investigation.

TABLE 7.14: ABSOLUTE DIFFERENCE BETWEEN HIGH EARTHQUAKE SUITE WITH & WITHOUT EQ38 (ELYSIAN PARK) FOR SAC3-A3-1 LQRY CONTROL SYSTEM

	Numerical Average Difference				Geometric-mean/50th Percentile Difference				84th Percentile Difference			
	Gr	**F1**	**F2**	**F3**	**Gr**	**F1**	**F2**	**F3**	**Gr**	**F1**	**F2**	**F3**
Peak Drift (% diff)		-0.15	0.35	0.49		-0.04	0.18	0.20		-0.24	0.46	0.86
Permanent Drift (% diff)		-0.47	-1.82	-2.87		-0.05	-0.51	-1.42		-0.18	-0.11	-0.55
Peak Acceleration (% diff)		-0.20	-0.43	0.09		-0.31	-0.46	0.08		0.07	-0.39	0.14
Hysteretic Energy (% diff)	-0.56	-0.16	0.14	-0.20	2.83	1.08	-3.25	2.51	-0.14	2.80	2.36	-2.85

7.5 IMPACT OF TRACKING PERMANENT DEFLECTIONS

Previous structural control investigations have shown the importance of including non-linear structural behaviour, with structural demands larger than those for a comparative linear analysis [Barroso et al. 2001]. The structural models used in this investigation include non-linear joint plasticity and yielding, allowing residual permanent deformation to be analysed. This section examines the impact of tracking the time-varying equilibrium position, a novel technique presented in Section 4.3.2, on controlled response.

To illustrate the effect of tracking the moving-zero, the results for the SAC3-A1 LQRy clipped optimal controller are presented for simulations including and excluding the tracking technique. For the clipped-optimal controllers the moving-zero displacements are subtracted from the lateral degrees of freedom for each floor before multiplication by the state feedback gains. Hence, control forces are determined based on displacement relative to the permanent deformation, which represents the final equilibrium position. This approach means that oscillations that are entirely positive or negative, have both positive and negative displacements relative to the permanent deflection. Velocities within the reduced state vector are unaffected by the time-varying equilibrium position. Although the reduction of accelerations is the target of the LQRy controller, results from each of the LQRy simulations

have shown reduced peak and permanent deformations in addition to accelerations. Hence, the following discussion is equally applicable for the displacement-based controllers.

Practically, the exclusion of moving-zero tracking means that during the negative half of any oscillation, the controller attempts to augment the response of the structure to push it back towards the original equilibrium position. This concept is illustrated in Figure 7.2(a) for the uncontrolled high suite Elysian Park Earthquake, where d_T and d_{NT} are the displacements used in the control law for the tracking and non-tracking cases, respectively. The resulting controlled floor 1 drifts are presented in Figure 7.2(b), showing the reduced permanent drifts that result from the extreme control forces that are applied to the structure when the moving-zero is excluded. As shown in Figure 7.2(b), the responses approximately follow the same path between 6 and 8 seconds, during which time the largest jolt in the earthquake record occurs. Following this large transient deflection, the responses separate, with the large control forces acting to re-yield the structure back towards its equilibrium position for the non-tracking case. Comparing the tracking response in Figure 7.2(b) with the uncontrolled response in Figure 7.2(a), the permanent deflections are reduced by over 2 inches, despite the inclusion of the permanent deflection tracking which effectively stops the control forces attempting to re-yield the structure back to its original position. It should be noted that increased joint flexibility resulting from yielding is not included in the structural models, which applies equal joint resisting moments independent of whether prior yielding has occurred.

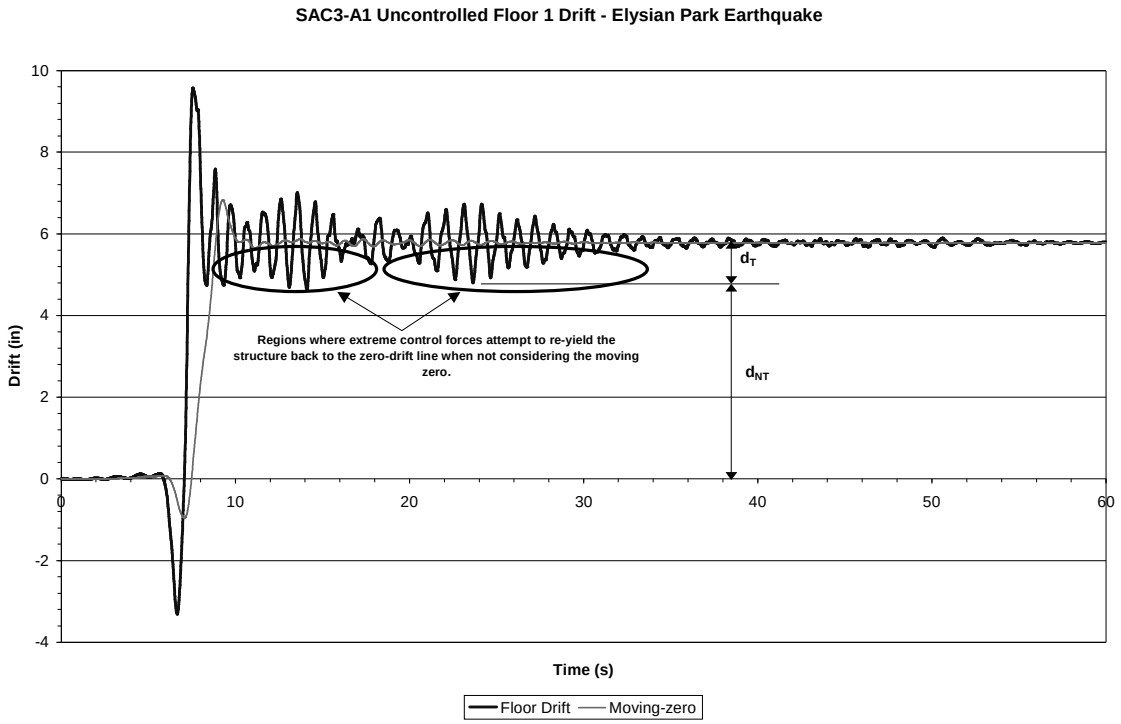

(a)

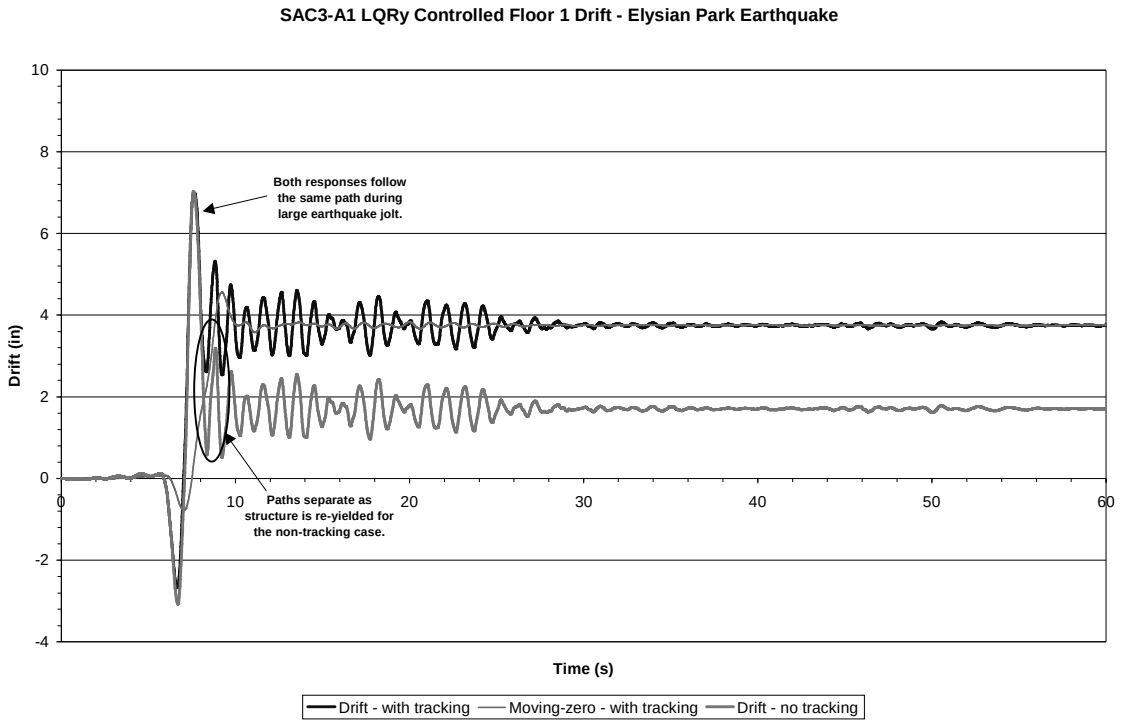

(b)

Figure 7.2: SAC3-A1 tracking comparison. (a) Uncontrolled floor 1 drift. (b) LQRy controlled floor 1 drift with and without tracking.

Table 7.15 presents the results for all three earthquake suites for simulations including, and excluding, moving-zero tracking. The impact of the moving-zero extends to all four response metrics, with several trends clearly visible:

i) The differences between the simulations including and excluding the moving-zero are most pronounced for the high earthquake suite, with very little difference observed for the low suite. This result highlights the contrast of near- and far-field seismic effects, with the far-field events in the low suites resulting in very little residual permanent deformation. Hence, the time-varying equilibrium position is very close to the original building position for the low suite, so very little adjustment to the control law or response results when tracking is not implemented.

ii) The reductions in both peak acceleration and hysteretic energy are smaller for the non-tracking cases. The average high suite 84^{th} percentile values for peak acceleration are -15.0% and +15.3% for the tracking and non-tracking cases respectively, while the hysteretic energy changes are -25.0% and -17.8% respectively. The higher accelerations are a result of the larger control forces that are applied in the incorrect direction during the half of the motion below the time-varying equilibrium point. The increased hysteretic energy, when tracking is excluded, is indicative of the re-yielding that occurs as the controller actuates each story relative to its original zero position. As the structure is re-yielded hysteretic energy is increased versus the tracking case, using this model. Since hysteretic energy gives an indication of the structural damage, it may be concluded that the exclusion of moving-zero tracking results in increased structural damage. It should be noted that the re-yielding that occurs is contrary to the nature of semi-active control, as energy may actually be supplied to the structure in the non-tracking case.

iii) Although permanent drift reductions are larger when the moving-zero is not used, peak drift reductions are actually slightly smaller. Increases in peak drift, when the moving-zero is not used, are most likely due to actuating in the wrong direction during the negative half cycle, as well as over-actuating during the rest of the oscillation. This action may in fact lead to structural instability. Hence, despite larger control forces due to not tracking the permanent deflections, the peak drift reductions are smaller when the moving-zero is not incorporated in the control law.

TABLE 7.15: RESULTS FOR SAC3-A1 ARCHITECTURE FOR LQRY CONTROLLER, WITH & WITHOUT TRACKING MOVING-ZERO

	Numerical Average				**Geometric-mean/50th Percentile**				**84th Percentile**			
	Gr	**F1**	**F2**	**F3**	**Gr**	**F1**	**F2**	**F3**	**Gr**	**F1**	**F2**	**F3**
High Suite (With Tracking)												
Peak Drift (%)		-22.35	-9.40	-7.18		-22.62	-8.66	-7.58		-22.99	-10.02	-5.10
Permanent Drift (%)		-17.68	-14.02	-12.42		-15.79	-26.83	-28.87		-23.38	18.10	14.07
Peak Acceleration (%)		-15.90	-21.12	-9.71		-16.31	-21.66	-9.54		-14.32	-19.79	-10.88
Hysteretic Energy (%)	-47.79	-23.11	-10.31	-20.78	-56.75	-20.38	-9.65	-21.65	-46.89	-21.30	-13.10	-18.79
High Suite (No Tracking)												
Peak Drift (%)		-19.02	-5.96	-3.09		-18.62	-5.71	-3.92		-20.56	-6.46	-1.13
Permanent Drift (%)		-43.05	-31.59	-20.20		-33.45	-40.28	-20.32		-54.46	-24.06	-23.36
Peak Acceleration (%)		17.81	-1.46	-2.14		9.96	-3.52	-2.89		38.46	5.42	1.90
Hysteretic Energy (%)	-28.08	-13.06	-4.95	-15.40	-27.56	-7.26	-18.99	-27.83	-27.68	-12.50	-10.95	-20.24
Medium Suite (With Tracking)												
Peak Drift (%)		-22.01	-7.59	-7.83		-20.81	-7.97	-9.55		-24.65	-6.32	-5.24
Permanent Drift (%)		-42.44	-16.03	-5.53		-64.19	-19.01	-24.87		-21.81	8.82	94.19
Peak Acceleration (%)		-23.24	-30.21	-13.32		-25.04	-30.28	-13.07		-20.77	-30.67	-14.85
Hysteretic Energy (%)	-69.37	-38.34	-24.76	-40.42	-76.21	-40.85	-30.00	-57.61	-64.92	-32.54	-28.05	-35.66
Medium Suite (No Tracking)												
Peak Drift (%)		-17.46	-6.42	-4.82		-16.84	-7.30	-6.83		-18.59	-3.99	-1.49
Permanent Drift (%)		-42.88	-17.85	2.21		-51.84	-32.62	-17.72		-28.71	27.80	46.84
Peak Acceleration (%)		17.17	-10.48	-9.54		4.92	-13.87	-9.82		38.95	-2.79	-8.22
Hysteretic Energy (%)	-49.85	-35.69	-23.03	-38.09	-60.66	-40.19	-26.86	-62.20	-58.00	-25.93	-20.30	-9.22
Low Suite (With Tracking)												
Peak Drift (%)		-23.48	-14.94	-18.78		-24.22	-18.30	-22.22		-21.93	-10.92	-17.36
Permanent Drift (%)		-44.81	-39.42	-38.79		-73.37	-84.02	-87.76		-72.45	-81.55	-85.63
Peak Acceleration (%)		-41.09	-45.00	-24.91		-45.48	-45.70	-25.25		-38.93	-45.21	-25.05
Hysteretic Energy (%)	-71.91	-61.14	-45.25	-57.77	-99.25	-98.13	-99.96	-100.00	-99.87	-47.93	-64.76	-99.93
Low Suite (No Tracking)												
Peak Drift (%)		-22.38	-16.36	-18.31		-24.00	-19.67	-21.95		-20.24	-12.80	-16.42
Permanent Drift (%)		-47.27	-26.70	-8.49		-71.84	-80.56	-85.81		-74.79	-74.73	-78.34
Peak Acceleration (%)		-39.99	-44.00	-24.53		-45.46	-45.21	-25.01		-37.53	-43.66	-24.34
Hysteretic Energy (%)	-58.52	-63.66	-46.18	-57.31	-99.46	-98.53	-99.97	-99.99	-97.18	-60.57	-78.36	-97.67

7.6 JERK DISTRIBUTION GRAPHICAL PERFORMANCE ASSESSMENT

In this investigation, the structural response for the different control systems and architectures has been assessed using peak drifts, permanent drifts, peak accelerations, and structural hysteretic energy, each determined at appropriate lognormal percentile levels. A performance measure not previously used to assess structural performance, although it was introduced in the JQR clipped optimal control design, is the total structural jerk, or time rate of change of structural acceleration. Structural jerk, presented in Section 4.7, is potentially related to both external damage and occupant safety, and with further development may be an area of great future potential. This section presents a graphical method of assessing the level of structural jerk for different controllers, using the LQR, LQRy, and JQR optimal controllers with linear simulations.

Figure 7.3 presents the distribution of structural jerk magnitudes for the uncontrolled, LQR, LQRy, clipped JQR, and unclipped JQR controllers. If using this type of jerk distribution as an assessment of the structural performance, it is desirable to have the distribution positioned as far to the left as possible. From Figure 7.3, it can be clearly seen that each of the controlled jerk distributions are situated further left than the uncontrolled response, with an order of magnitude difference between the controlled and uncontrolled distribution peaks. The LQRy and unclipped JQR jerk distributions are very similar, although the LQRy distribution has a slightly higher frequency to the left of the large peak. The LQR jerk distribution is comparable to that for the LQRy controller, however, there is a slight shift to the right for larger magnitudes to the right of the peak.

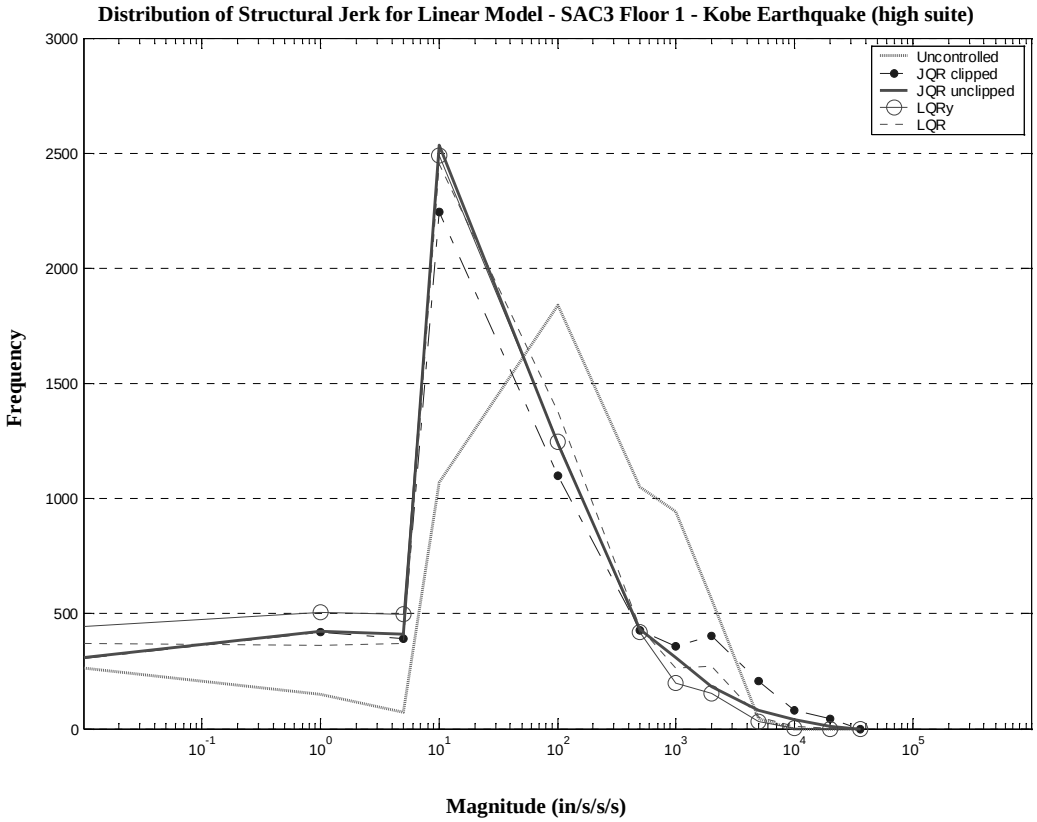

Figure 7.3: Floor 1 total structural jerk distribution for SAC3 linear model – Kobe Earthquake (high suite).

It should be noted that the effect of actuator saturation clipping on the jerk distribution for the JQR controller in Figure 7.3 is quite clear. The clipped distribution has a lower main peak, with a measurable amount of large magnitude values where the frequencies for the other clipped optimal controllers go to zero. When the actuator force is clipped, there is a significant amount of a "stick-slip" impulse due to the effect of non-linear saturation, resulting in an increase in structural jerk. The effect of this impulse on the structural jerk is illustrated in Figure 7.4, which presents the jerk for the uncontrolled and clipped JQR control cases during strong motion. It can be seen that during clipping the controlled jerk rapidly grows larger than the uncontrolled case, with the largest increase occurring when the control input is switched between positive and negative extremes. In the brief periods in between actuator clipping, the magnitude of the controlled jerks are, as designed and expected, lower

than the uncontrolled case. It should be noted that none of the optimal control designs explicitly accounts for saturation clipping.

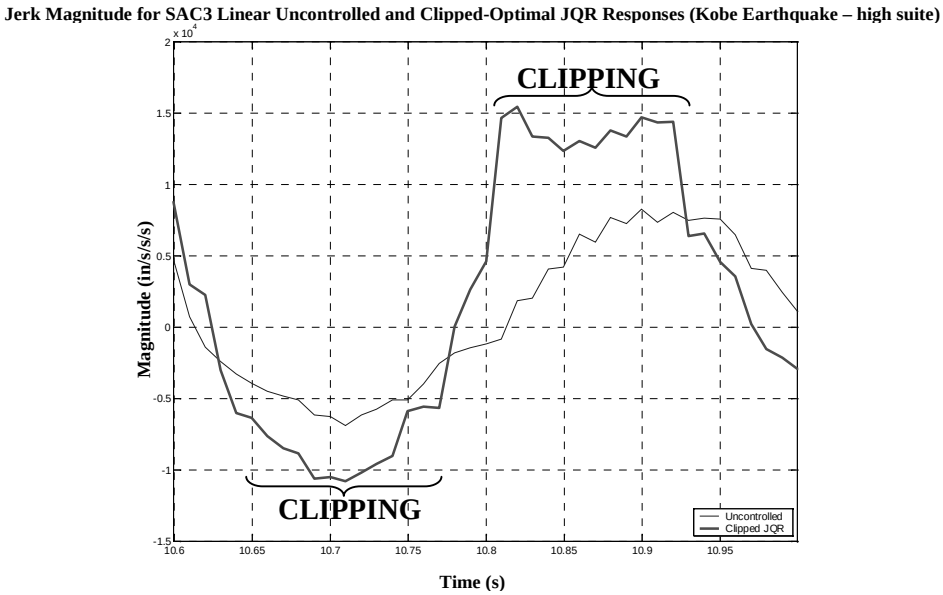

Figure 7.4: Effect of actuator force clipping on total structural jerk, during strong motion.

7.7 CHAPTER SUMMARY

This chapter has presented the normalised results for the SAC3 and SAC9 structural control simulations. Although the same maximum actuator authority was used within each of the simulations for each structure, the total amount of control input is dependent on the specific control law and the motion of the controlled structure. Normalisation is a means of processing results relative to the same datum, allowing comparisons to be made while still retaining the characteristics of the pre-normalised response. Two normalisation methods were presented with normalisation by the scaled change in structural hysteretic energy, and the $\mathbf{L_2}$-norm of the control input energy. For semi-active controllers the total system energy over an entire record remains constant, hence the change in hysteretic energy between the controlled and uncontrolled responses is proportional to the energy dissipated by the actuators. Both normalisations are indicative of the control input distribution, with the hysteretic energy

method representing the 50th percentile level, and the $\mathbf{L_2}$-norm method representing the 70.7th percentile. Normalised performance values (NPVs) were presented for the average geometric-mean response across all floors for each of the four performance metrics used in this investigation.

For the SAC3-A1 control architecture the LQRy controller was the only controller to show positive NPVs for each of the performance metrics across the entire response distribution. While the focus of the LQRy control design is on the minimisation of total structural accelerations, this result highlights the benefit of acceleration control as a means of reducing both internal occupant, and external structural, damage for the SAC3 building. The NPVs for the quasi-bang-bang controller showed the effect of applying a semi-active resisting stiffness to minimise the transient displacements in a decentralised fashion, with negative permanent drift NPVs observed for the high and medium earthquake suites. In addition, displacement regulation was seen to increase the total structural accelerations during the medium and high earthquake suites.

The NPVs for the SAC3-A2-1 architecture suggested that for centralised acceleration regulation it is beneficial to locate some actuator authority on the second floor, with larger acceleration NPVs observed for the LQRy controller. However, these larger acceleration NPVs were in addition to slight decreases in drift NPVs. For the decentralised resetable controller, the SAC3-A2-1 architecture produced increases in permanent drift and peak acceleration NPVs.

The SAC3-A3-1 control architecture resulted in a mixture of larger and smaller NPVs compared to the other SAC3 architectures. Considering the general trends of the NPVs at the 50th percentile level, it appears that maximum average response reductions, per unit of control

cost, are achieved through the placement of a small amount of actuator authority on the upper two floors, with most of the actuator authority retained on the first floor.

Two control architectures were presented for the SAC9 structure, using the clipped optimal LQRy and JQR controllers, and the decentralised resetable actuator. The difference between the control of squat shear buildings and tall slender buildings was highlighted by the smaller LQRy NPVs for the SAC9-A3 control architecture, indicating the difficulty of centralised acceleration control for tall structures using a very limited distribution of actuator authority. The NPVs for both the centralised and decentralised controllers were increased for the SAC9-A8 control architecture, highlighting the benefit of controlling the maximum number of floors for structural responses with significant participation of higher modes.

Most of the NPVs for both the SAC3 and SAC9 structures show an approximately exponential trend from the high to the low earthquake suites, giving extremely large performance reductions for the more likely, yet still sizable, seismic events. The peak ground accelerations for the low earthquake suite are substantially lower than those in the high and medium suites. Hence, as the energy associated with the excitation is related to the square of the ground acceleration, the approximately exponential trend in response reductions across the three earthquake suites is expected.

A comparison with a passive viscous damper system was presented from previous research that used the SAC structures and earthquake suites [Breneman 2000]. For both structures the passive actuator authority was unlimited, with 84^{th} percentile peak actuator authorities of 106% and 44% of the building weight for the SAC3 and SAC9 structures respectively. Compared to the LQRy and resetable semi-active control systems, which use a maximum actuator authority of approximately 13% of the building weight, the reduction in peak drift

and hysteretic energy were comparable to, and in some cases greater than, those for the passive system. The superior efficiency with which the reductions were obtained for the semi-active system is clearly seen through the substantially lower maximum actuator authority.

This chapter concludes with a discussion of three similar characteristics of both the SAC3 and SAC9 results:

i) Although each earthquake suite is designed such that the mean spectral accelerations fit the defined statistical performance levels, the spectral accelerations of individual earthquakes within the suites may not. The ability of the lognormal distribution to accurately represent the response distributions with minimal sensitivity to extreme events within the high earthquake suite was demonstrated, showing that the use of this distribution allowed an average response for the prescribed level of excedance to be obtained.

ii) The impact of tracking the time-varying equilibrium point was presented using the LQRy controller. It was shown that although permanent displacement NPVs were larger when the moving-zero was not included, the reduced hysteretic energy and acceleration NPVs suggest that the large control forces act to re-yield the structure back to its original position, resulting in additional structural damage. Hence, the overall performance of the controller is improved through the inclusion of the time-varying equilibrium point.

iii) An alternative method of assessing the structural performance is through the use of jerk distributions. An example distribution was presented for a linear SAC3 model, showing the desired distribution shift to the left that was obtained through control application. The

impact of actuator clipping on the total structural jerk was also presented, showing increased jerk due to the ‘stick-slip’ impulse created by the clipping effect.

The following chapter presents a summary of this investigation, and continues to draw conclusions about key analysis methods and findings that arose from this research.

8. SUMMARY & CONCLUSIONS

This thesis explores the creation and assessment of semi-active control algorithms for both squat shear buildings and tall flexible structures. If cost-effective, practicable, robust, semi-active or active, structural control systems can be developed for both new and retrofit applications, the potential reduction in loss of both property and lives due to seismic events is significant. Semi-active controllers offer many of the benefits of active systems, but have power requirements orders of magnitude smaller, and do not introduce energy to the system. Previous research into semi-active controllers has shown their potential in linear simulations with single earthquake excitations. A distinguishing feature of this investigation is the use of appropriate non-linear modelling techniques and realistic suites of seismic excitations in the statistical assessment of the semi-active control systems developed.

To assess the affect of structural architecture on control system performance, simulations were undertaken with three and nine story building models, designated the SAC3 and SAC9 structures respectively. These buildings were developed as part of the SAC Phase II Project, and are structures designed and built for the Los Angeles area. This region has a high seismic risk, making it a primary candidate for implementation of semi-active control systems. Structural performance was assessed using acceleration recordings of actual earthquakes representing probabilities of excedance of 2%, 10%, and 50% in 50 years, or approximate mean return periods of 2475 years, 474 years, and 72 years respectively, for the Los Angeles region.

Finite element models of the SAC3 and SAC9 structures were developed to include essential non-linear effects. Non-linear structural hysteretic behaviour and yielding were included in

the models using a lumped-plasticity model, based on the assumption that plasticity is confined to the beam-column joints. Non-linear behaviour due to P-delta effects was also included through the use of a geometric stiffness matrix, reducing the structural lateral stiffness as a function of static gravity load. A comparison of the participation of higher modes for the linear and non-linear SAC9 structural models was undertaken, showing that the inclusion of non-linear effects greatly increases the contribution of the third and fourth modes in particular. This higher mode participation has significant impact on the implementation of structural control for the SAC9 building, which would not be seen with linear modelling or single earthquake excitation.

During initial investigations, it was discovered that placing actuator units on each floor of the SAC9 structure resulted in augmented responses for both the centralised and decentralised controllers, with drift, peak acceleration, and hysteretic energy increases observed on several floors. This result is attributed to the interaction of actuators on adjacent floors, which occurs when higher modes participate in the structural response. This type of interaction was not observed for the SAC3 structure, due to its predominantly first mode response. The problem of actuator-actuator interaction was resolved through the use of tendons attached between actuators on the ground and higher controlled floors. To reduce the force application angle, each tendon spans two of the lateral bays. In addition, a clipped optimal ATMD was placed on the ninth floor so tendons are not required to span the entire height of the structure. The response reductions using this modified architecture were significant.

The question of how to measure damage is difficult, with different types of damage possible during extreme earthquake motions. In addition to damage of structural joints, internal walls, and external cladding, damage assessment must also consider occupant safety and the potential risk to people and equipment inside an oscillating structure. This investigation used

four response metrics to account for the different types of potential damage, with peak drift correlating to damage to internal walls and cladding, permanent drifts and hysteretic energy representative of damage to structural members and joints, and peak accelerations correlating to occupant safety. These metrics were considered of equal importance when assessing the structural performance, however, relative importance for practical applications is dependent on the intentions for building use. For example, the control of a hospital building is primarily concerned with occupant safety, whereas for a commercial building the primary focus may be on the minimisation of structural damage to reduce repair expenses and maintain property value. However, a combination of these two types of damage is clearly required in all applications.

The three earthquake suites each consist of 10 orthogonal pairs of earthquake records, with the mean spectral acceleration of the suite scaled to fit the defined levels of excedance. As individual earthquakes may exceed this probability level, a lognormal distribution was used to represent the response distributions for peak drift, permanent drift, and peak acceleration. As the energy distributions are not lognormal, a counted distribution was used. Through the presentation of the 50^{th}, 65^{th}, and 84^{th} percentile levels, the distribution shifting through the application of control was apparent. The ability of the lognormal distribution to accurately represent the response characteristics with minimal sensitivity to extreme single events was demonstrated for the high earthquake suite.

The impact of the actuator architecture on the efficacy of structural control was of interest in this investigation. In contrast to previous semi-active investigations, the maximum actuator authority was held constant for each of the control architecture simulations for the SAC3 and SAC9 buildings, with the distribution of this maximum actuator authority examined. In order to retain the practical applicability of this research, total actuator authority was limited to less

than 14% of the building weight for both structures. This level of actuation is much lower than that used in most previous investigations, and represents a significant limitation that must be accounted for in non-linear structural control response.

Although the same maximum actuator authority was used within the simulations for each structure, the total amount of control input is dependent on the specific control law and the motion of the controlled structure. To enable valid comparisons between controllers and control architectures, two types of normalisation were developed. The first method normalises the response reductions by the scaled change in hysteretic energy between the controlled and uncontrolled responses, while the second employs the $\mathbf{L_2}$-norm of the control energy, which represents the rms control energy value. Both normalisations are indicative of the control input distribution, with the hysteretic energy method representing the 50^{th} percentile level, and the $\mathbf{L_2}$-norm method representing the 70.7^{th} percentile. The use of the normalised performance values (NPVs) allows valid assessment of different structural responses despite any specific differences for each control system implementation.

For the SAC3 simulations, small increases in NPVs were generally seen between the SAC3-A1 and SAC3-A2 architectures, particularly for acceleration regulation, while overall NPV reductions were seen between the SAC3-A2 and SAC3-A3 architectures. These trends suggest that maximum actuator authority be retained at the base of squat shear buildings, as the benefits gained through second floor actuation appear insufficient to justify the added control architecture complexity.

The effect of control architecture on the control of the SAC9 building differs to that for the SAC3 structure, highlighting the necessity to tailor structural control to suit the anticipated nature of the building's response. Two architectures were investigated - the SAC9-A3

architecture, which has control forces applied to floors 2, 3, and 9, and the SAC9-A8 architecture, which actuates floors 2 through 9. In both architectures, the soft first story is not directly controlled to retain the isolation properties for which it was designed. General NPV increases were observed, for both the centralised and decentralised controllers, when the maximum actuator authority was distributed over eight floors rather than three. Although over 50% of the actuator authority was retained on floors 2 and 3, for tall structures with higher mode participation, it is desirable to distribute a small amount of the available actuator authority up the height of the structure, rather than at discrete locations only.

In addition to utilising common displacement focused regulator control laws, this research has developed acceleration and jerk focused control lows – the LQRy and JQR clipped optimal controllers:

i) *LQRy clipped optimal control:* For the SAC3 structure, the LQRy controller was the only controller to produce positive NPVs for each of the performance metrics across all three earthquake suites. Each of the displacement-focused controllers produced increased peak accelerations despite drift reductions. However, the converse is not true for the LQRy controller. This result implies that acceleration regulation is able to improve occupant safety while simultaneously reducing the structural damage. The SAC9-A3 control architecture highlighted the difficulty in controlling accelerations during multi-mode response of tall structures, using a limited distribution of actuator authority. However, the performance of the LQRy controller was greatly improved using the SAC9-A8 architecture.

ii) *JQR clipped optimal control:* The peak and permanent drift NPVs for the JQR controller were large, particularly for the high earthquake suite. However, the effect of jerk

regulation is to increase peak structural accelerations, with the controller acting to smooth the accelerations to reduce their rate of change. Additional development is required to widen the controller's effective band, and further classify its characteristics.

Previous research into non-linear structural control has not accounted for the time-varying equilibrium point that results from permanent deformations during large earthquake jolts. This deficiency results in the controller attempting to re-yield the structure back to its original (zero) position. Although this re-yielding does result in apparent permanent drift reductions, increases in peak drift, hysteretic energy and peak accelerations indicate an increase in the total structural damage. In addition, this damage would result in increased joint flexibility, which was not included in the non-linear structural models. This investigation employed a displacement moving-average to determine the time-varying equilibrium point, and then used instantaneous displacements relative to this point within the control laws. This new technique resulted in improved controller performance, and more accurately represents the dissipative capability of semi-active control laws.

This research has investigated the efficacy of semi-active control systems using non-linear structural models and realistic suites of earthquake records representing extremes of seismic excitations. In addition to displacement focused control laws, acceleration and jerk regulation control methods were developed, showing the potential damage reduction benefits attainable from these new control approaches. A statistical assessment of control architecture was developed and undertaken, examining the distribution of a constant maximum actuator authority for both squat shear buildings and tall slender structures. This assessment highlights the need to consider non-linear structural response characteristics when implementing semi-active control systems. Finally, statistical analysis of all results using normalised performance values show the efficacy of each control law and actuator type relative to

different magnitude seismic events. This research clearly presents, for the first time, the tradeoffs between control law, architecture type, non-linear effects, and seismic input characteristics for semi-active control of civil structures.

9. FUTURE WORK

Many questions have arisen from the findings of this research. This section presents the future work following from this initial investigation, and although not exhaustive, represents the areas where greatest potential benefit and further interest may lie:

- As this investigation was undertaken using computer simulation methods, experimental verification would help further identify both the benefits and the shortcomings of semi-active control systems. Experimental modelling techniques would need to include non-linear structural effects, as these have been shown to have a major influence on the structural performance. The effect of structural yielding may potentially be incorporated through the inclusion of either mechanical ratchet-type spring joints, or perhaps actively controlled joints that alter the non-linear restoring moment through the application of a variable magnetic field.

- Although the interaction of actuator dynamics and structural dynamics is assumed negligible in this investigation due to the large differences in frequency response, it would be beneficial to verify this assumption using non-linear modelling over an extensive range of actuator demands and designs.

- The primary focus of this research has been the comparison of different control systems for structural control, which now allows the selection of appropriate control algorithms and architectures for continued development. This continued development should use performance based engineering assessment, including the drift performance level definitions developed as part of NEHRP. However, the development of similar

performance level definitions are required for the peak acceleration and hysteretic energy performance, if a more complete assessment of overall structural damage is to be obtained.

- Actuator saturation was included in the simulations to account for practical actuator limitations, however, it was observed that this saturation resulted in an increase in total structural jerk. Saturation was not explicitly included in the optimal control laws, hence, a clear future development is their modification to include this effect. This approach may further enhance the performance of the LQRy and JQR clipped optimal controllers.

- As the control systems are further developed, it will become necessary to simultaneously develop guidelines for their practical implementation. Key practical features may become apparent through the experimental investigation, such as the ability to spread the actuator force vertical component when control forces are large, as well as methods of practically attaching the actuators and tendons to the structure.

10. REFERENCES

Barroso L.R. (1999). "Performance Evaluation of Vibration Controlled Steel Structures Under Seismic Loading." *Stanford University,* Thesis: PhD.

Barroso, L.R., Breneman, S.E., and Smith, H.A. (2000). "Comparison of Story Drift Demands of Various Control Strategies for the Seismic Resistance of Steel Moment Frames." *Proc. 12th World Conference on Earthquake Engineering,* Auckland, NZ.

Barroso, L.R., Breneman, S.E., and Smith, H.A. (2001). "Effects of Structural Modelling on Seismic Performance Estimation of Controlled Steel Structures." *Proc. 2001 American Control Conference,* Arlington, VA.

Barroso, L.R., Breneman, S.E., Smith, H.A. (1998). "Evaluating the Effectiveness of Structural Control Within the Context of Performance-based Engineering." *Proc. 6th US National Conference on Earthquake Engineering,* Paper 123.

Bobrow, J.E., and Jabbari, F. (1997). "A High-performance Semi-active Controller for Structural Vibration Suppression." *Smart Structures and Materials,* SPIE, Vol. 3041, 67-74.

Bobrow, J.E., Jabbari, F., and Thai, K. (1995). "An Active Truss Element and Control Law for Vibration Suppression." *Smart Materials and Structures,* Vol. 4, 264-269.

Bobrow, J.E., Jabbari, F., and Thai, K. (2000). "A New Approach to Shock Isolation and Vibration Suppression Using a Resetable Actuator." *ASME Transactions on Dynamic Systems, Measurement and Control,* Vol. 122, 570-573.

Breneman, S.E. (2000). "Design of Active Control Systems for Multi-level Seismic Resistance." *Stanford University*, Thesis: PhD.

BSSC (1997). "NEHRP Guidelines for the Seismic Regulation of Existing Buildings and Other Structures." *Technical Report FEMA 273,* FEMA.

Carlson, J.D. (1994). "The Promise of Controllable Fluids." *Proc. Actuator 94,* H. Borgmann, and K. Lenz, eds., AXON Technologie Consult GmbH, 266-270.

Chase, J.G., and Smith, H.A. (1995(a)). "H-infinity Control for Vibration Control of Civil Structures in Seismic Zones." *Technical Report No. 116,* The John A. Blume Earthquake Engineering Centre, Stanford, CA.

Chase, J.G., and Smith, H.A. (1995(b)). "Design of H-infinity Control System Architectures for Civil Structures." *Proc. 10th ASCE Engineering Mechanics Specialty Conference,* Colorado.

Clough, R.W., and Penzien, J. (1975). *Dynamics of Structures,* McGraw-Hill, New York, United States.

Den Hartog, J.P. (1947). *Mechanical Vibrations*, McGraw-Hill, Inc. New York, NY.

Dowdell, D.J., and Cherry, S. (1994). "Semi-active Friction Dampers for Seismic Response Control of Structures." *Proc. 5th US National Conference on Earthquake Engineering,* Vol. 1, 819-828.

Dyke, S.J. (1998). "Seismic Protection of a Benchmark Building Using Magnetorheological Dampers." *Proc. 2nd World Conference on Structural Control,* Kyoto, Japan.

Dyke, S.J., and Spencer, Jr., B.F. (1996). "Seismic Response Control Using Multiple MR Dampers." *Proc. 2nd International Workshop on Structural Control,* Hong Kong, 163-173.

Dyke, S.J., Spencer, Jr., B.F., Quast, P., and Sain, M.K. (1993). "Role of Control-Structure Interaction in Protective System Design." *ASCE Journal of Eng. Mech.,* Vol. 121, No. 2, 322-338.

Dyke, S.J., Spencer, Jr., B.F., Sain, M.K., and Carlson, J.D. (1996). "Modelling and Control of Magnetorheological Dampers for Seismic Response Reduction." *Smart Materials and Structures,* Vol. 5, 565-575.

Dyke, S.J., Spencer, Jr., B.F., Sain, M.K., and Carlson, J.D. (1998). "An Experimental Study of MR Dampers for Seismic Protection." *Smart Materials and Structures,* Vol. 7, 693-703.

Franklin, G.F., Powell, J.D., and Emami-Naeini, A. (1994). *Feedback Control of Dynamic Systems (3rd Edition),* Addison-Wesley, United States.

Gauch, R.R. (2000). *Statistical Methods for Researchers Made Very Simple,* University Press, Maryland, United States.

Gavin, H.P., Hose, Y.D., and Hansen, R.D. (1994). "Design and Control of Electrorheological Dampers." *Proc. 1st World Conference on Structural Control,* WP3:83-92.

Gupta, A. (1998). "Seismic Demands for Performance Evaluations of Steel Moment Resisting Frame Structures." *Stanford University*, Thesis: PhD.

Housner, G.W., Bergman, L.A., Caughey, T.K., Chassiakos, A.G., Claus, R.O., Masri, S.F., Skelton, R.L., Soong, T.T., Spencer, B.F., and Yao, J.T.P. (1997). "Structural Control: Past, Present, and Future." *Journal of Engineering Mechanics,* Vol. 123, No. 9, 897-971.

Humar, J.L. (1990), *Dynamics of Structures,* Prentice-Hall, New Jersey, United States.

Iwan, W.P., and Cifuentes, A. (1986). "A Model for System Identification of Degrading Structures." *EEESD,* Vol. 14, No. 6, 877-890.

Jabbari, F., and Bobrow, J.E. (2002). "Vibration Suppression with Resettable Device." *Journal of Engineering Mechanics,* Vol. 128, No. 9, 916-924.

Jansen, L.M., and Dyke, S.J. (2000). "Semi-Active Control Strategies for MR Dampers: A Comparative Study." *ASCE Journal of Engineering Mechanics,* Vol. 126, No. 8, 795-803.

Kageyama, M., and Yuzuru, Y. (1990). "Vibration Control Systems for Various Types of Structures." *Proc. US National Workshop on Structural Control,* USC, Los Angeles, CA.

Kawashima, K., Unjoh, S., and Shimizu, K. (1992). "Experiments on Dynamic Characteristics of Variable Dampers." *Proc. Japan National Symposium on Structural Response Control,* Tokyo, Japan, 121.

Kelly, J.M. (1986). "Aseismic Base Isolation: Review and Bibliography." *Soil Dynamics and Earthquake Engineering,* Vol. 5, No. 3, 202-216.

Kennedy, R.P., Cornell, C.A., Campbell, R.D., Kaplan, S., and Perla, H. F. (1980). "Probabilistic Seismic Safety Study of an Existing Nuclear Power Plant." *Nuclear Engineering and Design*, Vol. 59, No. 2, 315-338.

Kobori, T. (1990). "Technology Development and Forecast of Dynamical Intelligent Buildings (D.I.B)." *Intelligent Structures,* Elsevier Appl. Sci., New York, NY, 42-59.

Kobori, T., Takahashi, M., Nasu, T., Niwa, N., and Ogasawara, K. (1993). "Seismic Response Controlled Structure with Active Variable Stiffness System." *Earthquake Engineering and Structural Dynamics,* Vol. 22, 925-941.

Krawinkler, H., and Gupta, A. (1998). "Story Drift Demands for Steel Moment Frame Structures in Different Seismic Regions." *Proc. 6th US National Conference on Earthquake Engineering,* Seattle, Washington.

Limpert, E., Stahel, W.A., and Abbt, M. (2001). "Log-normal Distributions Across the Sciences: Keys and Clues." *Bioscience,* Vol. 51, No. 5, 341-352.

Mizoshita, Y., Hasegawa, S., and Takaishi, K. (1996). "Vibration Minimised Access Control for Disk Drives." *IEEE Transactions on Magnetics,* Vol. 32, No. 3, 1793-1798.

Mizuno, T., Kobori, T., Hirai, J., Matsunaga, Y., and Niwa, N. (1992). "Development of Adjustable Hydraulic Dampers for Seismic Response Control of Large Structures." *ASME PVP Conference,* PVP-Vol. 229, 163-170.

Palazzo, B., and Petti, R. (1994). "Seismic Response Control in Base Isolated Systems Using Tuned Mass Dampers." *Proc. 1st Conference on Structural Control,* FP5, 29-38.

Patten, W.N, He, Q., Kuo, C.C., Liu, L., and Sack, R.L. (1994). "Suppression of Vehicle Induced Bridge Vibration via Hydraulic Semi-active Vibration Dampers (SAVD)." *Proc. 1st World Conference on Structural. Control,* FA1, 30-38.

Patten, W.N. (1997). "New Life for the Walnut Creek Bridge via Semi-active Vibration Control." *Newsletter of the International Association for Structural Control,* Vol. 2, No. 1, 4-5.

Pekcan, G., Mander, J.B., Chen, S.S. (1999). "Design and Retrofit Methodology for Building Structures with Supplemental Energy Dissipating Systems." *Technical Report MCEER 14260-4300,* Multidisciplinary Centre for Earthquake Engineering Research, Buffalo, NY.

Peng, C.Y. (1992). "Identification Methodology for a Class of Hysteretic Structures." *Earthquake Engineering and Structural Dynamics,* Vol. 21, No. 8, 695-712.

Reinhorn, A.N., Soong, T.T., Wang, Y.P., Fukao, Y., and Abe, H. (1989). "1:4 Scale Model Studies of Active Tendon Systems and Active Mass Dampers for Aseismic Protection." *Technical Report NCEER-89-0026,* National Centre for Earthquake Engineering Research, SUNY Buffalo.

Sack, R.L., Kuo, C.C., Wu, H.C., Liu, L., and Patten, W.N., (1994). "Seismic Motion Control via Semi-active Hydraulic Actuators", *Proc. 5th US National Conference on Earthquake Engineering,* Chigago, IL, 311-318.

Sakamoto, M., Kobori, T., Nishi, Y., Murai, K., and Kagaya, H. (1994). "Practical Applications of Active and Hybrid Response Control Systems and their Verification by Earthquake and Strong Wind Observations." *Proc. 1st World Conference on Structural Control,* WP2, 90-99.

Sommerville, P., Smith, N., and Penyamurthula, S. (1997). "Development of Ground Motion Time Histories for Phase II of the FEMA/SAC Steel Project." *SAC Background Document Report,* Report No. SAC/BD-97/04.

Soong, T.T., Masri, S., and Housner, G.W. (1991). "An Overview of Active Structural Control Under Seismic Loads." *Earthquake Spectra,* Vol. 7, No. 3, 483-505.

Spencer, Jr., B.F., Dyke, S.J., Sain, M.K., and Carlson, J.D. (1997). "Phenomenological Model of a Magnetorheological Damper." *Journal of Engineering Mechanics,* ASCE, Vol. 123, No. 3, 230-238.

Spencer, Jr., B.F., Suhardjo, J., and Sain, M.K. (1994). "Frequency Domain Optimal Control Strategies for Aseismic Protection." *Journal of Engineering Mechanics,* ASCE, Vol. 120, No. 1, 135-159.

Thai, K., Jabbari, F., Bobrow, J.E. (1995). "Vibration Suppression Through Parametric Control: A General Framework." *ASME International Congress*, San Francisco, CA.

Villaverde, R. (1994). "Seismic Control of Structures with Damped Resonant Appendages." *Proc. 1st World Conference. on Structural Control*, Vol. 1, WP4-113-WP4-122.

Wen, Y. (1972). "Method for Random Vibration of Hysteretic Systems." *Journal of the Engineering Mechanics Division,* Vol. 102, 249-263.

Yang, G, Ramallo, J.C., Spencer Jr., B.F., Carlson, J.D., and Sain, M.K. (2000(a)). "Dynamic Performance of Large-Scale MR Fluid Damper." *Proc. 14th ASCE Engineering Mechanics Conference,* Austin, TX.

Yang, J.N., and Giannopolous (1978). "Active Tendon Control of Structures." *ASCE Journal of Engineering Mechanics,* Vol. 104, No. 3, 551-568.

Yang, J.N., Kim, J.H., Agrawal, A.K. (2000(b)). "Resetting Semi-active Stiffness Damper for Seismic Response Control." *Journal of Structural Engineering,* Vol. 126, No. 12, 1427-1433.
Yao, J.T.P. (1972). "Concept of Structural Control." *Journal of Engineering Structures Division,* ASCE, 98, 1567-1574.

Yi, F., Dyke, S.J., Caicedo, J.M., and Carlson, J.D. (2001). "Experimental Verification of Multi-input Seismic Control Strategies for Smart Sampers." *Journal of Engineering Mechanics,* Vol. 127, No. 11.

Yi, F., Dyke, S.J., Frech, S., and Carlson, J.D. (1998). "Investigation of Magnetorheological Dampers for Earthquake Hazard Mitigation." *Proc. 2nd World Conference on Structural Control*, Koyoto, Japan.